The RNA-binding protein Pumilio2 regulates cell fate decisions in the adult hippocampus neurogenic niche

by

Kenneth Klau

Graduate School Life Science Munich

Dissertation der Fakultät für Biologie

der Ludwig-Maximilians-Universität München

München

21.08.2024

Eidesstattliche Erklärung:

Hiermit versichere ich an Eides statt, dass die vorliegende schriftliche Dissertation mit dem Titel „The RNA-binding protein Pumilio2 regulates cell fate decisions in the adult hippocampus neurogenic niche“ von mir selbstständig verfasst wurde und dass keine anderen als die angegebenen Quellen und Hilfsmittel benutzt wurden. Die Stellen der Arbeit, die anderen Werken dem Wortlaut oder dem Sinne nach entnommen sind, wurden in jedem Fall unter Angabe der Quellen (einschließlich des World Wide Web und anderer elektronischer Text- und Datensammlungen) kenntlich gemacht. Weiterhin wurden alle Teile der Arbeit, die mit Hilfe von Werkzeugen der künstlichen Intelligenz de novo generiert wurden, durch Fußnote/Anmerkung an den entsprechenden Stellen kenntlich gemacht und die verwendeten Werkzeuge der künstlichen Intelligenz gelistet. Die genutzten Prompts befinden sich im Anhang. Diese Erklärung gilt für alle in der Arbeit enthaltenen Texte, Graphiken, Zeichnungen, Kartenskizzen und bildliche Darstellungen.

Die vorliegende Dissertation wurde weder ganz noch teilweise bei einer anderen Prüfungskommission vorgelegt.

Ich habe noch zu keinem früheren Zeitpunkt versucht, eine Dissertation einzureichen oder an einer Doktorprüfung teilzunehmen.

München, den 21.08.2024 Kenneth Klau

Betreuer

Prof. Dr. Michael A. Kiebler
Biomedizinisches Centrum München/Zellbiologie
Ludwig-Maximilians-Universität München

Erstgutachter:	Prof. Dr. Michael A. Kiebler
Zweitgutachter:	Prof. Dr. Christof Osman

Tag des Einreichens:	21.08.2024
Tag der Verteidigung:	11.12.2024

Table of Contents

Abstract

This study investigates the functional role of Pumilio2 (Pum2) in adult neurogenesis, revealing novel insights into its impact on cell fate determination and as a consequence, the emergence of a previously undescribed cell type in the neurogenic lineage: “transient state cells” (TSCs). Adult neurogenesis takes place both in the dentate gyrus (DG) and the subventricular zone of the lateral ventricle of the adult mouse brain. It is a highly regulated process orchestrated by sequentially active transcription factors controlling neural stem cell (NSC) differentiation into neurons and astrocytes. The transcriptional control of this differentiation process is well characterised, the post-transcriptional regulatory mechanisms, however, are understood to a lesser extent. Pilot experiments suggested that Pum2 among other RNA-binding proteins (RBPs) participates in this regulation. Therefore, this PhD project investigated the role of Pum2 in adult neurogenesis in the DG of Pum2 deficient mice. In these mice, a decreased rate in adult neurogenesis and NSC self-renewal was found, coupled with increased astrogenesis. Notably, voluntary physical activity rescued these defects in the adult neurogenic lineage, suggesting compensatory mechanisms in NSCs. We performed single-cell RNA sequencing (scRNA-seq) analysis to understand the reason for the decreased rate in neurogenesis. In line with the histological analysis, we observed a reduction of the neuronal linage upon Pum2 depletion. Strikingly, we identified a highly abundant cell cluster with mixed identity, expressing both neuronal and astrocytic markers. These transient state cells, with low abundancy in wild type (WT) animals, appeared abundant in Pum2-deficient mice. It is probable that these cells originate from NSCs, yet they appear to be unable to develop into mature granule cells. Histological analysis confirmed increased TSCs numbers upon Pum2 depletion. Additionally, *in vivo* downregulation of Pum2 by a retroviral approach in WT mice led to altered neuronal morphology combined with astrocytic features in differentiated cells. In the absence of Pum2, NSCs fail to commit to either a neuronal or astrocytic lineage, resulting in the accumulation of TSCs with mixed identity. Collectively, these results underscore the essential post-transcriptional regulatory role of Pum2 in the maintenance, differentiation, and cell fate determination of adult DG NSCs as well as the general importance of post-transcriptional regulation in NSC lineage commitment.

Abbreviations

(m)RNA	(messenger) ribonucleic acid
°C	degree Celsius
µL	Microlitre
Ago	Argonaute
Aldoc	Aldolase C
Ascl1	Achaete-scute homolog1
BDNF	Brain-derived neurotrophic factor
bHLH	Basic helix-loop-helix
BMP	Bone morphogenetic proteins
BrdU	Bromodeoxyuridine
BrdU	Bromodeoxyuridine
CA3	Cornu ammonis 3
CAG	Chicken beta-actin promoter
CaMKII	Calcium/Calmodulin-dependent protein kinase II
Ckb	Creatine kinase B-type
CNS	Central nervous system
DAPI	4′,6-diamidino-2-phenylindole
Dcx	Doublecortin
DG	Dentate gyrus
DMEM	Dulbecco’s modified eagle medium
DN	Differentiating neuron
DNA	Deoxyribonucleic acid
DPBS	Dulbecco's phosphate buffered saline
ECM	Extracellular matrix
EDTA	Ethylenediamine tetra acetic acid
eEF1A	Elongation factor 1A
EGFP	Enhanced green fluorescent protein
Eomes	Eomesodermin
FBS	Fetal bovine serum
FGF	Fibroblast growth factor
GABA	Gamma-aminobutyric acid
GCL	Granular cell layer

GO	Gene Ontology
GT	Gene trap
h	Hour
HCl	Hydrochloric acid
HEPES	4-(2-Hydroxyethyl)piperazine-1-ethanesulfonic acid
hNPC	Human neural progenitor cells
Hopx	Homeodomain-only protein
Hz	Hertz
IA	Immature astrocyte
IN	Immature neuron
IPC	Intermediate progenitor cell
KCl	Potassium chloride
KD	Knock down
KEGG	Kyoto Encyclopaedia of Genes and Genomes
kg	Kilo gram
KH_2PO4	Potassium dihydrogen phosphate
LB	Lysogeny broth
M	Mole
m/v	Mass to volume
mA	Milli amper
MA	Mature astrocyte
Mg	Milligram
$MgCl_2$	Magnesium chloride
min	Minute
miRNA	Micro RNA
mm	Millimetre
mM	Millimole
mm^3	Cubic millimetre
MN	Mature neuron
n	Number of replicates
Na_2HPO4	Disodium hydrogen phosphate
NaCl	Sodium chloride
NeuN	Neuronal nuclei

ng	Nanogram
Ngn2	Neurogenin 2
nm	Nanometer
nM	Nanomole
Nr2e1	nuclear receptor subfamily 2 group E member 1
Nrgn	Neurogranin
NSC	Neural stem cell
OCT	Optimal Cutting Temperature compound
p	Probability
Pax	Paired box protein
PBS	Phosphate-buffered saline
PCR	Poly chain reaction
PDL	poly-D-lysine
PFA	Paraformaldehyde
pH	Potential of hydrogen
PSA-NCAM	Polysialylated neural cell adhesion molecule
Pum1/2	Pumilio1/2
Rbfox3	Hexaribonucleotide binding protein-3
RBP	RNA-binding protein
Rgs4	Regulator of G-protein signalling 4
RIPA	Radioimmunoprecipitation assay buffer
RMS	Rostral migratory stream
RNP	Ribonucleoprotein
rpm	Rotation per minute
RT	Room temperature
s	Second
Scn1a/Scn8a	Sodium voltage-gated channel alpha subunit 1/8
scRNA-seq	Single-cell RNA sequencing
SDS	Sodium dodecyl-sulfate
SGZ	Subgranular zone
Shh	Sonic hedgehog
SOC	Super optimal broth with catabolite repression
Sox2/9	SRY-Box transcription factor 2/9

Stau	Staufen
SVZ	Subventricular zone
TAC	Thesis Advisory Committee
TAE	Tris-acetate-EDTA
Tbr2	T-box brain protein 2
TCEP	Tris(2-carboxyethyl)phosphine
TE	Tris-EDTA
Tmsb4x	Thymosin beta 4
TSC	Transient state cell
V	Volt
v/v	Volume to volume
VZ	Ventricular zone
Wnt	Wingless/Integrated
WT	Wild type

1 Introduction

1.1 The complexity and plasticity of the brain

It is a general accepted view that the human brain is the most complex organ in the body, consisting of an extensive neural network, including approximately 86 billion neurons and over 100 trillion synapses (Azevedo et al., 2009; Gebicke-Haerter, 2023). This provides the basis for our cognitive processes, emotional responses, and self-awareness (Azevedo et al., 2009). The brain's structure is characterized by a hierarchical organization, spanning individual neurons, functionally specialised regions, and integrated large-scale networks (Bullmore & Sporns, 2009). The enormous scale of the brain and its capacity for change and plasticity, highlights the immense challenge of deciphering and understanding its complex roles in cognition, behaviour, and overall experience (Marblestone et al., 2016). A detailed examination of the central units of this system, namely the neurons and glia cells, such as astrocytes, revealed that even single cells hold a high degree of complexity and intricate properties. Neurons come in diverse shapes, connectivity patterns, and neurotransmitter profiles, enabling them to perform many different functions and contribute to the brain's remarkable capabilities (Scala et al., 2021; Zeng & Sanes, 2017). Neurons transmit signals through electrical impulses (action potentials) and chemical messengers/neurotransmitters, forming complex communication networks (Sudhof, 2013). However, neurons do not function independently; glial cells play a vital role in supporting, nourishing and protecting neurons (Khakh & Deneen, 2019). Astrocytes, for example, assist in regulating the blood flow and neurotransmitter levels (Adermark et al., 2022; Marina et al., 2020). Oligodendrocytes are providing the myelin sheath, which insulates and supports axons (Bradl & Lassmann, 2010; Simons & Nave, 2015). Microglia represent the brain's resident immune cells (Clarke & Barres, 2013; Wolf et al., 2017). Importantly, this system is highly dynamic. Neuroplasticity allows the brain to remodel its connections throughout the lifespan and to change in response to experiences (Draganski et al., 2004). Environmental experiences greatly shape the brain, driving the formation and refinement of neural connections, primarily at the synapse level, and allowing structural changes through the addition of newborn neurons throughout the lifespan (Holtmaat & Svoboda, 2009; Zatorre et al., 2012). This ongoing development includes adult neurogenesis, the birth of new neurons, which can be significantly influenced in a positive or negative way by factors such as learning,

exercise, and stress (McEwen & Gianaros, 2011; van Praag et al., 1999). The regulation of gene expression by transcription factors is highly important in these processes, whereas RNA-binding proteins (RBPs) are essential in controlling the translation of genetic information into the proteins that build and modify neurons (Darnell, 2013; Pilaz & Silver, 2015). The understanding of the complex interplay between environmental experiences and the molecular mechanisms regulated by RBPs is crucial for explaining the mechanisms by which our brains undergo continuous adaption and change (Leslie & Nedivi, 2011).

1.1.1 The mouse brain

Mice share several fundamental similarities with humans with respect to their brains, including structures, functions, genetics and cellular processes (Beauchamp et al., 2022; Wong et al., 2023). The genetic composition of mice is well-characterised and can be modified, thereby allowing investigations into the role of specific genes on brain development, function and disease (Nestler & Hyman, 2010; Svenson et al., 2012). Furthermore, their shorter lifespan allows to observe the effects of ageing and pharmacological treatments across generations (Allen et al., 2023; Finch & Tanzi, 1997; Miller, 2001). Mouse models are of great value in the study of neurological disorders, as they help to understand disease mechanisms and allow the development of potential treatments (Dawson et al., 2018; Miller et al., 2010). This is possible through the availability of well-established experimental tools and techniques. Despite the fundamental similarities, the human and the mouse brain exhibit striking differences. A key distinction between the mouse and human brains is their sheer size. However, the ratio to their body size is similar with approximately 1:40 (Herculano-Houzel, 2009; Jerison & Count, 1955). In addition, the human brain is far more complex with a significant larger volume and more complex cortical surface which enables enhanced cognitive capacities (Azevedo et al., 2009). This evolves by early signals from the dorsomedial tissue in the developing brain that play a crucial role in determining the folding patterns (gyrification) of distant regions of the neocortex (Chizhikov et al., 2019). At the cellular level, human neurons show an increased dendritic complexity, which may allow more complex information processing (Jacobs et al., 1997; Masoli et al., 2024). The overall structure of the brain is similar between humans and mice, however, the proportions of its regions and the specific structures within them differ (Hofman, 1989). The human prefrontal cortex, which is critical for

higher-order functions such as planning and decision-making, is more developed than the one from rodents (Miller & Cohen, 2001). These structural and cellular differences have broad influence for how these brains process information and regulates species-specific behaviours (Geschwind & Rakic, 2013). Despite these differences, studying the mouse brain provides valuable insights into fundamental processes that allow us to understand the human brain.

1.1.2 Embryonic neurogenesis

Embryonic neurogenesis is a tightly orchestrated developmental process that forms the central nervous system (CNS) (Berninger et al., 2006; Bystron et al., 2008). In mice, this process is well characterised, however, key aspects are still not fully understood (Florio & Huttner, 2014; Gotz & Huttner, 2005). The process begins with the development of the neural plate, a thickened region of the ectoderm (Tam & Behringer, 1997). The neural plate subsequently folds to create the neural tube, which serves as the origin to the CNS (Copp et al., 2003). Within the neural tube, neural stem cells (NSCs), initially termed neuroepithelial cells, reside within the ventricular zone (VZ) (Gotz & Huttner, 2005). These NSCs undergo symmetric proliferative divisions to expand their pool (Noctor et al., 2001). A key transition point marks the emergence of radial glial cells (RGCs), a specialized NSC type that originates from neuroendocrine cells after embryonic day 13 in mice (Kriegstein & Gotz, 2003). RGCs evolve a long basal process that extends towards the pial surface, representing the outermost boundary of the brain. These processes serve as a scaffold for the migration of neurons (Rakic, 1972; Sidman & Rakic, 1973; Stiles & Jernigan, 2010). RGCs primarily divide asymmetrically in a self-renewing way, while at the same time giving rise to either neurons directly or intermediate progenitor cells (IPCs) (Huttner & Kosodo, 2005). IPCs in the subventricular zone (SVZ) undergo further divisions to generate the vast number of neurons required for brain development (Haubensak et al., 2004). The process of neuronal differentiation is complex, following the inside-out principle in which deep cortical layers are generated first, followed by increasingly more superficial layers (Angevine & Sidman, 1961; Stiles & Jernigan, 2010). Crucially, neurogenesis happens in a spatiotemporal manner, orchestrated by complex signalling cascades and transcriptional networks. Morphogens like Sonic Hedgehog (Shh), Bone Morphogenetic Proteins (BMPs), Wnts, and Fibroblast Growth Factors (FGFs) play important roles in shaping the developing nervous system along the dorsal-ventral and

anterior-posterior axes (Bertrand & Dahmane, 2006; Jessell, 2000). These signals act on transcription factors within NSCs, such as those of the paired box protein (Pax), SRY-Box transcription factor (Sox), and basic helix-loop-helix (bHLH) families, regulating their proliferative capacity, cell fate determination, and differentiation (Guillemot, 2007). Newly born neurons detach from the VZ and begin to migrate, often guided by the supportive scaffolds of RGC processes (Noctor et al., 2001; Rakic, 1972). There are diverse modes of neuronal migration, including soma translocation where the cell body moves directly along the radial glial fibre, and locomotion, where the neuron extends a leading process for dynamic movement (Marin et al., 2006). During migration, neurons begin to differentiate, extending axons and dendrites to form early connections (McAllister, 2000). Factors like Reelin, secreted by Cajal-Retzius cells, are essential for ensuring neurons migrate to their correct positions within the developing cortex's layered structure (D'Arcangelo et al., 1995). When reaching their target destinations, neurons start to mature by undergoing wide synaptogenesis and refining their connections (McAllister, 2000). This process is a balance between integration into functional circuits and apoptosis (programmed cell death), a mechanism that eliminates excess or improperly connected neurons (Kuan et al., 2000). While the main processes of neurogenesis are conserved, mouse models reveal species-specific features. The mouse cortex has a comparable larger SVZ with outer RGCs, a specialised subtype with enhanced proliferative capacity, which most likely contributing to the enlarged cortical size of higher mammals (Hansen et al., 2010). Disruptions in the proper development can lead to severe neurodevelopmental disorders (Barkovich et al., 2012).

1.1.3 Adult hippocampal neurogenesis and its contributor to memory, pattern separation, and mood

Adult neurogenesis, the generation of new neurons in the mature brain, contrasts with the long-held dogma of a static CNS. In mice, two neurogenic niches are present in the adulthood, the SVZ at the lateral ventricles, and the subgranular zone (SGZ), a part of the dentate gyrus (DG), which is a subregion within the hippocampus (Altman & Das, 1965; Gage, 2000; Lim & Alvarez-Buylla, 2014). Adult neurogenesis is a dynamic process, which is controlled by intrinsic and extrinsic factors. Transcription factors such as Sox2, nuclear receptor subfamily 2 group E member 1 (Nr2e1) and Achaete-scute homolog 1 (Ascl1) are essential for maintaining the stem cell identity

and the regulation of cell fate progression (Knobloch & Jessberger, 2017). Neurotrophic factors, including the brain-derived neurotrophic factor (BDNF), play a pivotal role in promoting neuronal differentiation, survival and synaptic integration (Lu et al., 2014). Physical exercise, environmental enrichment, and specific cognitive tasks enhance hippocampal neurogenesis, thereby demonstrating the plasticity of the adult brain (Sahay et al., 2011). Conversely, stress, the process of ageing, and various pathological conditions have been shown to have a negative impact on adult neurogenesis (Dranovsky & Hen, 2006). Within the SVZ, quiescent NSCs possess astrocytic characteristics comparable to RGCs (Doetsch et al., 1999). Upon activation, quiescent NSCs give rise to rapidly proliferating transit-amplifying progenitors (Doetsch et al., 1997). These transit-amplifying progenitors undergo further differentiation into neuroblasts, which migrate along the rostral migratory stream (RMS) towards the olfactory bulb, where they integrate as interneurons (Lois & Alvarez-Buylla, 1994; Zhao et al., 2008). The hippocampal SGZ has a similar hierarchical organization. In brief, RGCs generate IPCs, which subsequently undergo division and transition into neuroblasts that differentiate into neurons (Kempermann et al., 2004). The RGCs, which express the homeodomain-only protein (Hopx), are in the SGZ (Berg et al., 2019; Pilz et al., 2018; Seri et al., 2001). Upon activation through Notch or Wnt signalling or GABA neurotransmitter release, RGCs differentiate into proliferative IPCs that express T-box brain protein 2 (Tbr2) (Bonaguidi et al., 2011; Kempermann et al., 2004; Lugert et al., 2010). IPCs undergo further divisions and differentiate into neuroblasts, which begin to express markers of neuronal differentiation, such as doublecortin (Dcx) (Hodge et al., 2012; Urban & Guillemot, 2014; Zhao et al., 2008). Newborn neurons migrate a short distance into the granule cell layer, where they start to express Hexaribonucleotide Binding Protein-3 (Rbfox3, also known as NeuN, named due to the protein Rbfox3 which is found in neuronal nuclei). These newborn neurons initially develop the dendrites into the molecular layer (ML) and subsequently project their axons through the hilus towards their targets in the Cornu Ammonis 3 (CA3) region of the hippocampus, where they integrate into the existing circuitry, playing a crucial role in learning and memory formation (Sahay et al., 2011; Toni et al., 2007; van Praag et al., 1999; Zhao et al., 2006) (**Figure 1**). The newborn neurons undergo a competitive selection process during their early development. This holds true for newborn granule cells in the hippocampus, where the newborn neurons compete for limited resources,

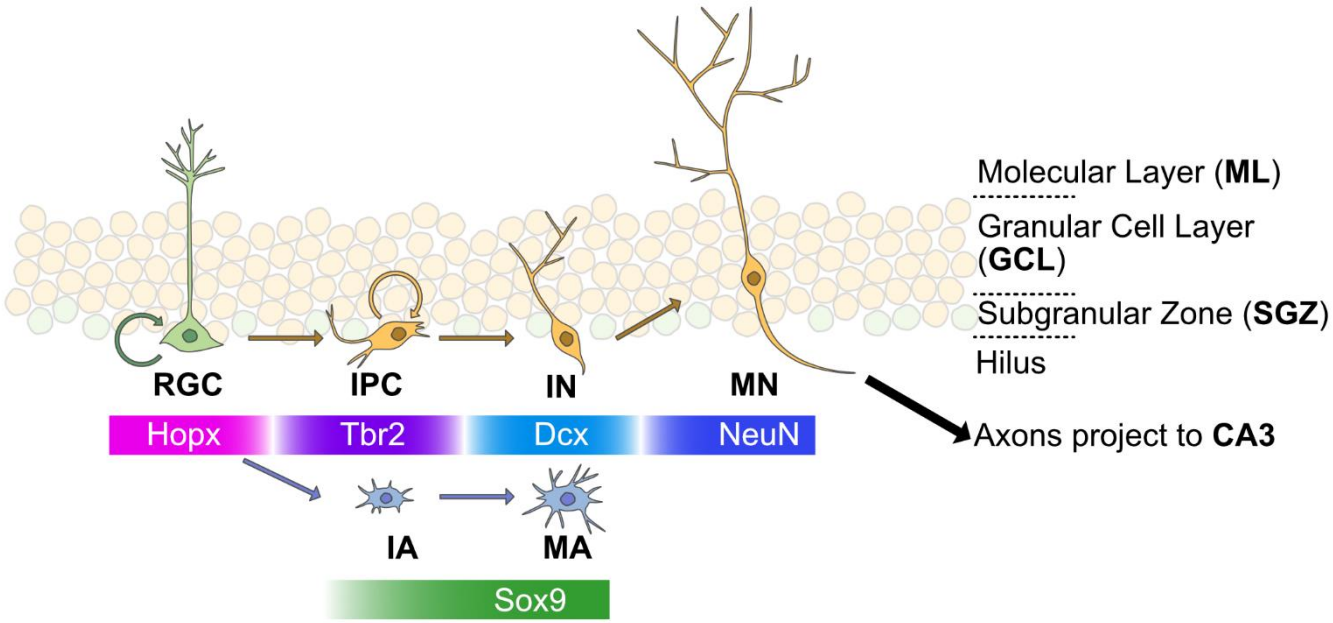

Figure 1: Differentiation pathways of RGCs in the DG. RGCs within the subgranular zone (SGZ) can follow neurogenic or astrogenic lineages, respectively. Neurogenesis: RGCs differentiate into Tbr2+ intermediate progenitor cells (IPCs), which further develop into Dcx+ immature neurons (INs). INs mature into NeuN+ neurons, which extend extending dendrites into the molecular layer (ML) and projects their axons into the CA3 region. Astrogenesis: RGCs transition into immature astrocytes (IAs) before maturing into Sox9+ mature astrocytes (MAs). Adapted with the help of Dr. Barbara Nitz from (Berg et al., 2018).

including neurotrophic factors and GABAergic depolarising inhibition as well as activity-dependent selection. This competition results in the elimination of a significant number of GCs. Only a small percentage is successfully integrated into the existing brain circuitry (Bergami & Berninger, 2012). Adult neurogenesis is an important process that has been shown to do more than simply replace lost neurons. It is crucial for the brain's lifelong capacity for change and adaptation to novel or changing environments (Deng et al., 2010). It introduces young, highly plastic neurons into existing neuronal circuits, which may allow the formation of new connections and the modification of existing ones (Christian et al., 2014; Schmidt-Hieber et al., 2004). This ongoing rewiring may be responsible for the brain's remarkable capacity to adapt to novel experiences, learn new skills, and potentially recover from certain injuries (Goncalves et al., 2016; Kempermann et al., 2018). An important characteristic of newly born neurons in the DG is their enhanced excitability and plasticity during maturation, indicating the potential for their unique contribution to specific cognitive functions (Ge et al., 2007;

Schmidt-Hieber et al., 2004). This is consistent with the long-standing hypothesis that hippocampal neurogenesis is involved in pattern separation, the process of discriminating between similar experiences or storing distinct memories in the face of overlapping inputs (Aimone et al., 2009; Clelland et al., 2009). Selective disruption of adult neurogenesis, often through targeted irradiation or viral injection, has provided evidence for its involvement in hippocampal-dependent learning (Jessberger et al., 2009). The performance of animals with depleted neurogenesis is impaired in tasks that require spatial memory and the ability to differentiate between similar contexts, such as contextual fear conditioning (Jessberger et al., 2009; Sahay et al., 2011). These findings demonstrate the important role of new neurons in the formation and refinement of memory within the hippocampus. In addition to its role in learning and memory, an aberrant adult hippocampal neurogenesis may also contribute to the development of mood disorders, including depression and anxiety (Snyder et al., 2011). A major risk factor for these kinds of disorders is stress, which can suppress neurogenesis (Mirescu & Gould, 2006). The artificial increase in the birth of new neurons often act in an antidepressant-like way (Malberg et al., 2000; Sahay & Hen, 2007). Studies also hint that increased neurogenesis may be important to protect against age-related cognitive decline, which allow to explore future treatments that aim to preserve brain function in aged humans (Drapeau et al., 2003; Kuhn et al., 1996). This indicates that maintaining a healthy rate of hippocampal neurogenesis may be crucial for emotional well-being, resilience in the context of life's challenges and age-related decline. In addition to neurogenesis, the adult brain is also capable of astrogenesis, the formation of new astrocytes (Ge et al., 2012). In contrast with the long-held view of astrocytes as only supportive cells, recent research has demonstrated that they actively modulate synaptic activity, regulating neurotransmitter release and reuptake (Allen & Eroglu, 2017; Bazargani & Attwell, 2016; Chalmers et al., 2024). New research suggests that adult-born astrocytes may promote synaptic plasticity and therefore influencing learning and memory processes (Chalmers et al., 2024; Santello et al., 2019). Furthermore, astrocytes assist in maintaining brain homeostasis, indicating that astrogenesis may be a crucial factor in the brain's resilience to disease and ageing (Khakh & Deneen, 2019).

1.1.4 Evidence on human adult neurogenesis

Although adult neurogenesis has been well-documented in rodents, it is more often recognised as a dynamic process that may also occur in humans. The retrospective birth dating of cells by carbon birth dating in humans indicate that minimal neurogenesis occurs in the adult human cortex and dynamics of neurogenesis in the adult human hippocampus provided evidence for the existence in these regions (Spalding et al., 2013; Spalding et al., 2005). In early studies, suggested markers for neurogenesis, including doublecortin (Dcx), polysialylated neural cell adhesion molecule (PSA-NCAM) and Ki67, were identified in the adult human hippocampus (Eriksson et al., 1998; Knoth et al., 2010; Sanai et al., 2011). However, research indicates a decline in neurogenesis during childhood until the levels of neurogenesis potentially becoming very low or being undetectable in adulthood (Sorrells et al., 2018). This contrasts with findings in mice, where hippocampal neurogenesis is observed throughout lifespan, with a significant decline after three months of age (Altman & Das, 1965; Kempermann et al., 2004; Knoth et al., 2010). Furthermore, the role of the SVZ as a neurogenic niche may differ between species, with a potentially lower olfactory bulb contribution in humans (Sanai et al., 2004). Therefore, additional research will be essential to elucidate whether the neurogenic capacity observed in mice is applicable to the adult human brain (Kempermann et al., 2015).

1.2 RBPs act as master regulator of gene expression

Hippocampal neurogenesis is not only driven by transcription factors, as it was long believed. Recent research demonstrated the crucial role of RBPs in regulating gene expression and localization at the post-transcriptional level (Fernandez-Moya et al., 2014; Gebauer et al., 2021; Hentze et al., 2018). Understanding RBP function offers new avenues for unravelling the complexities of this important process. RNA undergoes a series of transformations that impact its stability from transcription over localization and translation into functional proteins (Hentze et al., 2018). RBPs bind with RNAs to control diverse cellular processes (Gerstberger et al., 2014). They act as master regulator at every step of this lifecycle, controlling RNA processing and recognizing specific codes within RNA transcripts (Fernandez-Moya et al., 2021; Gebauer et al., 2021). By recognizing *cis*-acting factors like mRNA sequences and/or structural elements, they form complex complexes called ribonucleoprotein particles (RNP) or RNA granules, which vary in size and makeup (Bauer et al., 2022; Doyle &

Kiebler, 2011; Fritzsche et al., 2013; Kiebler & Bassell, 2006). RNPs are shaping numerous facets of RNA metabolism (Doyle & Kiebler, 2011). They are forming to regulate RNA from early on within the nucleus. Transcription produces a precursor mRNA (pre-mRNA) molecule. RBPs play a crucial role in shaping pre-mRNAs through splicing, 5'-capping, 3'-polyadenylation and directing their exit from the nucleus (Doyle & Kiebler, 2011; Dreyfuss et al., 2002; Macchi et al., 2004). They influence alternative splicing events, mature mRNA and the polyadenylation (Gerstberger et al., 2014; Vuong et al., 2016). These events imprint a distinctive "*RNA signature*" onto each transcript, which consists of specific sequences and structures. This functions like a blueprint for specific RBPs that direct the mRNAs within the cytoplasm (Doyle & Kiebler, 2011). Following this, RBPs facilitate nuclear export of the mRNA into the cytoplasm (Kohler & Hurt, 2007). Within the cytoplasm, RNPs are dynamically remodeled allowing precise control over mRNA stability, localisation to subcellular destinations, and localised protein synthesis where it is required (Buxbaum et al., 2015; Doyle & Kiebler, 2011; Medioni et al., 2012; Schieweck, Riedemann, et al., 2021). The localized protein synthesis is achieved by the transport of RNPs along the cytoskeleton via the direct or indirect interaction of RBPs with molecular motors (Buxbaum et al., 2015; Gumy et al., 2014; Kiebler & Bassell, 2006; Mofatteh & Bullock, 2017). Therefore, RBPs play a critical role in mRNA localization, ensuring it reaches the correct subcellular destination for translation (Martin & Ephrussi, 2009). Furthermore, RBPs directly control translation by influencing initiation, elongation, and termination (Licatalosi & Darnell, 2010). Finally, RBPs regulate mRNA stability, determining its lifespan and the amount of protein being produced (Schoenberg & Maquat, 2012). RBPs apply their effects by recognizing specific RNA sequences and/or structural motifs (Schieweck, Ninkovic, & Kiebler, 2021). They act in all cell types, demonstrating critical roles in development, cell differentiation and stress response (Gerstberger et al., 2014; Hentze et al., 2018). Aberrant RBP function has been linked to numerous diseases, such as cancer, neurodegenerative, neuropsychiatric and neurological disorders, as well as viral infections (Lukong et al., 2008; Pereira et al., 2017). Therefore, RBPs are essential regulators of gene expression at a post-transcriptional level (Mitchell & Parker, 2014). Their significance, together with recent technological advances in identifying RNA-protein interactions, makes RBP biology an important

area of research with far-reaching implications for understanding fundamental biology together with disease pathogenesis.

1.2.1 RBPs act as key players in neuronal development, plasticity, and disease

The CNS, including the brain with its labyrinth of connections, relies on precisely controlled gene expression for optimal development and function (Holt & Schuman, 2013; Schieweck, Ninkovic, & Kiebler, 2021). Neurons, with their incredibly long extensions, complex architecture and specialized roles, need to quickly modify protein levels in specific subcellular compartments by mRNA localization to respond to signals (Holt & Schuman, 2013). As previously stated, RBPs are actively shaping the fate of mRNAs and influencing the subsequential protein expression (Hentze et al., 2018; Schieweck, Ninkovic, & Kiebler, 2021). This is of high importance in neurons for several cellular processes including axonal outgrowth, shaping dendritic branches, strengthening or weakening synapses long-term and is therefore, also important for memory formation and learning (Doyle & Kiebler, 2011; Holt & Schuman, 2013; Klann & Dever, 2004; Sahoo et al., 2018; Yoon et al., 2016). The delivery of RNPs to synapses marks a remarkable degree of precision but the transport is not unidirectional (Doyle & Kiebler, 2011). However, the delivery of mRNAs and subsequently the translation is influenced by the synapse's activity level (Doyle & Kiebler, 2011). Translation-suppressing RBPs in dendritic transport might indicate that mRNAs may be transported to their synaptic destinations in a state of translational inactivity (Dahm & Kiebler, 2005; Fritzsche et al., 2013). The "*sushi belt model*" provides a possible explanation for dendritic mRNA trafficking in which RNPs continuously circulate in both directions within dendrites, ready to supply activated synapses with the right mRNA. This may involve activity-dependent 'tags', such as a prion-like switch protein in synapses, which attract dynamic microtubules that extend into dendritic spines and allow the precise delivery, anchoring and disassemble of individual RNPs followed by local translation of mRNAs (Doyle & Kiebler, 2011). The newly synthesized protein then participates in the remodelling and strengthening of the synapse (Bauer et al., 2019; Buxbaum et al., 2014; Doyle & Kiebler, 2011; Park et al., 2014). An investigation regarding the transport of *regulator of G-protein signalling 4 (Rgs4)* mRNA underscored the reasonability of the "*sushi-belt model*" (Bauer et al., 2019). The synaptic transport depends on signals within its 3'-untranslated region (Bauer et al., 2019). After serving its purpose at the synapse, an mRNA can be broken down or

potentially repackaged into an RNP for further transport and/or translation (Bauer et al., 2019). Dysfunction of post-transcriptional regulators can lead to a disrupted protein localization (Lecuyer et al., 2007). This has been linked with the onset of a range of neurological, neurodevelopmental and neurodegenerative conditions and is therefore underscoring their significance within the CNS (Boczonadi et al., 2014; De Conti et al., 2017; Sartor et al., 2015; Wan et al., 2012).

1.2.2 The role of Pumilio2 from translation regulation to adult neurogenesis

RBPs have been shown to be important regulators for neurogenesis. The mammalian Pumilio2 (Pum2) protein, a member of the highly conserved PUF protein family of RBPs, might represent a potential key regulator in neurogenesis (Goldstrohm et al., 2018; Wang et al., 2018; Zhang et al., 2017). Pum2, with its specific recognition motive (UGUANAUA) in the 3'-UTR of mRNAs, has remarkable control over protein expression, influencing mRNA translation, stability, and even transport (Goldstrohm et al., 2018; Hotz & Nelson, 2017; Martinez et al., 2019; Van Etten et al., 2012; White et al., 2001; Zhang et al., 2017). Their role in repressing translation was observed across yeast, flies, and frogs (Nakahata et al., 2003; Parisi & Lin, 2000; Wickens et al., 2002). One key mechanism involves the shortening of the mRNA's poly-A tail. Pum proteins can recruit the CCR4-NOT deadenylase complex, leading to mRNA instability and preventing translation (Goldstrohm et al., 2007; Van Etten et al., 2012). Additionally, Pum2 can directly prevent translation initiation by binding to the 5' cap of mRNAs, competing with the essential translation factor eIF4E (Cao et al., 2010). Pum2's influence on protein expression extends beyond initiation. It can interfere with translation elongation process in combination with Argonaute (Ago) proteins and elongation factor 1A (eEF1A) to form an inhibitory complex (Friend et al., 2012). Recent findings revealed, Pum2 can also activate translation, specifically boosting the expression of GABAergic synapse components like Gephyrin (Schieweck, Riedemann, et al., 2021). Yet, the precise way Pum2 influences localized protein synthesis and its role in global protein expression remains unknown. Given Pum2's effects on translation and its diverse RNA targets, it is a critical regulator of cell function. Beyond direct translation control, Pum2 also influences mRNA localization, essential for processes like cellular migration (Hotz & Nelson, 2017). Pum2 is also influencing the process of neuronal development and synaptic function (Dong et al., 2018; Siemen et al., 2011; Vessey et al., 2010). While a significant amount of research exists, its full role within

neurons remains enigmatic. In developing neurons, Pum2 actively prevent the localization of certain mRNAs into axons, thereby shaping axonal protein production (Martinez et al., 2019). Studies in *Drosophila* revealed Pum's impact on dendritic development, synaptic function, and neuronal excitability through its regulation of key proteins (Mee et al., 2004; Menon et al., 2009; Menon et al., 2004; Schweers et al., 2002; Ye et al., 2004). Pum2 has been shown to be a crucial regulator of the precise timing of diverse neuronal subtypes and cell fate decisions during embryonic corticogenesis (Parra & Johnston, 2022; Pilaz & Silver, 2015; Vessey et al., 2012; Zahr et al., 2018). Normally, mRNAs encoding various neuronal specification proteins are co-expressed within neural progenitors. Pum2 influences this by forming a complex with 4E-T to repress the translation of these mRNAs of which a vast number is essential for transcriptional control and neuronal development, such as the transcription factors Pou3f3/Brn1, Tle4 and members of the proneurogenic bHLH family, such as Neurog1, Neurog2 and Ascl1 (Zahr et al., 2018). Disrupting either Pum2 or 4E-T results in the aberrant expression of proteins and the disruption of neuronal layer development (Zahr et al., 2018). The mechanism by which eIF4E/4E-T controls neurogenesis by regulating proneurogenic proteins, has been previously observed (Yang et al., 2014). Pum2 plays a key role in the asymmetric division of neural progenitors, such as RGCs, where it represses the translation of these mRNAs during RGC division (Gotz & Huttner, 2005; Vessey et al., 2012). There it forms RNP complexes with mRNA targets, encoding cell fate determinants to promote differentiation and supress stem cell characteristics, which are segregated into differentiating daughter cells, such as the IPCs (Vessey et al., 2012). Disrupting Pum2 function leads to a depletion of the progenitor pool (Vessey et al., 2012). This highlights the importance of Pum2-mediated RNA regulation in maintaining the balance between stem cell maintenance and neuronal differentiation and maturation during brain development (**Figure 2A**). Pum2 plays a dynamic role in hippocampal neurons, forming RNA granules with key RBPs like FMRP and potentially Stau2 within the somatodendritic region (Fritzsche et al., 2013; Vessey et al., 2006; Zhang et al., 2017). Furthermore, the interaction with Stau2 has been demonstrated to be indispensable for synaptic plasticity and long-term memory formation (Dubnau et al., 2003). Notably, Pum2 and Stau2 seem to regulate a shared pool of mRNA targets, indicating Pum2's role in activity-dependent control of local translation (Heraud-Farlow & Kiebler, 2014;

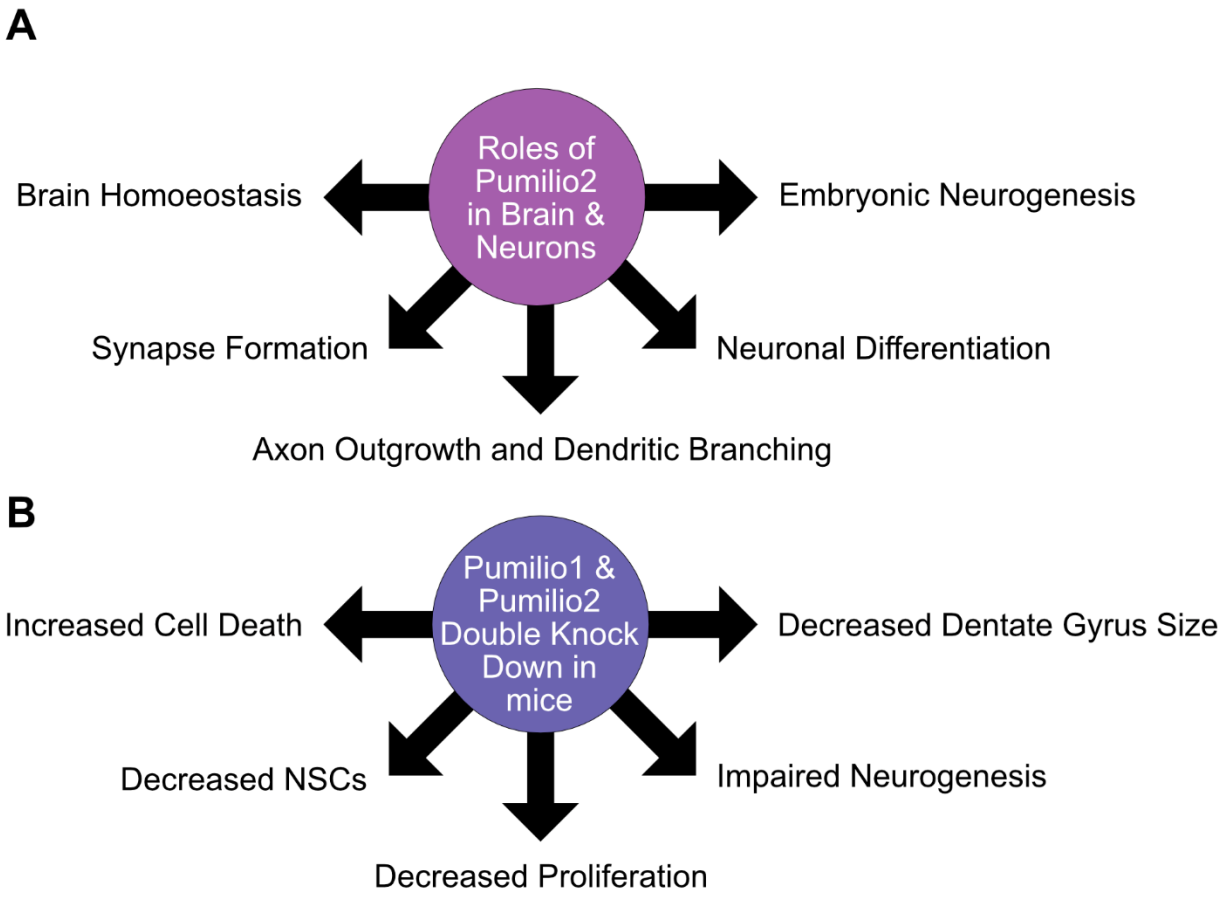

Figure 2: Known roles of Pum2 in neurons and the brain. (**A**) Pum2 as important regulator of different processes in neurons and the brain. (**B**) The cartoon shows the effect of the double depletion of Pum1 & 2 in the same mouse. The results of the double depletion are adapted from M. Zhang et al. (Zhang et al., 2017).

Schieweck, Riedemann, et al., 2021; Zahr et al., 2018; Zhang et al., 2017). Pum2 together with Pum1 potentially also plays a crucial role in the development of the hippocampus. This aligns with the observation of Pum2 and Pum1 depletion, which enhances the protein levels of its mRNA targets, thereby providing further evidence for its function as a translational repressor in neurogenesis (Zhang et al., 2017). Depletion of Pum1 and Pum2 disrupts hippocampal neurogenesis and increases cell death, reduces DG size and increases IPC density, highlighting their important role in neuronal survival and differentiation (Zhang et al., 2017) (**Figure 2B**). Furthermore, the depletion of Pum2 in mice is related to spontaneous epileptic seizures (Follwaczny et al., 2017; Siemen et al., 2011). Pum2's mRNA targets during development overlap with those found in mature neurons, indicating that, Pum2 is likely to act within a complex network of RBPs to regulate gene expression and cell fate decisions during brain development and mature brain with great precision (Fritzsche et al., 2013). In immature neurons (INs), Pum2 controls dendritic outgrowth, whereas in mature neurons (MNs),

loss of Pum2 leads to a reduction in dendritic spines, an increase in elongated filopodia, and to a boost in excitatory signalling. Pum2 appears to reduce neuronal excitation by repressing the translation of key molecules like sodium channels (Scn1a, Scn8a) and the AMPA receptor subunit Gria2 (Dong et al., 2018; Driscoll et al., 2013; Vessey et al., 2010). Notably, mutations in the sodium channel Scn8a are also linked to epilepsy (Blanchard et al., 2015; Martin et al., 2007). This is important for the precise temporal expression of neuronal characteristics. Interestingly, Pum2's role in maintaining stem cell populations extends beyond the brain. It acts as a translational regulator in germ cell development (Fox et al., 2005; Moore et al., 2003). This underscores Pum2's broader significance in cell fate regulation.

1.3 Aim of the project

The aim of the thesis is to elucidate the specific role of the RBP Pum2 in modulating adult neurogenesis within the mammalian brain. As previously stated, adult neurogenesis underpins critical brain processes like learning, memory formation, and adaptation to environmental changes in which Pum2 has been implicated to play an important role. Dysregulation of adult neurogenesis is implicated in a range of neurodevelopmental and neurodegenerative disorders, making it a potential therapeutic target. Yet, despite the importance of lifelong ongoing neurogenesis and the known important contribution of RBPs in this process, the specific role of Pum2 in the adult neurogenesis is not sufficiently explored. Understanding the precise role by which Pum2 shapes the birth and integration of new neurons is likely to provide insights into the fundamental biology of the brain and to potentially open new avenues for therapeutic interventions in neurological disorders where neurogenesis is impaired.

For this doctoral thesis, I utilised a Pum2 deficient mouse line (Siemen et al., 2011). These animals display a downregulation of Pum2 in the whole brain and the hippocampus of 90% (Follwaczny et al., 2017).

Specifically, this work sought to address the following research questions:

- **I)** At which level does Pum2 contribute to adult neurogenesis?
- **II)** Do the newly born neurons develop normally in Pum2 deficiency?
- **III)** Is the Pum2 deficient brain capable to overcome the reduced neurogenesis?
- **IV)** Does the downregulation of Pum2, specifically in the adult brain, affect neurogenesis?

2 Material and Methods

2.1 Materials

Table 1: List of primary antibodies

Antibody	Species	Company	Dilution
α-BrdU	rat (monoclonal)	Abcam	1:300
α-Ckb	rabbit (polyclonal)	Sigma Aldrich	1:1000
α-Dcx	guinea pig (polyclonal)	Merck Millipore	1:1000
α-Dcx	rabbit (polyclonal)	Abcam	1:1000
α-GFP	chicken (polyclonal)	Aves Labs	1:1000
α-Hopx	rabbit (polyclonal)	Sigma Aldrich	1:1000
α-Ki67	rabbit (polyclonal)	Thermo Fisher Scientific™	1:1000
α-NeuN	rabbit (monoclonal)	Abcam	1:500
α-Sox9	rabbit (polyclonal)	Sigma Aldrich	1:2000
α-Tbr2	rabbit (monoclonal)	Abcam	1:1000
α-Tmsb4x	mouse (polyclonal)	Abcam	1:1000

Table 2: List of secondary antibodies

Antibody	Species	Company	Dilution
α-chicken-A488	donkey	Jackson Immuno Research; Thermo Fisher Scientific™	1:1000
α-guinea pig-Cy3	goat	Jackson Immuno Research; Thermo Fisher Scientific™	1:1000
α-mouse-A555	donkey	Molecular Probes (LifeTechnologies)	1:1000
α-rabbit-A647	donkey	Molecular Probes (LifeTechnologies); Thermo Fisher Scientific™	1:500
α-rat-A488	goat	Molecular Probes (LifeTechnologies); Thermo Fisher Scientific™	1:1000

Table 3: List of buffers, media, and solutions

Buffer/Medium/Solution	Components
0-medium (HEK 293GPG cells)	DMEM (1x) + GlutaMAX™ + 25 mM HEPES; 10% (v/v) FBS;
10% Sucrose solution	10% sucrose in 1x PBS;
1x PBS (1 L)	1.44 g Na_2HPO4; 8 g NaCl; 0.2 g KH_2PO4; 0.2 g KCl;
1x TAE buffer	1 mM EDTA disodium salt; 40 mM Tris base; 20 mM acetic acid;
30% Sucrose solution	30% (m/v) sucrose in 1x PBS;
3x SDS sample buffer	188 mM Tris-Cl (pH 6.8); 3% (m/v) SDS; 30% (v/v) glycerol; 15% (v/v) β-mercaptoethanol;
4% PFA	4% (m/v) PFA in 1x PBS;
70% Ethanol	70 mL EtOH in 33.31 mL ultra-pure water;
Ampicillin-LB media	100 mg/L ampicillin in LB media;
Blocking solution (Immunostaining)	1x PBS with 0.5% (v/v) Tween20 and 5% (m/v) BSA; pH 7.1;
Blocking solution (Western Blot)	1x PBS with 0.5% (v/v) Tween20 and 2% (m/v) BSA; pH 7.1;
Blotting buffer	25 mM Tris-HCl; 192 mM glycine; 20% (v/v) methanol; 0.02% (m/v) SDS;
Borate buffer (0.1M, pH 8.5)	0.1 M boric acid; 25 mM NaOH;
Cryoprotection solution (500 mL)	150 g sucrose; 40 mM phosphate buffer; 150 mL ethylene glycol;
DAPI solution	2 µg/mL DAPI in ultra-pure water;
Elution buffer	0.5 M glycine; 3 M Urea; 3M guanidinium hydrochloride; 70 mM TCEP-HCl; pH 2.5;
Ethanol (50%, RNase free)	50 mL EtOH in 53.31 mL ultra-pure water;
Ethanol (70%, RNase free)	70 mL EtOH in 33.31 mL ultra-pure water;
Growth medium (HEK 293GPG cells)	DMEM (1X) + GlutaMAX™ + 25 mM HEPES; 10% (v/v) FBS; Geneticin (50 mg/ml); Tetracycline (1mg/ml); Puromycin (10 mg/ml);

HCl (4M)	33.3% (v/v) 12 M HCl in ultra-pure water;
Imaging buffer	0.7 M N-acetyl-cysteine in PBS; pH 7.4;
Kanamycin-LB media	50 mg/L Kanamycin in LB media;
LB media (1 L)	10 g peptone; 5 g yeast extract; 10 g NaCl;
Lower buffer	1.5 M Tris-HCl; 0.4% (m/v) SDS; pH 8.8;
NaOH (10M)	0.39 g/L NaOH in ultra-pure water;
NaOH (50mM)	1.97 g/L NaOH in ultra-pure water;
P19 medium	DMEM (1X) + GlutaMAX™ + 25 mM HEPES; 10% (v/v) FBS; 1% (v/v) penicillin/streptomycin; 1% (v/v) non-essential amino acids;
PBS-T	1x PBS with 0.5% (v/v) Tween20;
PDL solution	1 mg/mL PDL in ultra-pure water;
RIPA buffer	10 mM Tris-HCl, pH 8.0; 1 mM EDTA; 0.5 mM EGTA; 1% (v/v) Triton-X; 0.1% sodium deoxycholate; 0.1% (m/v) SDS; 140 mM NaCl;
SDS running buffer	25 mM Tris-HCl; 192 mM glycine; 1% SDS;
SOC media	2.5 mM KCl; 10 mM $MgCl_2$; 20 mM glucose; in LB media;
Sodium citrate buffer	10 mM sodium citrate; 0.05% (v/v) Tween 20; pH 6.0;
Streptomycin-LB media	33 mg/L Streptomycinsulfat in LB media;
TBS5 buffer	Tris-HCl, pH 7.8; 5 M NaCl; 1 M KCl; 1 M $MgCl_2$;
TE buffer	1 mM EDTA, pH 8.0; 10 mM Tris-HCl, pH 8.0;
Transfection medium (HEK 293GPG cells)	DMEM (1x); GlutaMAX™; 25 mM HEPES;
Tris-HCl (40mM) pH 5.5	4.84 g/L Tris-base in ultra-pure water;
Triton-X (0.01%)	1x PBS; 0.01% (v/v) Triton-X100; pH 7.1;
Upper buffer	0.5 M Tris-HCl; 0.4% (m/v) SDS; pH 6.8;

Table 4: List of chemicals

Chemical	**Company**
Acetic acid	Carl Roth®

Agarose powder	Biomol
Albumin bovine fraction	Serva
Cycloheximide	Carl Roth®
DMEM (1X) + GlutaMAX™ (4,5 g/L D-glucose) + 25mM HEPES; Gibco™	Thermo Fisher Scientific™
EDTA disodium salt	Carl Roth®
Ethanol	Sigma-Aldrich®
Ethylene Glycol	Carl Roth®
Geneticin	Thermo Fisher Scientific™
GenJet™ Plus DNA transfection reagent	SignaGen Laboratories
Glycine	Carl Roth®
Guanidinium hydrochloride	Merck KGaA/Sigma Aldrich
HCl (37%; 12M)	Carl Roth®
KCl	Carl Roth®
KH_2PO4	Carl Roth®
$MgCl_2$	Carl Roth®
Na_2HPO4	Carl Roth®
N-acetyl-cysteine	Sigma-Aldrich®
NaCl	Carl Roth®
NaOH	Carl Roth®
PDL	Sigma-Aldrich®
Puromycin; Gibco™	Thermo Fisher Scientific™
SDS	Carl Roth®
Sodium deoxycholate	Carl Roth®
Sucrose	Merck KGaA/Sigma Aldrich
Tetracycline	Sigma-Aldrich®
Tris base	Carl Roth®
Tris(2-chlorehyl)phosphat (TCEP)-HCl	Sigma-Aldrich®
Tri-sodium citrate dihydrate	Carl Roth®
Triton-X	Carl Roth®
Tween 20	Sigma-Aldrich®
Urea	Carl Roth®

Water (RNase free)	Sigma-Aldrich®
β-mercaptoethanol	Sigma-Aldrich®

Table 5: List of expendable materials

Expendable material	**Company**
1,5 mL tube	Starlab international GmbH
100/20 mm cell culture dish	CELLSTAR® Greiner Bio One
15 mL tube	CELLSTAR® Greiner Bio One
24 well plate	CELLSTAR® Greiner Bio One
24 well plate (glass bottom)	CELLSTAR® Greiner Bio One
35/10 mm cell culture dish	CELLSTAR® Greiner Bio One
50 mL tube	CELLSTAR® Greiner Bio One
Cover glass	Marienfeld Superior
FastPrep 24 tubes (Lysis Matrix D)	MP Biomedicals™
Glass Replacement 1.14MM 3.5"	World Precision Instruments
Immerge pen	Vector Laboratories
Injection syringe	Omnican® Carl Roth®
Microscopy slides	Thermo Fisher Scientific™ / Epredia
Mould	Polysciences Inc.
Nanoliter2020 Injector	World Precision Instruments
Needle (blue)	Sterican® Carl Roth®
Needle (brown)	Sterican® Carl Roth®
Nitrocellulose membrane	Amersham™
Nunc EasYFlaskTM 175 cm^2	Thermo Fisher Scientific™
PCR tubes	Starlab international GmbH
Polypropylene centrifuge tubes	Beckman Coulter
PVDF syringe filter 0.45 µm	Starlab international GmbH
Syringe	Sterican® Carl Roth®
Ultracentrifuge tube	Beckman Coulter

Table 6: List of kits and consumables

Kit and Consumable	Company
0.5% Trypsin/EDTA solution (10X); Gibco™	Thermo Fisher Scientific™
1kb DNA ladder	Serva
ACD-RNAscope Kit	Bio-Techne®
Aqua-Poli-Mount	Polysciences Inc.
BLOCK-iT™ Pol II miR RNAi Expression Vector Kit with EmGFP	Thermo Fisher Scientific™
DPBS (1X) [-] Calcium, [-] Magnesium; Gibco™	Thermo Fisher Scientific™
Extract-N-Amp™ PCR ReadyMix™	Sigma-Aldrich®
FBS	Thermo Fisher Scientific™
Gateway™ BP Clonase™ II Enzyme-Mix	Thermo Fisher Scientific™
Gateway™ LR Clonase™ II Enzyme-Mix	Thermo Fisher Scientific™
Gel Loading Dye Purple (6x)	New England BioLabs®
Tissue-PCR-Kit Extract-N-Amp™	Sigma-Aldrich®
HEPES Buffer Solution (1M); Gibco™	Thermo Fisher Scientific™
LB-ampicillin plates	Self-made
LB-kanamycin plates	Self-made
LB-streptomycin plates	Self-made
Miniprep Kit	Qiagen
Non-Essential Amino Acids; Gibco™	Thermo Fisher Scientific™
OCT mounting medium	Tissue-Tek®
Penicillin/Streptomycin; Gibco™	Thermo Fisher Scientific™
Triple Color Protein-Standard III	Serva

Table 7: List of instruments and equipment

Instrument/Equipment	Company
300 Volt Power Supply	Peqlab
4-channel peristaltic pump	Gilson
5417 R centrifuge	Eppendorf™
Axio Observer.Z1 inverted microscope	Carl Zeiss
Epredia™ CryoStar™ NX70 Kryostat	Thermo Fisher Scientific™
FastPrep-24 5G Instrument	MP Biomedicals™
Galaxy 170S CO2 Incubator	New Brunswick/Eppendorf™
Gel Doc System	Peqlab
GFL 1003 Wasserbad	Gemini Lab
Horizontal Midi Gel Systems	Peqlab
HybEZ Hybridization Oven	Advanced Cell Diagnostics
Innova®44 Incubator Shaker Series	Orbital Shakers
Innova™ 44 Incubator	New Brunswick/Eppendorf™
KS 260 basic (orbital shaker)	IKA
Mini-PROTEAN® Tetra System	Bio-Rad
Nanodrop 2000c	Thermo Fisher Scientific™
Odyssey CLx	Li-Cor
Optima ™ XPN-80 ultracentrifuge	Beckman Coulter
Piston Gradient Fractionator	BIOCOMP
PowerPac Basic	Bio-Rad
S1000 Thermo Cycler	Bio-Rad
Steam Device	Braun
Stereotaxic Instrument	Kopf®
TCS SP8 confocal microscope	Leica
ThermoMixer® C	Eppendorf™

Table 8: List of mouse strains

Strain	Background	Nomenclature
Pum2 GT	C57BL6/J	B6;129P2-Pum2Gt(XE772)Byg
WT	C57BL6/J	-

Table 9: List of plasmids

Construct	Vector	miRNA Sequence
attB1-EmGFP-miRNA(empty)-attB2	pcDNA™ 6.2-GW/EmGFP-miR	-
attP1-ccdB-CM^R-attP2	Gateway™pDONR™221	-
CAG-attR1-Cm^R-ccdB-attR2	RV-CAG-Dest.	-
CAG-GFP-miRNA(Pum2) – Oligo1	CAG-GFP	5’-AGAAGGAGGAAAGAGCTGGCT-3’
CAG-GFP-miRNA(Pum2) – Oligo3	CAG-GFP	5’-TTAACTGGATGGAAGTGCCAC-3’
CAG-GFP-miRNA(Scrambled)	CAG-GFP	5’-AAATGTACTGCGCGTGGAGAC-3’

Table 10: List of Oligonucleotides

Oligonucleotide	Oligonucleotide sequence
miRNA forward 1	5’-GCTGAGAAGGAGGAAAGAGCTGGCTGTTTTGGCCACTGACTGACAGCCAGCTTTCCTCCTTCT-3’
miRNA forward 2	5’-TGCTGTTAACTGGATGGAAGTGCCACGTTTTGGCCACTGACTGACGTGGCACTCATCCAGTTAA-3’
miRNA reverse 1	5’-CCTGAGAAGGAGGAAAGCTGGCTGTCAGTCAGTGGCC

	AAAACAGCCAGCTCTTTCCTCCTTCTC-3’
miRNA reverse 2	5’-CCTGTTAACTGGATGAGTGCCACGTCAGTCAGTGGCCA AAACGTGGCACTTCCATCCAGTTAAC-3’
Pum2 forward primer	5’-AAATGGCACCCATCATTGTT-3’
Pum2 reverse primer 1 (WT)	5’-CCGTTGTCTGCAGTGTCTGT-3’
Pum2 reverse primer 2 (GT)	5’-ACCAGCGTTTCTGGGTGA-3’

Table 10: List of RNAscope probes

Probe	**Channel**	**Catalogue Number**	**Company**
Aldoc	C3	429531-C3	Bio-Techne®
Nrgn	C1	499441	Bio-Techne®
Tmsb4x	C2	472851-C2	Bio-Techne®

2.2 Methods

2.2.1 Genotyping of Pum2 mice

$Pum2^{GT/GT}$ and $Pum2^{WT/WT}$ mice were genotyped via PCR to confirm their genetic modification status. The DNA from ear biopsies, obtained by animal caretakers, was extracted by adding a mix of 60µL Extract-N-Amp Tissue mix and 20µL of Tissue Prep solution from the Tissue-PCR-Kit Extract-N-Amp™. The samples were incubated for 4h at 55°C. The reaction was stopped at 95°C for 4min. 60µL of neutralization solution was added. A PCR master mix was prepared containing 10 µL Extract-N-Amp™ PCR ReadyMix™, 1 µL of each Pum2 primer (Pum2 forward primer, Pum2 reverse primer 1, Pum2 reverse primer 2), and 3 µL of RNase-free water. 16 µL of master mix was dispensed into individual PCR tubes for each biopsy, along with positive (heterozygous) and negative (water) controls. 4 µL of neutralised biopsy lysate was added to each corresponding tube and mixed briefly by vortexing. PCR amplification was performed in a thermocycler using the following program:

Step	Temperature	Time	Repeat
1	94°C	180s	
2	94°C	30s	
3	60°C	30s	30 cycles
4	72°C	80s	
5	72°C	120s	
6	4°C	∞	

Following PCR amplification, 4 µL of 6x gel loading dye was added to each sample and mixed by gentle vortexing. 10 µL of each prepared sample was loaded into individual wells of a 1.5% agarose gel; a 1kb DNA ladder was loaded into the first well for size comparison. Electrophoresis was performed in 1x TAE buffer at 150V for 30 min. The gel was then imaged using the gel doc system. Successful amplification was indicated by the following band patterns: $Pum2^{WT/WT}$ mice exhibited a band at 460 bp, $Pum2^{GT/GT}$ mice exhibited a band at 280 bp, and $Pum2^{WT/GT}$ mice exhibited both bands (460 bp and 280 bp).

2.2.2 Production of miRNA plasmids

Oligonucleotides encoding the desired miRNA were hybridised. Each dimerization reaction contained 5 µL of each corresponding oligonucleotide (200 µM), 2 µL 10x annealing buffer (BLOCK-iT™ Pol II miR RNAi Expression Vector Kit with EmGFP),

and 8 µL RNase-free water. The mixture was heated up to 95°C for 4 min, cooled down to room temperature (RT) for 10 min, then briefly vortexed and centrifuged. Hybridised oligonucleotides were diluted to 500 nM and subsequently to 10 nM in annealing buffer and RNase-free water. 10 nM hybridised oligonucleotides were ligated into linearised pcDNA™ 6.2-GW/EmGFP-miR vector (5 ng/µL) using a mixture of 4 µL 5x ligation buffer, 9 µL RNase-free water, and 1 µL T4 DNA ligase (BLOCK-iT™ Pol II miR RNAi Expression Vector Kit with EmGFP). Ligation proceeded for 1 h at RT. 2 µL of the ligation product was transformed into XL1-Blue competent cells via heat shock. Transformed cells were cultured overnight at 37°C on LB-streptomycin plates, and three colonies were selected per plate. The plasmids were isolated from overnight bacterial cultures using a miniprep kit from Qiagen and quantified using a NanoDrop spectrometer. Sanger sequencing by Eurofins Genomics confirmed successful miRNA integration. A Gateway™ BP Clonase™ II Enzyme Mix was used to clone the GFP-miRNA sequence from the pcDNA™ 6.2-GW/EmGFP-miR vector into the Gateway™pDONR™221 vector. The reaction contained 75 ng of each vector, 1 µL TE buffer, and 1 µL BP clonase, incubated for 1 h at 25°C. Proteinase K treatment inactivated the clonase. The plasmids were transformed into Top10 bacteria via heat shock, selected on LB-kanamycin plates, isolated using the miniprep kit, quantified by NanoDrop, and sequence-verified by Eurofins Genomics. The GFP-miRNA sequence was transferred from Gateway™pDONR™221 to the RV-CAG-Dest vector using Gateway™ LR Clonase™ II Enzyme Mix. The reaction setup was identical to the Gateway™pDONRTM221 cloning step as described above. Plasmids were transformed into Top10 bacteria via heat shock, selected on LB-ampicillin plates, isolated using the miniprep kit, quantified with NanoDrop, and sequence-verified by Eurofins Genomics.

2.2.3 Retrovirus production

Retroviral particles encoding miRNAs targeting Pum2 and a control miRNA were produced in HEK 293GPG cells (obtained from the Magdalena Götz laboratory at the BMC). Cells were seeded in 10cm plates at $6x10^6$ cells/plate and cultured in selective growth medium. After two days, the medium was replaced with prewarmed 0-medium, and cells were incubated at 37°C with 5% CO_2 for 2 h. Transfection was performed using the GenJet™ Plus DNA Transfection Reagent. Briefly, in separate 9 mL volumes of transfection medium, 180 µL GenJet™ and 120 µg of the respective plasmid were

added and gently mixed. After incubation at RT for 15 min, the transfection mixture was added dropwise to HEK 293GPG cells. Medium changes with fresh 0-medium were performed at one- and four days post-transfection (DPT). Virus-containing medium was collected at six, eight, and eleven DPT, filtered (0.45 µm PVDF filter), and concentrated by ultracentrifugation (27,000 rpm, 2 h, 4°C). The virus pellet was resuspended overnight in TBS5 buffer at 4°C and then stored at -80°C. The viral titre was determined in collaboration with Paulina Chlebik and Martina Bürkle (Magdalena Götz laboratory) using a P6 mouse astrocyte culture.

2.2.4 Stereotactic injection

Stereotactic injections were performed together with Dr. Gregor Pilz. Mice were anesthetised with MMF (0.05mg/kg Medetomin, 5mg/kg Midazolam, 0.05mg/kg Fentanyl) through intraperitoneal injection and kept on a heating pad under aseptic conditions. Reflexes were monitored to check the anaesthesia depth. An eye gel was applied on the eyes to prevent the drying-out. Once anesthetised, mice were secured in a stereotactic apparatus. An incision exposed the skull, which was washed with saline. A small cranial window was created via trepanation over the DG (coordinates: 2mm posterior to bregma, 1.6mm lateral to midline). A fine glass capillary loaded with retroviral suspension (500 nL retrovirus, 4 ng/mL Fast Green FCF) was slowly inserted 2mm into the brain. The suspension was injected at a rate of 50 nL/min. Following injection, the capillary was removed, and the incision was sutured. Anaesthesia was antagonised with a subcutaneous injection of Atipamezole (2.5mg/kg), Flumazenil (0.5mg/kg), and Buprenorphine (0.1mg/kg). Post-operative analgesia included oral application of Meloxicam (5mg/kg) two times a day for three consecutive days. Mice were housed in groups of four based on viral treatment and perfused three weeks post-injection.

2.2.5 BrdU treatment of mice

This experiment was primarily conducted by Christin Illig. Mice at the age of 8 weeks, including both $Pum2^{WT/WT}$ and $Pum2^{GT/GT}$ genotypes, were given BrdU (50 mg/mL) with 5% sucrose in their drinking water for two weeks to label proliferating cells during early stages of the neurogenesis lineage. To examine later stages of the lineage, BrdU-supplemented water was replaced with normal drinking water for an additional two weeks. At the end of the two-week period for early stage and four week period for late stage, mice were sacrificed and perfused.

2.2.6 BrdU treatment of mice with voluntary physical activity

This experiment was primarily conducted by Christin Illig. Mice at the age of 8 weeks, including both Pum2WT/WT and Pum2GT/GT genotypes, were used in this study. To label proliferating cells during early stages of the neurogenesis lineage, drinking water was supplemented with BrdU (50 mg/mL) and 5% sucrose for two weeks. During this period, mice were also provided with voluntary access to a running wheel to explore the effects of physical activity. To examine later stages of the lineage, BrdU-supplemented water was replaced with normal drinking water, and the running wheels were removed for additional two weeks. At the end of the two-week period for early stage and four-week period for late stage, mice were sacrificed and perfused.

2.2.7 Transcardial perfusion of mice

Mice were deeply anesthetised via an intraperitoneal injection of MMF (0.05mg/kg Medetomin, 5mg/kg Midazolam, 0.05mg/kg Fentanyl) and monitored for the absence of reflexes before proceeding. Following fixation to a dissection board, transcranial perfusion was initiated by inserting a needle into the left ventricle. Mice were transcardial perfused first with 1x PBS for 20 min, followed by 4% PFA solution for an additional 20 min. After perfusion, brains were carefully extracted and post-fixed in 4% PFA overnight at 4°C. Brains were then cryoprotected by sequential overnight incubations in 10% sucrose followed by 30% sucrose until tissue sank. Sucrose-infiltrated brains were embedded in OCT mounting medium, frozen using a dry ice/ethanol bath, and stored at -80°C until ready for cryosectioning.

2.2.8 Cryosectioning of mouse brains

Brains embedded in OCT mounting medium were trimmed, attached to cryostat specimen plates using additional OCT, and positioned within the cryostat chamber. Brains were sectioned coronally through the entire hippocampus. Sections were collected at either 40 µm thickness for immunostaining or 10 µm thickness for RNAscope. During sectioning, slices were either directly mounted onto microscopy slides and stored at -80°C or collected in 1x PBS and subsequently transferred to a cryoprotection solution for storage at -20°C.

2.2.9 Immunostaining of mouse brain sections

Free-floating brain sections were washed 3 times for 10 min with 1x PBS at RT. For antigen retrieval, sections were treated with 4M HCl for 15 min, followed by three 10-

min washes with 0.1M borate buffer at RT. Sections were then washed twice with 1x PBS for 10 min each at RT and blocked with immunostaining blocking solution for 2 h at RT to minimize non-specific antibody binding. Sections were incubated overnight at 4°C with diluted primary antibodies in blocking solution. The following day, sections were washed three washes with 1x PBS at RT and were incubated for 2 h at RT with secondary antibodies diluted in blocking solution. After a 5 min DAPI incubation, sections were washed three times with 1x PBS for 10 min each at RT. Finally, sections were mounted onto microscopy slides with Aqua-Poly-Mount and stored at RT until imaging.

2.2.10 Consecutive immunostaining of mouse brain sections

Free-floating brain sections were washed 3x in 1x PBS for 10 min each at RT followed by antigen retrieval in citrate buffer for 1 h at ≥99°C in a humidified chamber. Sections were then adhered to PDL-coated glass-bottom 24-well plates and dried (until transparent) for approximately 20 min. After 3x washes with 1x PBS, sections were blocked for 2 h with an immunostaining blocking solution at RT. Sections were incubated for 5 days in blocking solution containing primary antibodies at 4°C. Following three PBS washes at RT, sections were incubated with blocking solution and secondary antibodies for 2 days at 4°C. After three short washes with 1xPBS, sections were incubated with DAPI for 5 min, washed again 3x with 1xPBS, and imaged in imaging buffer. Post-imaging, antibodies were eluted with a 1:1 mixture of elution buffer and ultra-pure water for 3x 5 min washes at RT. Sections were washed again 3x with 1x PBS at RT, and the immunostaining procedure was repeated using the indicated set of primary/secondary antibodies.

2.2.11 RNA detection on mouse brain slices using RNAscope

Frozen brain sections mounted on slides were thawed and air-dried for 45 min at RT, followed by brief PBS washes. Slides were baked at 60°C for 30 min and post-fixed with 4% PFA for 15 min at 4°C. Sections were dehydrated with an ethanol series from 50%, 70% and 2x 100% for 5 min each at RT, air-dried, and treated with hydrogen peroxide for 10 min at RT. After PBS washes, sections underwent antigen retrieval in preheated retrieval buffer at ≥99°C for 5 min and were immediately washed with ultra-pure water. Slides were dehydrated with 100% ethanol and air-dried for 20 min at RT. A hydrophobic barrier was created around each section using the immerge pen. Sections were treated with Protease III at 40°C for 20 min in a humidified chamber and

washed with ultra-pure water. Probes against Nrgn/Tmsb4x and Aldoc (ACD-BIO) were mixed and hybridised at 40°C for 2 h in a humidified chamber. Slides underwent multiple washes with preheated wash buffer before sequential signal amplification using AMP1, AMP2, and AMP3 at 40°C for 30 min each in a humidified chamber with washes between amplification steps. HRP-C1 was applied at 40°C for 15 min in a humidified chamber followed by Vivid 520 fluorophore development (1:1500 in TSA buffer) at 40°C for 30 min in a humidified chamber. HRP-C1 was inactivated with HRP blocker at 40°C for 15 min in a humidified chamber. This process was repeated with HRP-C2 (Vivid 570) and HRP-C3 (Vivid 650). Slides were washed in PBS and counterstained with DAPI for 1 min at RT. Sections were mounted with Aqua-Poly-Mount and stored overnight at 4°C before imaging.

2.2.12 P19 mouse cell line culture

P19 cells, obtained from the laboratory of Magdalena Götz, were thawed at 37°C and seeded in 10 mL prewarmed P19 medium in a 10 cm plate. Cells were incubated at 37°C with 5% CO_2 for one day. For routine passaging, cells were washed with prewarmed DPBS, briefly treated with 3 mL trypsin at 37°C for 3 min, followed by resuspended in P19 medium. Cells were split 1:1 after one day and 1:10 after additional two days in culture. For experiments, P19 cells were seeded at a 1:50 dilution in 2 mL prewarmed P19 medium in a live-cell imaging plate and incubated for half a day at 37°C with 5% CO_2. Cells were then either transiently transfected using the calcium phosphate method (Goetze et al., 2004) or transduced with 10 µL retrovirus that was added to the P19 medium. Following a one day incubation, the medium was replaced with fresh prewarmed P19 medium. Cells were cultured for an additional two days, with a medium change after one day. On the final day, cells were washed with prewarmed DPBS and fixed with 4% PFA for 15 min at RT.

2.2.13 Immunostaining of P19 mouse cell line

Fixed P19 cells were washed three times with 1x DPBS and permeabilised with 0.1% Triton-X in DPBS for 5 min at RT. After further washes 3x for 10 min in 1x DPBS, cells were blocked with an appropriate blocking serum for 2 h at RT. Primary antibody incubation was performed overnight at 4°C in blocking serum. The following day, cells were quickly washed three times with 1x DPBS and incubated with secondary antibodies diluted in blocking serum for 2 h at RT. Cells were counterstained with DAPI for 5 min, washed 3x for 10 min with 1x DPBS, and stored in 1x DPBS until imaging.

2.2.14 Fluorescence microscopy and image processing

Fluorescence imaging of immunostained P19 cell cultures was performed using a Zeiss Axio Observer.Z1 inverted phase-contrast fluorescence microscope. Stained mouse brain sections were imaged using a Leica TCS SP8 confocal microscope.

2.2.14.1 Widefield fluorescence microscopy

Fluorescence images of fixed P19 cells were acquired using a Zeiss Axio Observer.Z1 inverted microscope equipped with a Plan-Apochromat 63x/1.40 Ph3 M27 oil immersion objective, COLIBRI.2 LED light source, and Axiocam 506 mono camera. Image acquisition was controlled using ZEN 2.6 pro (blue edition, Zeiss) software. GFP-positive cells were imaged using excitation wavelengths of 385nm, 470nm, and 625nm, with exposure times ranging from 50ms to 300ms depending on laser intensity. Raw images were analysed using ZEN 3.2 (blue edition, Zeiss). For presentation purposes, images were minimally adjusted for intensity, brightness, contrast, and magnification. No other image processing was applied.

2.2.14.2 Confocal fluorescence microscopy

Confocal images of fixed mouse brain sections were acquired using a Leica TCS SP8 microscope, focusing on the DG subregion of the hippocampus. Excitation wavelengths included 405nm, 488nm, 552nm, and 638nm. Acquisition gain was set at 800V for the 405nm laser and 50V for the remaining lasers. Scan speed ranged from 200Hz to 600Hz with a 63x objective. Raw images were analysed using Arivis Vision 4D (Version 3.5) or ImageJ (Version 1.53f51). Images used for presentation were minimally adjusted for intensity, brightness, contrast, magnification, and Z-projection. Scale bars are included in the figures.

2.2.15 Analysis of imaging data

2.2.15.1 Endogenous expression and knockdown of Pum2 in P19 cell line

Widefield fluorescence microscopy images were acquired to assess Pum2 knockdown efficiency in the P19 cell line expressing miRNA targeting Pum2. Images included phase contrast and channels corresponding to DAPI, EGFP, and Alexa647 spectra. Analysis was performed using Zeiss Zen 3.5 (blue edition) software, focusing exclusively on EGFP-positive cells. The soma of each EGFP-positive cell was manually outlined (excluding the nucleus). For background correction, a nearby cell-

free region was selected for each measured cell. Cells with overlapping fluorescence signals were excluded from the analysis.

2.2.15.2 Analysis of the proliferation rate in the DG

To assess hippocampal proliferation rates in mice with and without physical activity, BrdU labelling was employed. Confocal fluorescence microscopy was used to acquire tiled images using emission spectra corresponding to DAPI, Alexa555/Cy3, and Alexa647/Cy5. Tiles were stitched together to generate complete images. Image analysis was performed using Arivis Vision 4D (Version 3.5). A 3D model of the DG was generated based on the DAPI signal and used to mask out surrounding regions. BrdU-positive signals were quantified and analysed in relation to DG volume or localization within the DG. Results were subjected to statistical analysis.

2.2.15.3 Analysis of the proliferating, cycling, neurons and glia cells

To investigate the cellular composition of proliferating cells in both normal and physically active mice, BrdU labelling was combined with immunostaining for the following cell type-specific markers:

- Ki67: marker for actively cycling cells
- NeuN: marker for mature neurons (MNs)
- Dcx: marker for immature neurons (INs)
- Tbr2: marker for intermediate progenitor cells (IPCs)
- Hopx: marker for radial glia cells (RGCs)
- Sox9: marker for (mature) astrocytes (MAs)

Following the previously described procedures, images were analysed with a focus on quantifying not only BrdU-positive cells but also cells co-labelled with BrdU and specific cell type markers. The ratio of BrdU-positive cells expressing a given marker to the absolute number of BrdU-positive cells was calculated, followed by statistical analysis.

2.2.15.4 Transient state cell on RNA level

Confocal fluorescence microscopy images were acquired for RNAscope analysis. Using a HC PL APO 63x objective, a single tile image was captured within the inner region of the DG, just before the two blades converge. Image acquisition included emission spectra corresponding to DAPI, Vivid 520, Vivid 570, and Vivid 650 dyes. RNAscope targets included:

- Nrgn: Developing neuronal gene
- Tmsb4x: Progenitor/Immature neuronal gene
- Aldoc: Glia gene

Nuclei within a single image plane were used as reference points to identify individual cells. Cells exhibiting co-localization of all three target genes, detected by RNAscope, within their immediate surrounding of the DAPI staining were classified as transient state cells (TSC). Additionally, the location of TSCs was categorised as either the subgranular zone (first two cell layers) or the granular cell layer (remaining cell layers). The ratio of transient state cells to total nuclei was calculated, followed by statistical analysis.

2.2.15.5 Number and morphological analysis of transient state cells

To investigate transient state cells in the DG of $Pum2^{WT/WT}$ and $Pum2^{GT/GT}$ mice, immunostaining, and confocal fluorescence microscopy (as previously described) were employed. The analysis focused on the following aspects:

- **Cell Count:** Transient state cells co-expressing Ckb and Tmsb4x were quantified, providing a comparative measure of population density between the two mouse genotypes.
- **Dendrite Length:** The length of dendrites exhibiting co-localization of Ckb and Tmsb4x signals was measured.
- **Dendritic Extension:** The proportion of dendrites extending into the molecular layer was determined.
- **Cell Body Morphology:** Cell body shapes were carefully observed for insight into overall cell morphology.

2.2.16 Dissection and protein sample preparation of the hippocampus

$Pum2^{WT/WT}$ and $Pum2^{GT/GT}$ genotypes were sacrificed via cervical dislocation. The skull was carefully opened, and the brain was removed and immediately placed in cold HBSS. Hemispheres were separated, and the brain stem, cerebellum, diencephalon, and meninges were removed. The hippocampus was carefully dissected using a fine needle (blue), avoiding the white matter according to established protocol (Hagihara et al., 2009). Hippocampi from a single mouse were pooled in an ultra-vortexing tube containing 200µL RIPA buffer. Samples were ultra-vortexed (6m/s, 60s) and

transferred to a 1.5 mL tube. 100µL of 6x SDS buffer was added, and samples were boiled for 5 min at 95°C. Lysates were stored at 4°C.

2.2.17 SDS-Page and Western Blot

Prior to loading, protein samples (in 6x SDS buffer) were boiled for 5 min at 95°C. 10 µL of each sample and 5 µL of protein ladder were loaded onto a 12% SDS gel and run at 100V for 90 min in SDS running buffer. Proteins were transferred to a nitrocellulose membrane using blotting buffer and constant current (100mA) for 90 min. The membrane was blocked with blocking solution (2 h, RT, 100 rpm) and incubated overnight at 4°C (100 rpm) with primary antibodies diluted in blocking solution. The following day, membranes were washed 3x with PBS-T for 10 min and incubated with secondary antibodies in blocking solution (1 h, RT, 100 rpm). After another 3x of 10 min PBS-T washes, membranes were imaged using a Li-Cor imager.

2.2.18 Polysome Profiling

$Pum2^{WT/WT}$ and $Pum2^{GT/GT}$ were perfused with PBS containing cycloheximide (2mg/mL cycloheximide in DMSO diluted 1:500 in PBS) to stall translation. Following PBS perfusion, brains were extracted, and the hippocampus was dissected as previously described, snap-frozen in liquid nitrogen, and stored at -80°C. Hippocampal tissue was lysed in 350 µL polysome lysis buffer and carefully pipetted up and down three times. Samples were homogenised using an injection needle and centrifuged (13,000 rpm, 5 min, 4°C). The supernatant was carefully layered onto a sucrose gradient (18-50%) within an ultracentrifuge tube. Samples were ultracentrifuged at 35,000 rpm for 1.5 h (4°C) with an SW55Ti rotor. Following centrifugation, samples were analysed using a polysome profiler. Analysis was performed in GraphPad. Monosome and polysome peaks were separated, the area under the curve was determined for each, and the ratio was calculated. Results were subjected to statistical analysis.

2.2.19 Statistical analysis

Data processing, visualisation, and statistical analysis were performed using the following software. Microsoft Excel was used for general data management, while GraphPad Prism 8 was used as tool for creating graphs and conducting statistical tests. Additionally, RStudio 4.2.0 was utilised for specific data processing tasks and comparing our gene lists to previously published data. The Shapiro-Wilk normality test was used to determine data distribution. For data analysis (excluding RNAscope and

transient state cell immunohistochemistry), results represent the average of three technical replicates per biological replicate (mouse). Statistical significance of differences between conditions was determined using the following tests, as appropriate:

- Student's t-test: Normal distributed data with similar standard deviation
- Welch´s t-test: Normal distributed data with unequal standard deviation
- Mann-Whitney test: Non-normal distributed data with similar standard deviation

Results with p-values <0.05 were considered statistically significant (*p < 0.05, **p < 0.01, ***p < 0.001, n.s. ≥ 0.05).

2.2.20 10x Illumina single-cell RNA sequencing

Single-cell RNA sequencing (scRNA-seq) was principally carried out by Dr. Christina Koupourtidou, assisted by Dr. Stefanie Ohlig, Sabine Thomas and myself. $Pum2^{WT/WT}$ and $Pum2^{GT/GT}$ mice were sacrificed via cervical dislocation. Following brain extraction, non-hippocampal regions (including the brain stem, diencephalon, and meninges) were removed. Hippocampal dissection, focusing on the DG, was performed according to established protocols (Hagihara et al., 2009). A single-cell suspension was generated from the dissected tissue. Cells were encapsulated in droplets and processed with a 10x sequencing chip for Illumina RNA sequencing. Raw sequencing results were formatted as matrices suitable for downstream analysis.

2.2.21 scRNA-seq data processing

Dr. Christina Koupourtidou performed initial scRNA-seq data preprocessing and established the Scanpy workflow. I conducted subsequent downstream analysis and bioinformatics. This preprocessing and downstream analysis was carried out in Python using JupyterLab and utilised the Scanpy toolkit (Wolf et al., 2018). The workflow was designed in accordance with the guidelines outlined by the Theis Lab (https://www.sc-best-practices.org/preamble.html).

2.2.22 Using text-based AI for language precision

In my dissertation I employed text-based AI programs, DeepL (DeepL Write, 2024) and Google Gemini (Google Gemini, 2024), to enhance the language presentation. The programs provided support with sentence restructuring, grammar correction, and suggestions for alternative wording. Importantly, it did so without generating de novo

text, altering the core content of the provided text or introducing its own conceptual ideas. I carefully reviewed and edited all generated suggestions to ensure they accurately reflected the intended arguments and were consistent with the existing research in the field and my findings.

3 Results

3.1 Shift towards astrogenic cell generation in the DG of Pum2 deficient mice

3.1.1 Ongoing proliferation of new cells with a decrease in the size of the DG in Pum2 deficiency

To begin exploring the role of Pum2 in adult neurogenesis, we were aiming to investigate the effect of the Pum2 deficiency on the proliferation rate in the DG. To investigate this, we employed a well-established BrdU labelling technique to track the proliferation and differentiation of RGCs and IPCs in the DG (Gratzner, 1982; Nowakowski et al., 1989). This approach allows for the identification of newly generated cells and their subsequent maturation into neurons or astrocytes. The role of Pum2 in adult neurogenesis was studied in young adult mice of 8 weeks as they have transitioned out of adolescence into adulthood with a relatively high neurogenesis rate in the DG. Mice were given the thymidine base analogue BrdU to drink for two weeks, allowing us to trace newly generated cells within the neurogenic niche up to the stage of INs. This experiment was performed by technical assistant Christin. Following perfusion and brain preparation for immunostaining (**Figure 3A**). Immunostaining for BrdU and cell nuclei with DAPI confirmed active cell division within the DG (**Figure 3B**). I evaluated the overall size of the DG by measuring its size and normalizing it against $Pum2^{WT/WT}$ mice. Surprisingly, my analysis revealed a statistically significant decrease in the size of the DG in $Pum2^{GT/GT}$ mice (**Figure 3C**). However, the density of BrdU-positive cells in the DG, as well as the per-section count (40µm), showed no statistically significant difference (**Figure 3D, E**). Even though this could vary between sections of the same brain. These results demonstrate that the experimental approach can effectively trace proliferation within the DG under both WT and Pum2-deficient conditions. Furthermore, the reduction in DG size suggests a potential role of Pum2 in controlling the cell number within the DG for example by controlling the cell cycle activity.

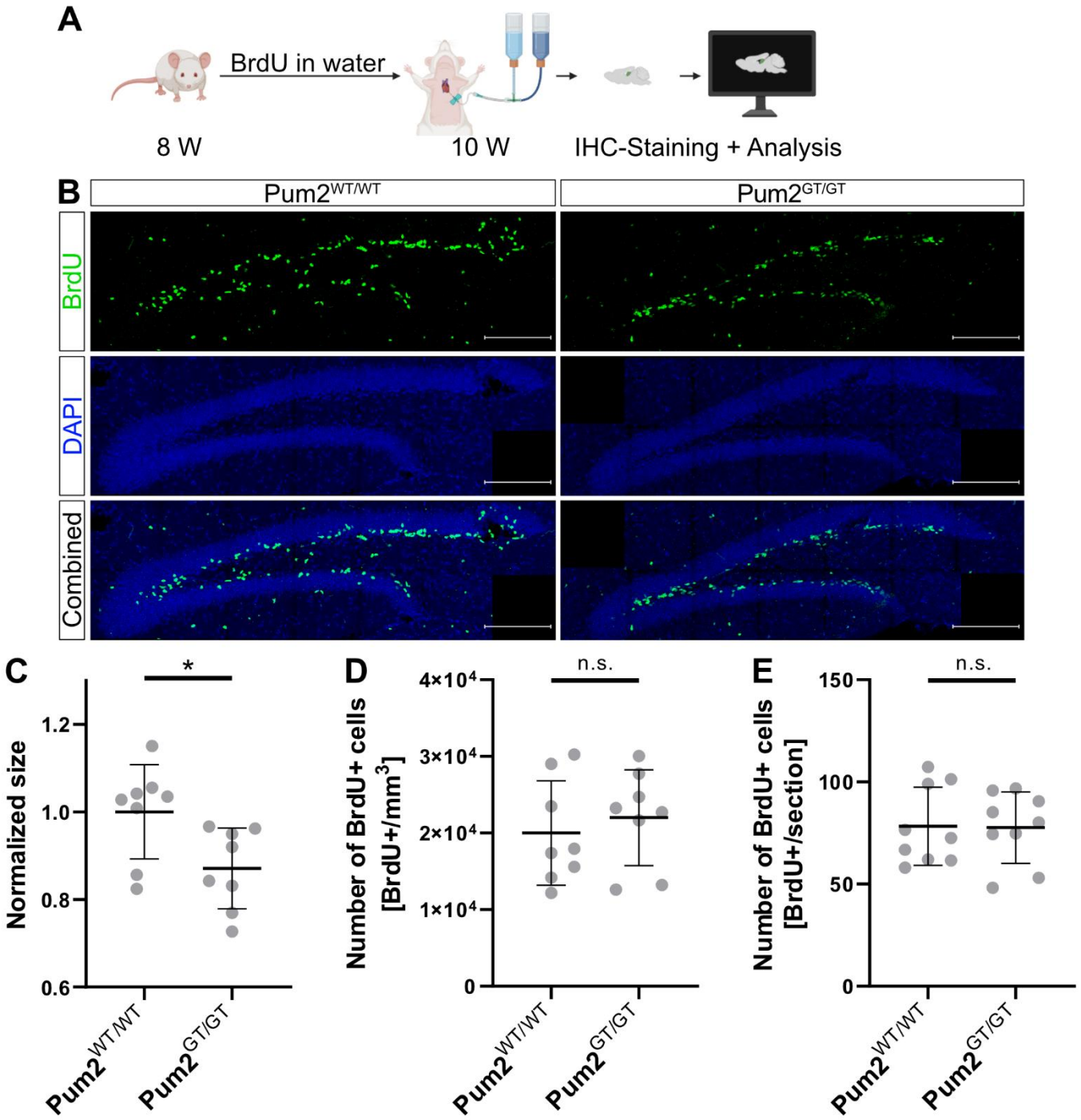

Figure 3: Pum2 deficiency reduces DG size despite stable cell proliferation. (**A**) Experimental outline of BrdU labelling of Pum2$^{WT/WT}$ and Pum2$^{GT/GT}$ mice over 2 weeks. Created with BioRender.com. Agreement number: WC2759Y4P4 (**B**) Representative Z-stack images of BrdU and DAPI immunostaining on sagittal DG sections (40µm thick) of Pum2$^{WT/WT}$ and Pum2$^{GT/GT}$ mice. Scale bars: 200µm. (**C**) Dot plot displaying the normalised DG size of Pum2$^{WT/WT}$ and Pum2$^{GT/GT}$ mice defined by the shape of the DAPI signal. (**D**) Dot plot displaying the number of BrdU-labelled cells relative to 1mm^3. (**E**) Dot plot displaying the number of BrdU-positive cells in sagittal DG sections (40µm thick). Mean and standard deviation are shown. Circles indicate independent biological replicates (n = 8, 9). Asterisks represent p-values obtained by (**C**) unpaired Welch's t-test and (**D, E**) unpaired Student's t-test (*p < 0.05, n.s. ≥ 0.05).

3.1.2 Pum2 deficiency leads to an increase of actively cycling cells

The initial results demonstrated a reduction in the size of the DG but no difference in newly proliferated cells that might be due to a role of Pum2 in controlling the cell cycle activity. To investigate deeper the potential role of Pum2 in cell cycle activity, we examined its impact on the cell cycle directly, using immunostaining techniques. We utilised sections obtained from the previously described experiment (**Figure 3A**) to perform a combined staining for Ki67 and BrdU, allowing us to compare $Pum2^{WT/WT}$ and $Pum2^{GT/GT}$ mice (**Figure 4A**). The combination of Ki67 and BrdU allows to address the newly proliferated cells that are in an active cell cycle. Importantly, Ki67 is a reliable marker that specifically identifies cells actively engaged in the cell cycle (Sun & Kaufman, 2018). My analysis revealed a statistically significant increase in the density of cells that were within the active cell cycle in $Pum2^{GT/GT}$ mice compared to their $Pum2^{WT/WT}$ counterparts (**Figure 4B**). This intriguing finding was further reinforced, when we specifically analysed those cells that were both actively cycling (Ki67 positive) and had incorporated BrdU compared to all BrdU incorporated cells. This approach allows us to focus on cells that are undergoing potentially multiple rounds of division during the BrdU uptake period. Again, a similar pattern emerged – a notable increase was observed in $Pum2^{GT/GT}$ mice (**Figure 4C**). These results, coupled with our earlier observation that Pum2 deficiency affects the size of the DG, strongly suggest that Pum2 might play an important role in regulating cell cycle dynamics. It appears that the absence of Pum2 leads to a higher proportion of cells actively engaged in cell cycle.

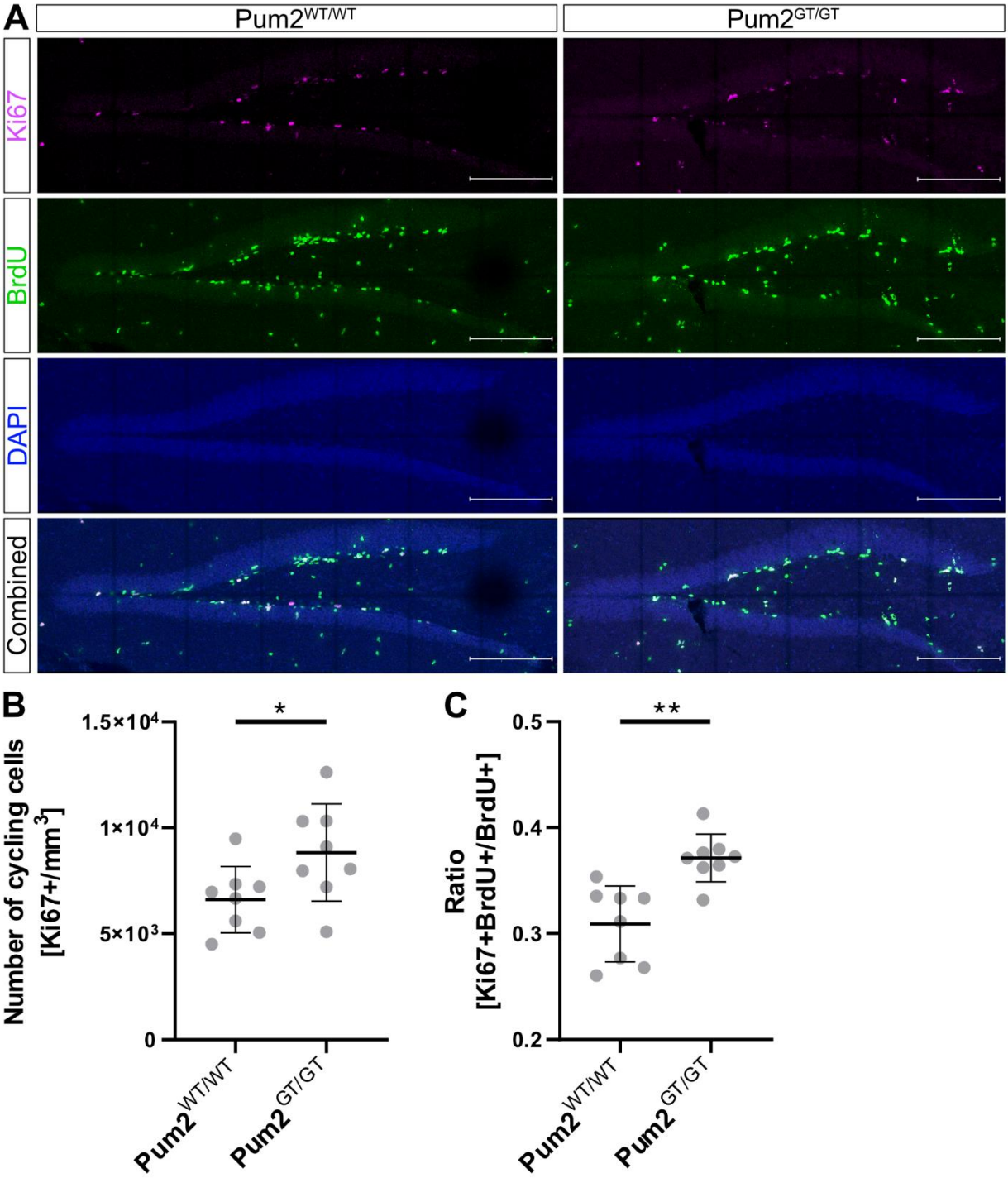

Figure 4: Pum2 deficiency increases the number of cycling cells. (**A**) Representative Z-stack images of Ki67, BrdU and DAPI immunostaining on sagittal DG sections (40µm thick) of $Pum2^{WT/WT}$ and $Pum2^{GT/GT}$ mice. Scale bars: 200µm. (**B**) Dot plot displaying the number of Ki67-labelled cells relative to $1mm^3$. (**C**) Dot plot displaying the ratio of Ki67- and BrdU-labelled cells relative to all BrdU-labelled cells. Mean and standard deviation are shown. Circles indicate independent biological replicates (n = 8). Asterisks represent p-values obtained by (**B, C**) unpaired Welch's t-test (**p < 0.01, *p < 0.05).

3.1.3 Pum2 deficiency leads to a decrease of newly generated INs

The initial findings of our study successfully validated the robustness and reliability of our experimental approach, paving the way for a more in-depth investigation into the proliferative capacity of cells within the DG. Having established this foundation, we turned our attention to elucidating the specific role of Pum2 in the intricate process of adult neurogenesis, focusing our analysis on the neuronal lineage within the DG. To begin to investigate the precise timepoint, when Pum2 acts in the process of adult neurogenesis, we carefully selected the cellular marker indicative for INs. INs were specifically stained with a microtubule-associated protein, Dcx, a protein whose expression is uniquely limited to this stage of neuronal development (Zhao et al., 2008). To visualise the marker, we utilised sections obtained from the previously described experiment for immunostaining (**Figure 3A**). The immunostaining incorporated the aforementioned marker together with BrdU, allowing us to assess any potential changes within the neurogenic lineage on the stage of INs (**Figure 5A**). Surprisingly, my analysis revealed no statistically significant changes in the cell density for Dcx-positive INs (**Figure 5B**). To further investigate the differentiation of newly proliferated cells into INs, we performed a quantitative analysis comparing the number of cells co-expressing the IN marker Dcx and the proliferation marker BrdU with the total number of BrdU-positive cells. This ratio provides a valuable metric for assessing the proportion of recently divided cells that have embarked on a neuronal differentiation pathway. A statistically significant decrease was observed in the proportion of newly proliferated INs relative to the overall population of newly generated cells (**Figure 5C**). These results strongly implicate a role of Pum2 in the regulation of neurogenesis at the stage of IN development or potentially even earlier. Notably, while Pum2 appears to be important for the rate of IN production, it does not seem to play a role in density of INs within the DG.

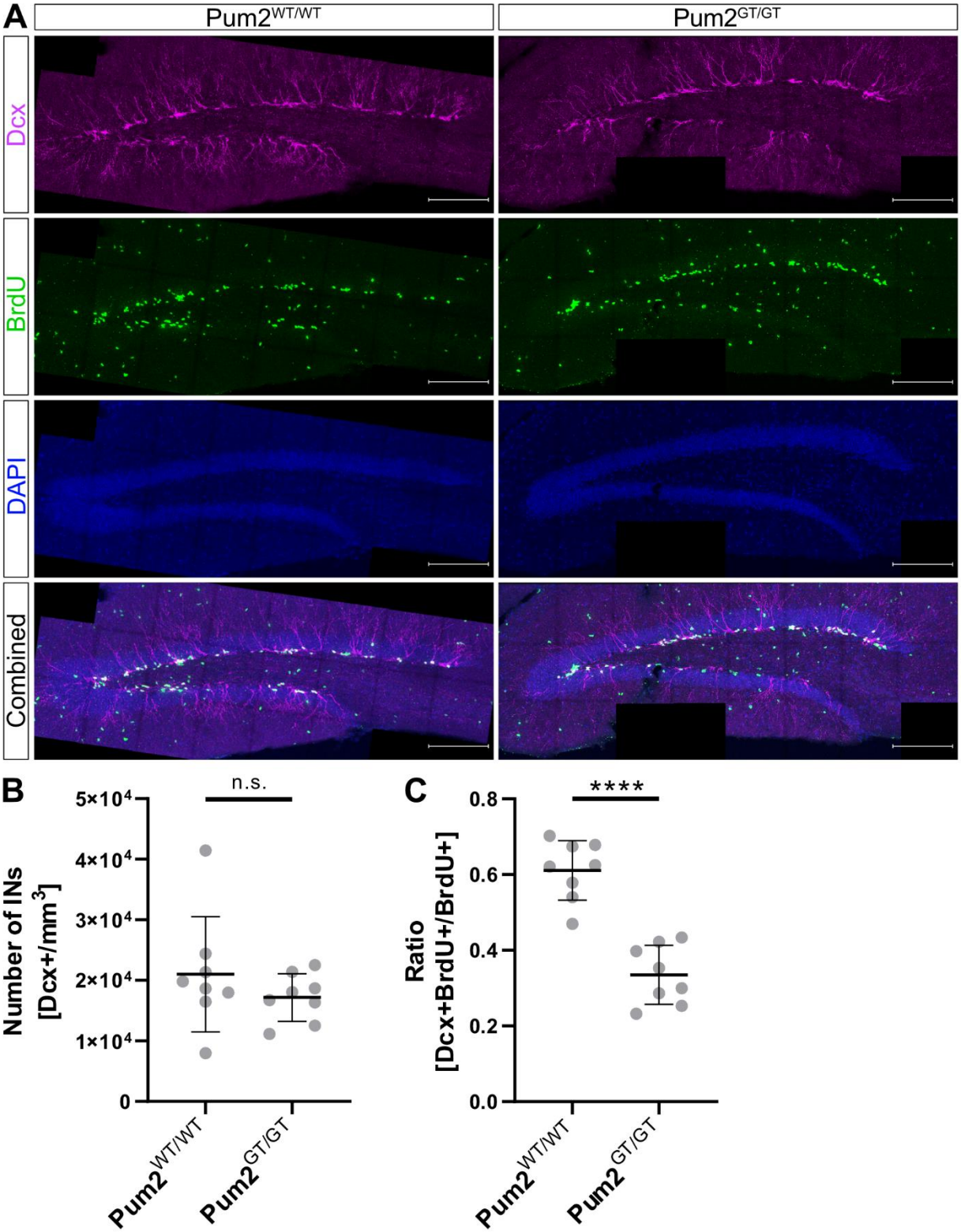

Figure 5: Pum2 deficiency decreases the generation of new immature neurons (INs). (**A**) Representative Z-stack images of Dcx, BrdU and DAPI immunostaining on sagittal DG sections (40µm thick) of $Pum2^{WT/WT}$ and $Pum2^{GT/GT}$ mice. Scale bars: 200µm. (**B**) Dot plot displaying the number of Dcx-labelled cells relative to $1mm^3$. (**C**) Dot plot displaying the ratio of Dcx- and BrdU-labelled cells relative to all BrdU-labelled cells. Mean and standard deviation are shown. Circles indicate independent biological replicates (n = 8). Asterisks represent p-values obtained by (**B, C**) unpaired Student's t-test (****$p < 0.0001$, n.s. ≥ 0.05).

3.1.4 Pum2 deficiency leads to a decrease of newly generated intermediate progenitor cells

The previous findings align with our initial hypothesis, solidifying the notion that Pum2 plays a pivotal role in adult neurogenesis. To further refine our understanding, we next sought to pinpoint the precise stage at which Pum2 exerts its influence in this complex process. To delineate the specific stage within adult neurogenesis where Pum2 exerts its effect, we rigorously investigated cellular markers characteristic of IPCs. We focused on Tbr2 staining, as this transcription factor serves as a critical regulator in early brain development and adult hippocampal lineage progression of IPCs (Hodge et al., 2012; Lv et al., 2019). Immunostaining of sections from our prior experiment (**Figure 3A**) was performed to visualise these markers. Specifically, we combined Tbr2 with BrdU, facilitating an assessment of potential alterations within the neurogenic lineage at the IPC stage (**Figure 6A**). Our analysis demonstrated no statistically significant difference in the overall density of Tbr2-positive IPCs (**Figure 6B**). However, by a similar analysis as previously described for INs, we observed a notable decrease in the proportion of newly proliferated IPCs relative to the total population of newly generated cells (**Figure 6C**). These findings strongly suggest that Pum2 plays a crucial role in the early stages of neurogenesis, potentially as early as the IPC stage. While Pum2 appears to be essential for the rate of IPC production, it does not seem to affect the overall density of IPCs within the DG. Taken together with our previous results, this evidence points to a potential disruption in the proliferation of cells within the neuronal lineage, rather than a change in the overall cellular composition of the DG.

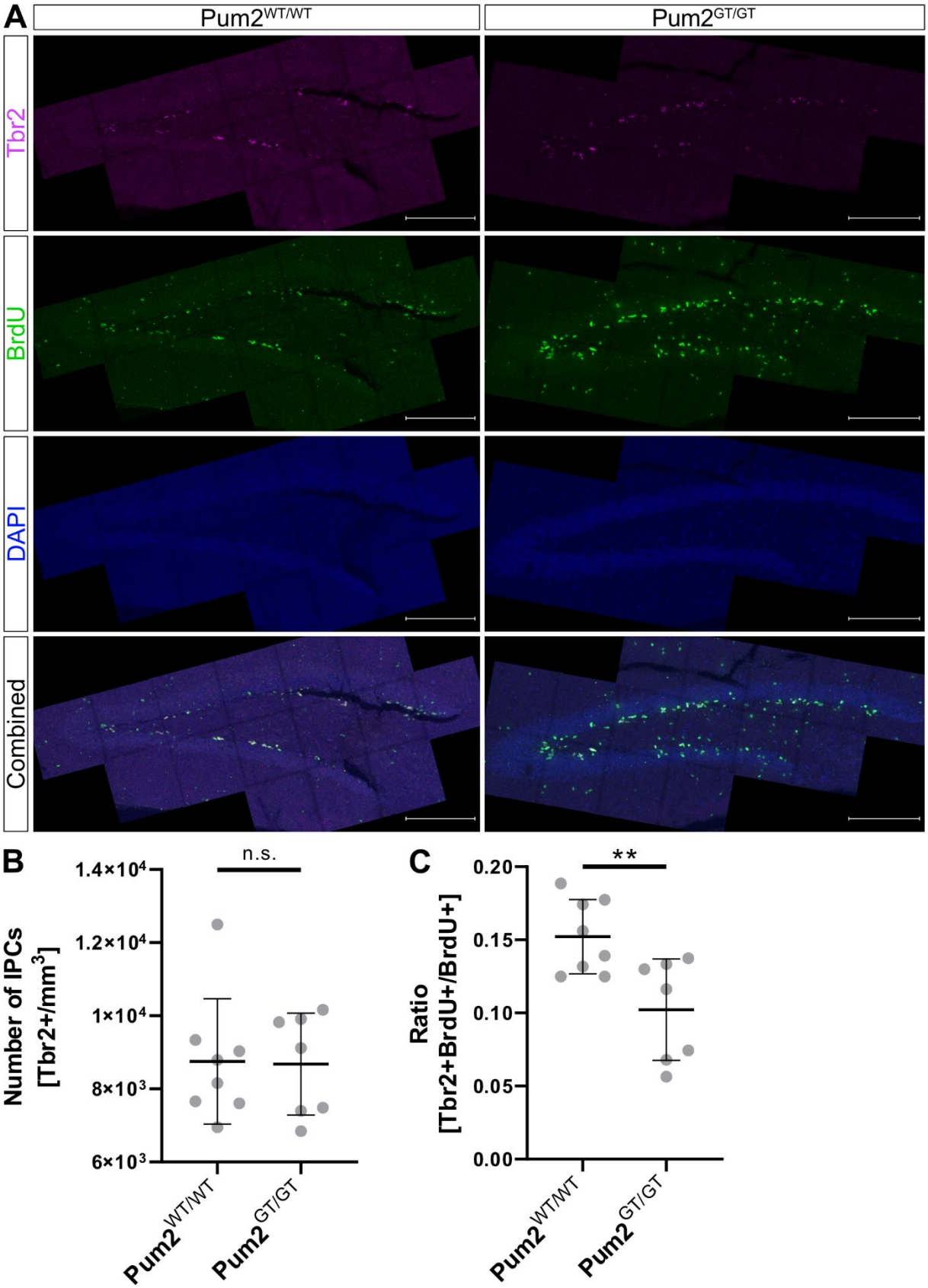

Figure 6: Pum2 deficiency reduces IPC generation. (**A**) Representative Z-stack images of Tbr2, BrdU and DAPI immunostaining on sagittal DG sections (40µm thick) of $Pum2^{WT/WT}$ and $Pum2^{GT/GT}$ mice. Scale bars: 200µm. (**B**) Dot plot displaying the number of Tbr2- labelled cells relative to $1mm^3$. (**C**) Dot plot displaying the ratio of Tbr2- and BrdU-labelled cells relative to all BrdU-labelled cells. Mean and standard deviation are shown. Circles indicate independent biological replicates (n = 7, 8). Asterisks represent p-values obtained by (**B, C**) unpaired Student's t-test (**$p < 0.01$, n.s. ≥ 0.05).

3.1.5 The self-renewal of radial glia cell is affected by Pum2 deficiency

Our previous findings strongly indicated a disruption in neuronal lineage proliferation under Pum2 deficiency. This observation led us to investigate the origin of the neuronal lineage within the adult DG. Specifically, we sought to determine whether RGC populations, the primary source of new neurons in the DG, were similarly affected. To explore this, we targeted a specific cellular marker for RGCs. We stained for Hopx, a protein expressed in RGCs with a putative role in their development (Berg et al., 2018). While Hopx's precise function remains under investigation, its expression pattern renders it a valuable tool for identifying this cell type. Utilizing sections from our prior experiment for immunostaining (**Figure 3A**), we combined Hopx with BrdU to evaluate potential alterations in the RGC population (**Figure 7A**). Our analysis revealed a trend towards a reduction in the overall density of Hopx-positive RGCs, although this did not reach statistical significance (**Figure 7B**). In contrast to the overall density of RGCs, a similar analysis to that described previously, revealed a statistically significant decrease in the proportion of newly proliferated RGCs relative to the total population of newly generated cells. This decrease mirrored the trend observed in previous cell types (**Figure 7C**). This striking finding implies that Pum2 acts on the level of RGCs by modulating their proliferation and potentially balancing their differentiation. Consistent with our observations in other cell types, the overall density of RGCs remains unaffected in the short term and seems not to change the DG composition. However, Pum2 deficiency appears to selectively hinder the ability of RGCs to replenish themselves, raising the possibility of long-term RGC depletion.

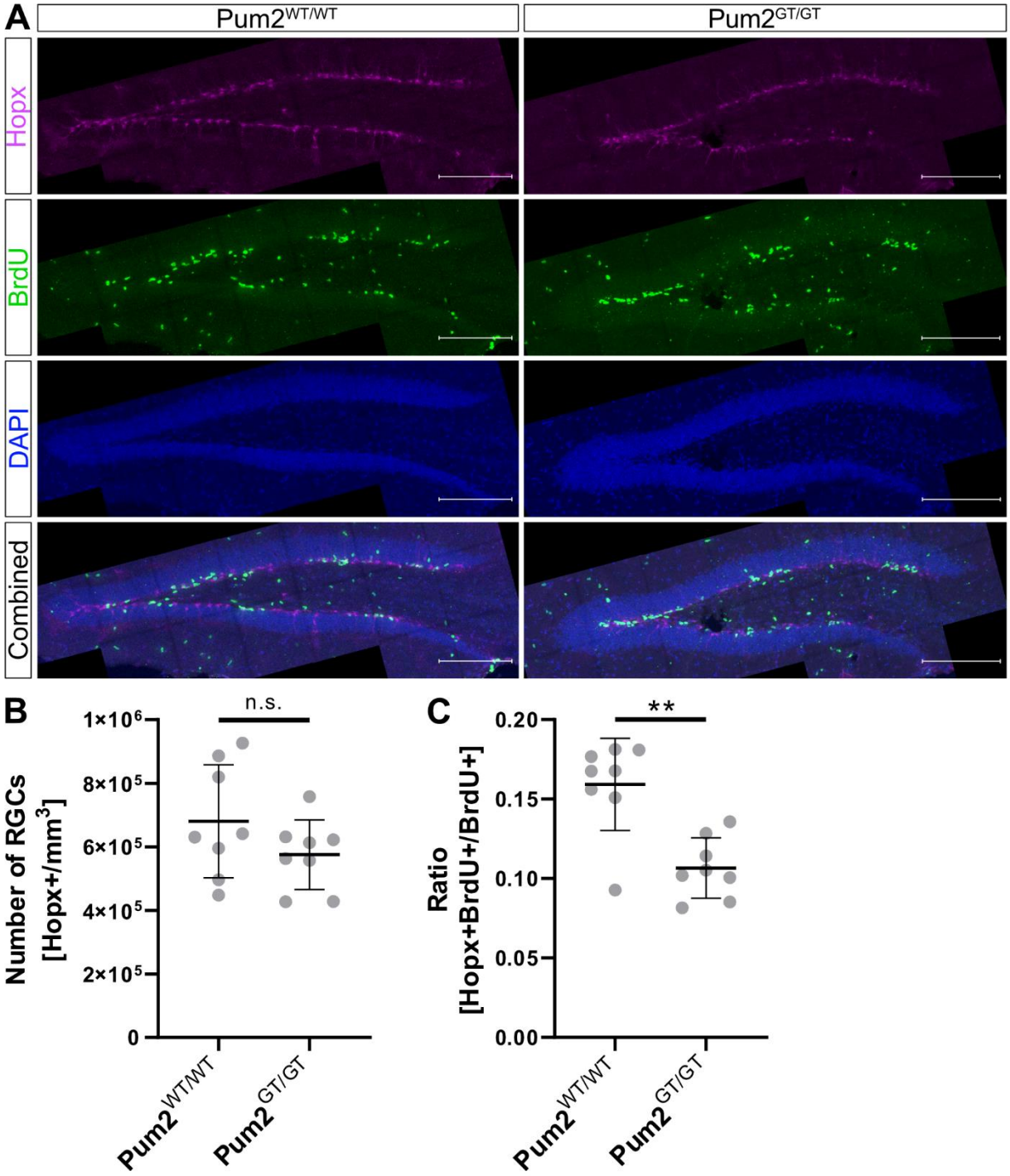

Figure 7: Pum2 deficiency reduces the generation of new RGCs. (**A**) Representative Z-stack images of Hopx, BrdU and DAPI immunostaining on sagittal DG sections (40µm thick) of $Pum2^{WT/WT}$ and $Pum2^{GT/GT}$ mice. Scale bars: 200µm. (**B**) Dot plot displaying the number of Hopx-labelled cells relative to $1mm^3$. (**C**) Dot plot displaying the ratio of Hopx- and BrdU-labelled cells relative to all BrdU-labelled cells. Mean and standard deviation are shown. Circles indicate independent biological replicates (n = 8). Asterisks represent p-values obtained by (**B**) unpaired Student's t-test and (**C**) Mann-Whitney U test (**$p < 0.01$, n.s. ≥ 0.05).

3.1.6 Newly generated mature astrocyte population is increased upon Pum2 deficiency

Our previous results demonstrated disruptions in both neuronal lineage proliferation and RGC self-renewal under Pum2 deficiency, suggesting a role for Pum2 on the level of RGCs and potentially in balancing RGC cell fate decisions. To further investigate this hypothesis, and to assess potential effects on the broader glial cell population, I shifted my focus to astrocytes, utilizing Sox9 as a well-established marker. Sox9 is a protein essential for astrocyte development and function (Ge et al., 2012; Klum et al., 2018). I employed immunostaining on sections from the previous experiment (**Figure 3A**), combining Sox9 with BrdU to evaluate changes within the astrocyte population (**Figure 8A**). My analysis revealed a statistically significant increase in the density of Sox9-positive astrocytes within the DG (**Figure 8B**). Concurrently, a similar analysis to that described previously, the proportion of newly proliferated astrocytes relative to the total population of newly generated cells also exhibited a statistically significant increase (**Figure 8C**). These findings suggest that Pum2 deficiency has a dual effect on astrocytes within the DG. There is a concurrent increase in the proportion of newly proliferated cells that differentiate into astrocytes. This suggests that Pum2 plays a role in regulating the cell fate decision of RGCs, with Pum2 depletion shifting the balance from neurogenesis towards astrogenesis. Interestingly, despite the increase in newly proliferated astrocytes, we did not observe a corresponding increase in astrocyte density within the DG. This could be attributed to the migration of these newly formed astrocytes out of the DG or potentially a yet unidentified cell fate commitment for these cells that express Sox9 as an intermediate marker.

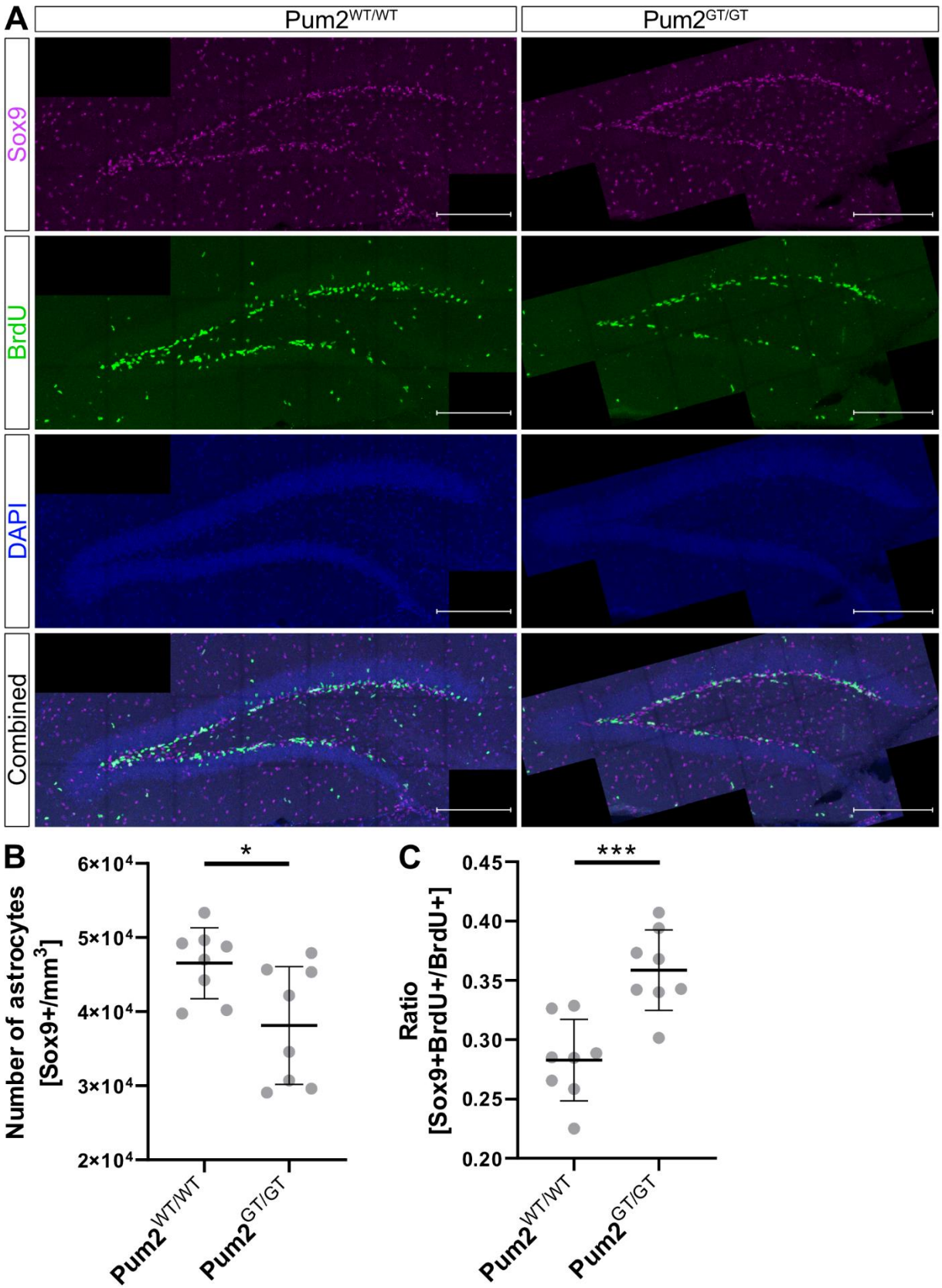

Figure 8: Pum2 deficiency disrupts astrocyte generation and density. (**A**) Representative Z-stack images of Sox9, BrdU and DAPI immunostaining on sagittal DG sections (40µm thick) of $Pum2^{WT/WT}$ and $Pum2^{GT/GT}$ mice. Scale bars: 200µm. (**B**) Dot plot displaying the number of Sox9-labelled cells per $1mm^3$. (**C**) Dot plot displaying the ratio of Sox9- and BrdU-labelled cells relative to all BrdU-labelled cells. Mean and standard deviation are shown. Circles indicate independent biological replicates (n = 8). Asterisks represent p-values obtained by (**B, C**) unpaired Student's t-test (***$p < 0.001$, *$p < 0.05$).

3.1.7 Changes of absolute cell number of specific cell types

Our previous analyses focused on cell densities, revealing changes specifically in Sox9-positive astrocytes under Pum2 deficiency. However, these results reflect the relative composition of the DG rather than absolute cell numbers. To address this, I next analysed the absolute cell numbers of the previously described cell types, independent of DG size. I focused on Ki67-positive cycling cells, Dcx-positive INs, Tbr2-positive IPCs, Hopx-positive RGCs, and Sox9-positive astrocytes. These cell types represent critical components of the DG, providing a comprehensive overview. The analysis revealed no statistically significant reduction in the number of actively cycling cells (Ki67+) in $Pum2^{GT/GT}$ mice (**Figure 9A**). While the IPC population (Tbr2+) did not exhibit a statistically significant decrease, it displayed a notable downward trend in $Pum2^{GT/GT}$ mice (**Figure 9B**). I confirmed a statistically significant decrease in the IN population (Dcx+) in $Pum2^{GT/GT}$ mice (**Figure 9C**). Similarly, the RGC population (Hopx+) was statistically significant reduced in $Pum2^{GT/GT}$ mice (**Figure *9*D**). In line with the previous findings on astrocytes, a statistically significant decrease in the total astrocyte population (Sox9+) was observed in $Pum2^{GT/GT}$ mice (**Figure 9E**). Collectively, the findings indicate that Pum2 plays a critical role in maintaining cell numbers within the DG, as its deficiency leads to a statistically significant reduction across various cell types, potentially explaining the observed decrease in DG size. While our analysis of cell densities suggests that Pum2 plays a relatively minor role in directly shaping the overall cellular composition of the DG. This finding raises the possibility that Pum2 may play a critical role in cell survival, particularly during early developmental stages as no increase of cell death could be observed in the adult DG (data not shown).

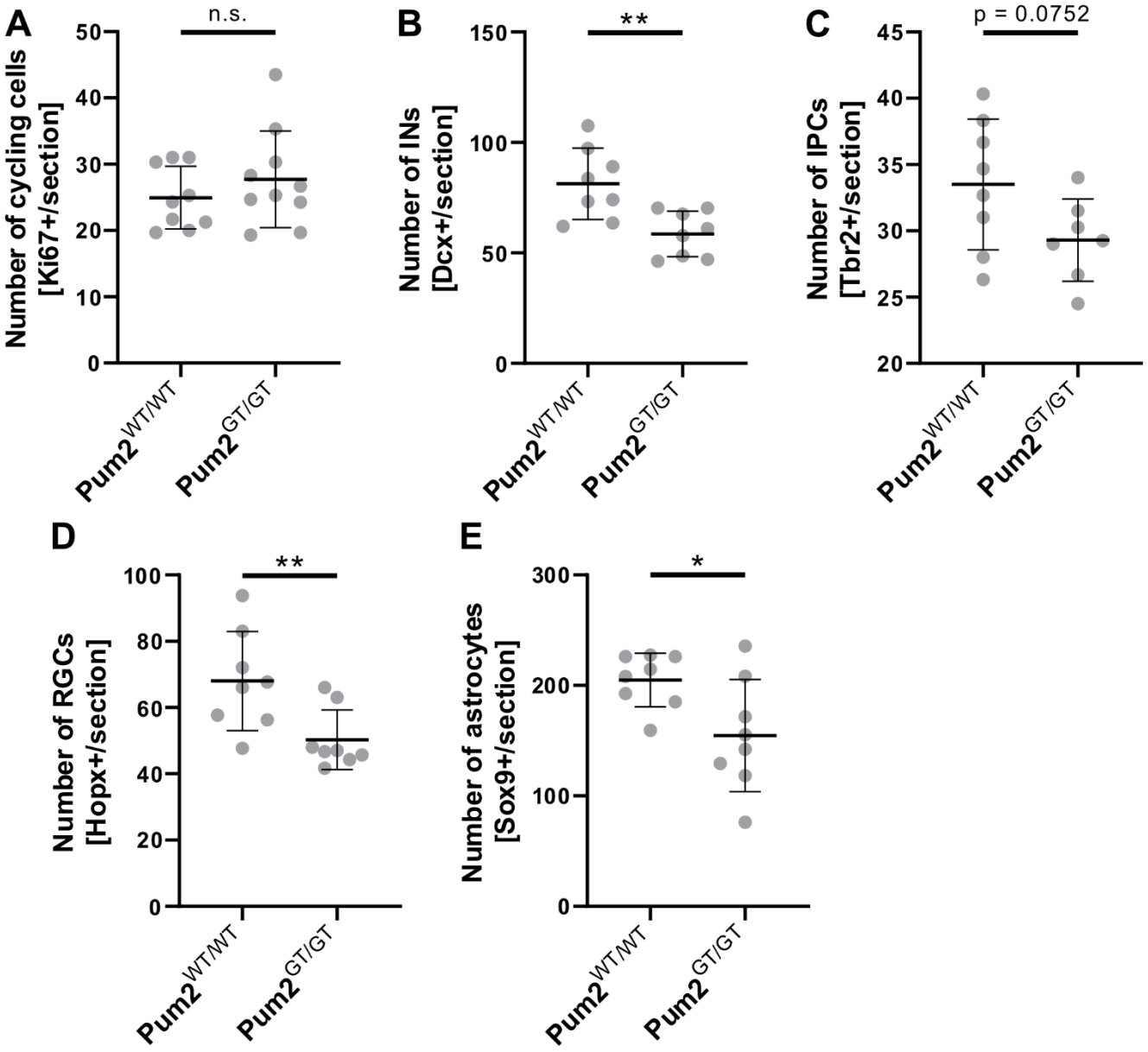

Figure 9: Pum2 deficiency leads to loss of cell identity in the DG. (**A**) Dot plot displaying the number of Ki67-positive cells in the DG per sagittal sections (40µm thick). (**B**) Dot plot displaying the number of Dcx-positive cells in sagittal DG sections (40µm thick). (**C**) Dot plot displaying the number of Tbr2-positive cells in sagittal DG sections (40µm thick). (**D**) Dot plot displaying the number of Hopx-positive cells in sagittal DG sections (40µm thick). (**E**) Dot plot displaying the number of Sox9-positive cells in sagittal DG sections (40µm thick). Mean and standard deviation are shown. Circles indicate independent biological replicates (n = 8). Asterisks represent p-values obtained by (**A**) unpaired Welch's t-test, (**B, C, E**) unpaired Student's t-test and (**D**) Mann-Whitney U test (**p < 0.01, *p < 0.05, n.s. ≥ 0.05).

3.1.8 Decrease of newly generated mature neurons

Our previous experiments focused on Pum2's role in adult neurogenesis within young adult mice. While valuable, this approach did not address the maturation potential of these newly generated neurons and the effect of Pum2 deficiency on those neurons. To investigate this aspect, we adopted a protocol allowing for a four-week maturation period, as established for studying mature neurons *in vivo* (Cheng et al., 2011). This extended timeframe provides newly generated neurons sufficient time to differentiate, migrate, and integrate into the DG. Christin Illig performed this experiment with mice treated as follows: eight weeks-old mice received BrdU over two weeks, followed by a two-week BrdU-free period before perfusion at 12 weeks of age (**Figure 10A**). To assess the population of newly generated mature neurons, we used immunostaining for NeuN in combination with BrdU (**Figure 10B**). This analysis revealed a reduction in the newly generated mature neuron population under Pum2 deficiency (**Figure 11A**). Additionally, this approach allowed me to compare the localization of BrdU-positive cells within the DG after two and four weeks of maturation. I divided the DG into the granular cell layer (GCL) and the subgranular zone (SGZ), with the SGZ defined as the first two cell layers bordering the hilus. This analysis demonstrated a time-dependent shift of BrdU-positive cells towards the GCL between the two weeks and four weeks maturation timepoints. Interestingly, no statistically significant localization difference was observed between $Pum2^{GT/GT}$ and $Pum2^{WT/WT}$ mice (**Figure 11B**). In summary, these results consistently support our previous findings of reduced neurogenesis upon Pum2 depletion. However, my analysis indicates that the localization of newly generated cells within the DG remains unaltered over the maturation period. The decrease in newly generated MNs, coupled with the unaffected migration of new cells, suggests that Pum2 is not essential for cell migration within the DG. This implies that other factors may be responsible for guiding the movement of newly generated cells, regardless of their fate.

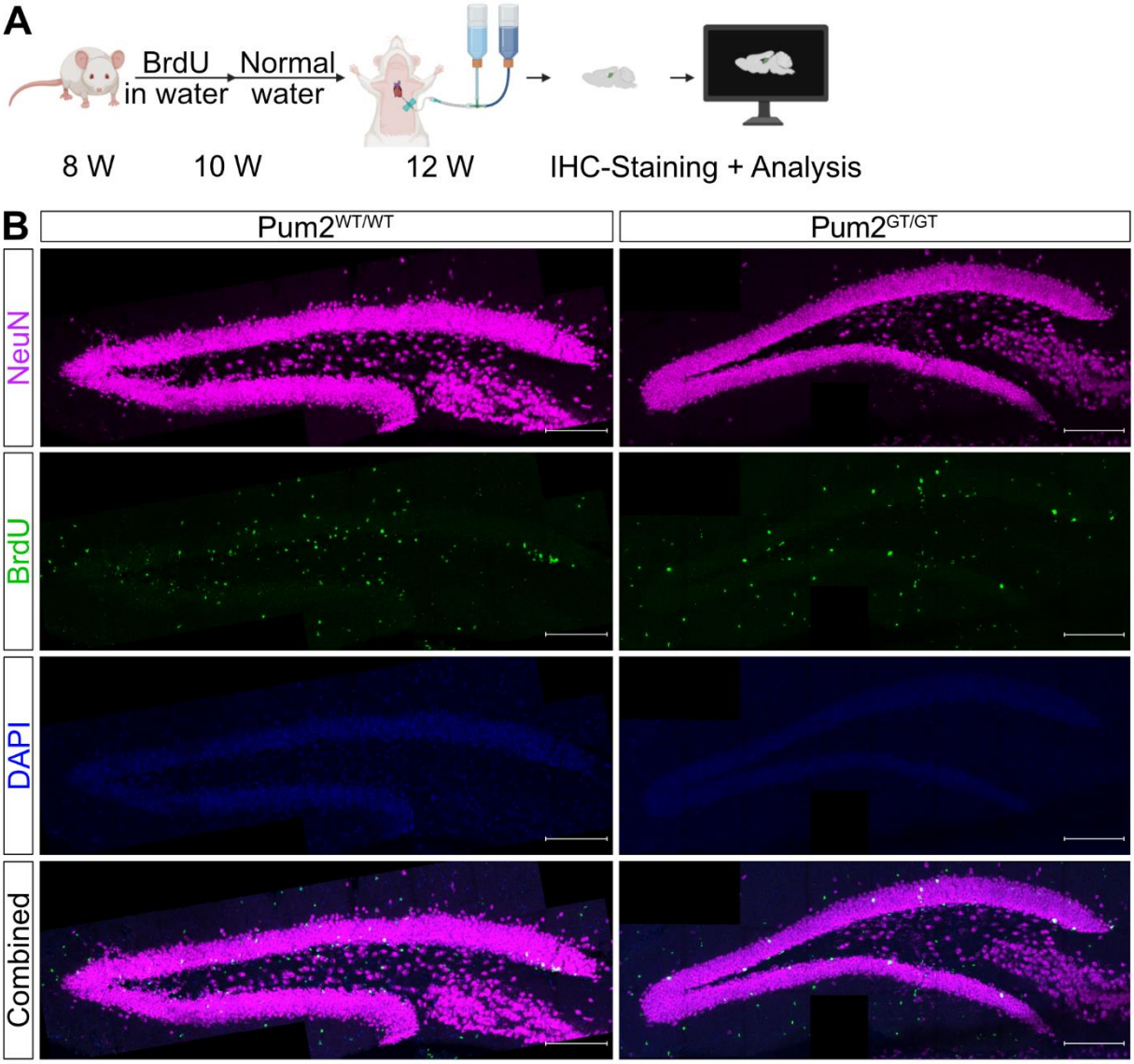

Figure 10 Detection of MNs in the DG. (**A**) Experimental outline of the BrdU-labelling of Pum2$^{WT/WT}$ and Pum2$^{GT/GT}$ mice with additional 2 weeks of maturation time. Created with BioRender.com. Agreement number: CY2759YDDI (**B**) Representative Z-stack images of NeuN, BrdU and DAPI immunostaining on sagittal DG sections (40µm thick) of Pum2$^{WT/WT}$ and Pum2$^{GT/GT}$ mice. Scale bars: 200µm.

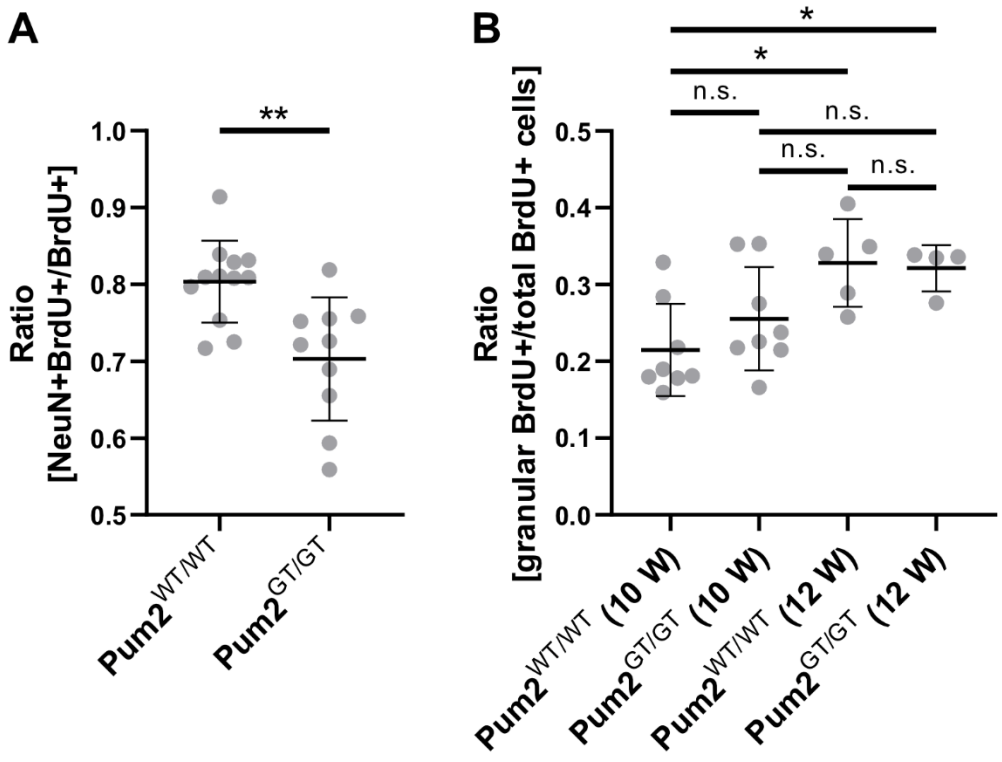

Figure 11: Pum2 deficiency reduces the generation of new MNs in the DG. (**A**) Dot plot displaying the ratio of NeuN and BrdU-labelled cells relative to all BrdU labelled cells. (**B**) Dot plot displaying the ratio of BrdU-labelled cells in the granular cell layer relative to all BrdU labelled cells after two and four weeks. Mean and Standard Deviation are shown. Mean and standard deviation are shown. Circles indicate independent biological replicates (n = 4, 5, 8, 9, 12). Asterisks represent p-values obtained by (**A**) unpaired Student's t-test and (**B**) Mann-Whitney U test (**p < 0.01, *p < 0.05, n.s. ≥ 0.05).

3.2 DG neurogenic nice plasticity sufficient to counteract Pum2 deficiency

3.2.1 Recovery of proliferating cells through voluntary physical activity

To investigate whether Pum2-deficient brains retain sufficient plasticity to potentially overcome the previously described phenotypes, Christin Illig repeated the initial proliferation tracing experiment with the addition of freely accessible running wheels within the cages (**Figure 12A**). Immunostaining of BrdU confirmed ongoing cell division within the DG (**Figure 12B**). I assessed the overall DG size by measuring its perimeter and normalizing these measurements to those obtained from $Pum2^{WT/WT}$ mice in our previous analysis. This analysis revealed a statistically significant increase in the size of the DG in $Pum2^{WT/WT}$ mice exposed to the running wheel (**Figure 13A**). Remarkably, the DG size in $Pum2^{GT/GT}$ mice not only recover to the $Pum2^{WT/WT}$ condition without running wheel but reached a size comparable to that of $Pum2^{WT/WT}$ mice with running wheel access (**Figure 13A**). The analysis of BrdU-positive cell density in the DG of $Pum2^{WT/WT}$ mice with running wheels did not show a statistically significant increase (**Figure 13B**). However, when considering the total number of BrdU-positive cells per 40µm section, a statistically significant increase was observed in $Pum2^{WT/WT}$ mice exposed to running wheels compared to their control counterparts (**Figure 13C**). Conversely, in $Pum2^{GT/GT}$ mice exposed to running wheels, the density of BrdU-positive cells was statistically significant reduced compared to $Pum2^{GT/GT}$ mice without running wheels. Additionally, a downward trend was noted when compared to control $Pum2^{WT/WT}$ mice (**Figure 13B**). Surprisingly, the total number of BrdU-positive cells per 40 µm section remained unchanged across $Pum2^{GT/GT}$ mice with running wheels, control $Pum2^{WT/WT}$ mice, and $Pum2^{GT/GT}$ mice without running wheel access (**Figure 13C**). These results indicate that physical activity can partially rescue the proliferative capacity of cells within the DG under Pum2 deficiency. Notably, we observed an unexpected increase in DG size, suggesting a potential compensatory mechanism that could counteract the neurogenesis deficit associated with Pum2 loss.

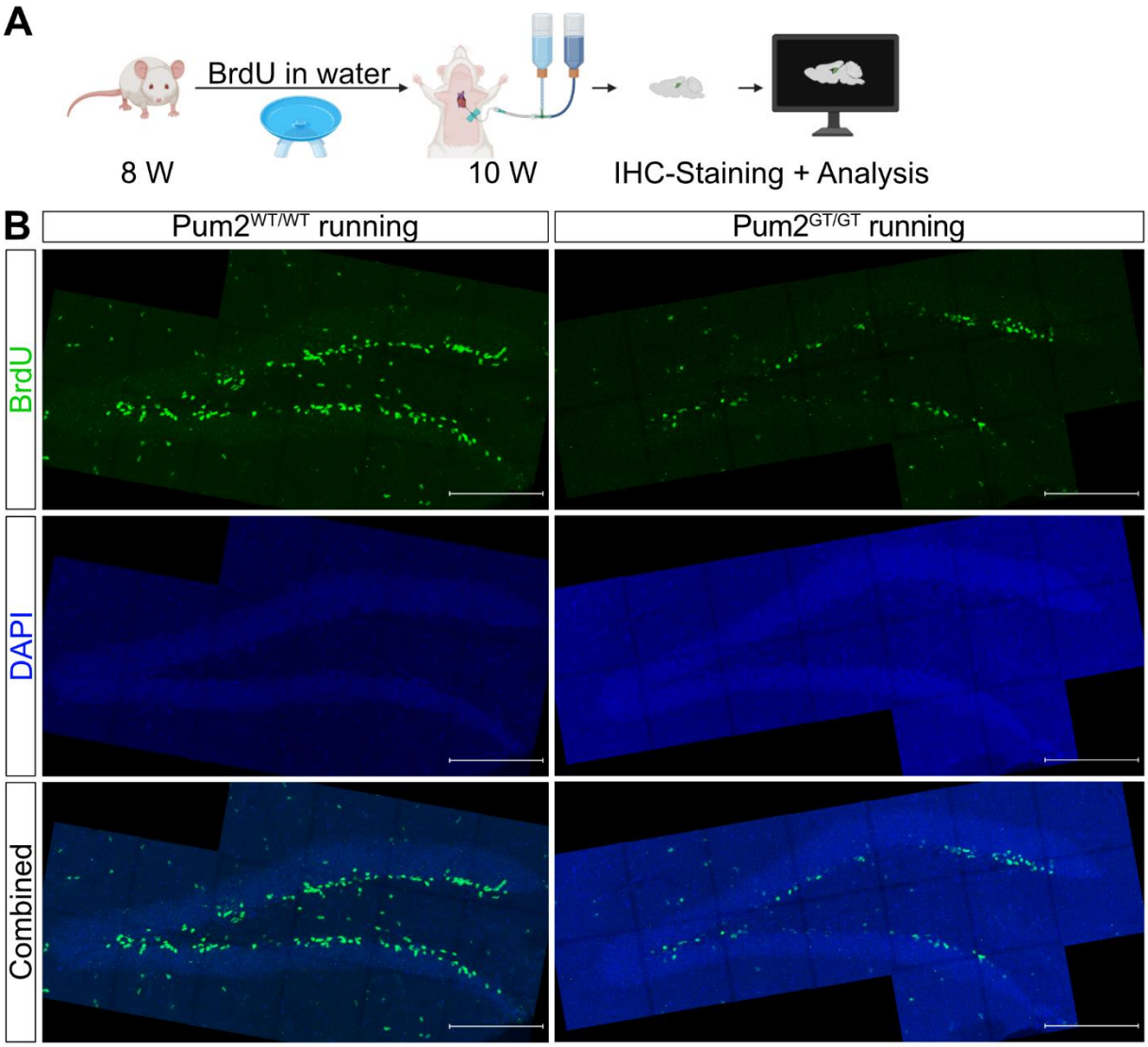

Figure 12: Detection of proliferating cells in the DG. (**A**) Experimental outline of the BrdU-labelling of Pum2$^{WT/WT}$ and Pum2$^{GT/GT}$ mice over 2 weeks with voluntary access to a running wheel. Created with BioRender.com. Agreement number: OG2759Y842 (**B**) Representative Z-stack images of BrdU and DAPI immunostaining on sagittal DG sections (40µm thick) of Pum2$^{WT/WT}$ and Pum2$^{GT/GT}$ mice. Scale bars: 200µm.

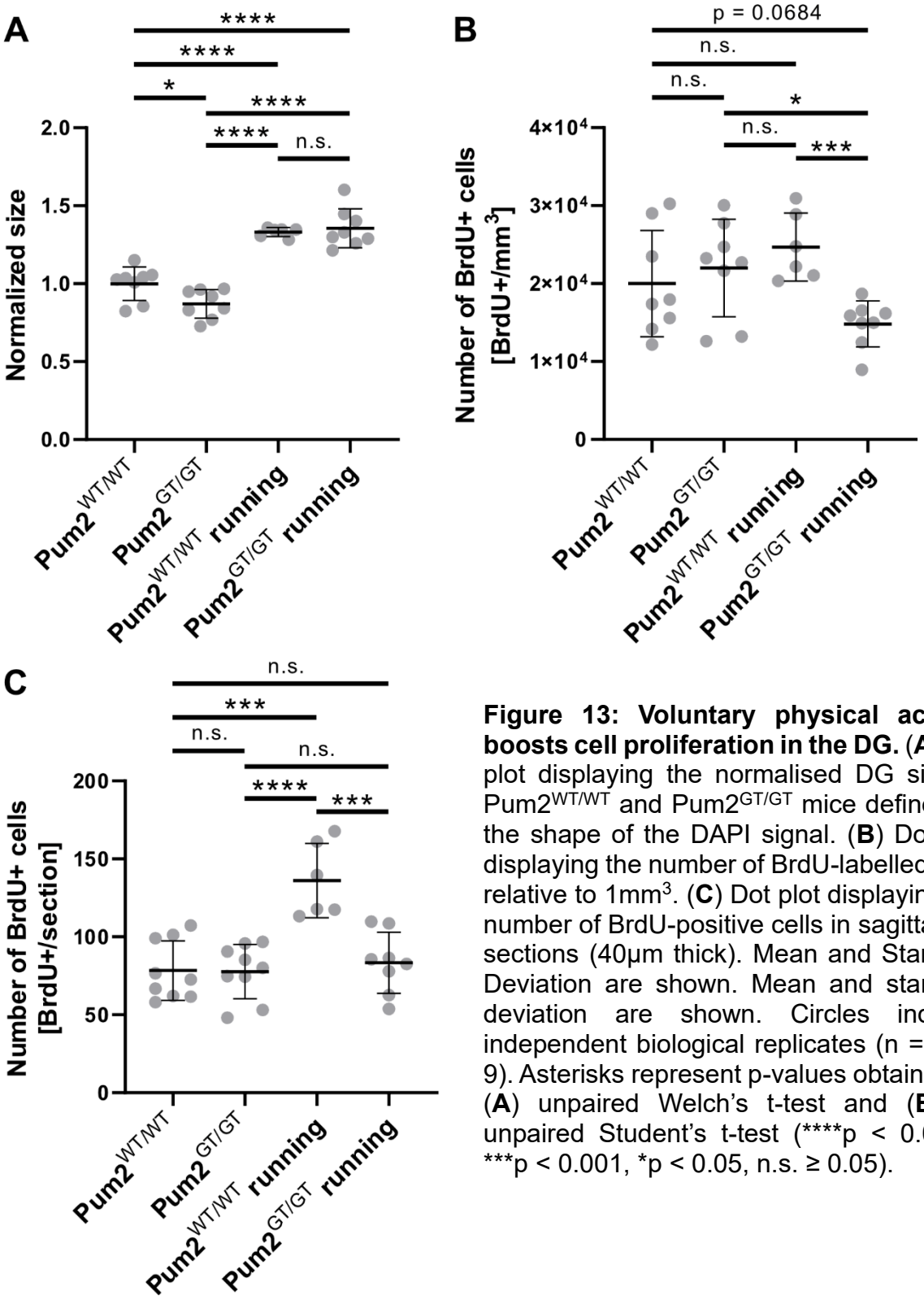

Figure 13: Voluntary physical activity boosts cell proliferation in the DG. (**A**) Dot plot displaying the normalised DG size of $Pum2^{WT/WT}$ and $Pum2^{GT/GT}$ mice defined by the shape of the DAPI signal. (**B**) Dot plot displaying the number of BrdU-labelled cells relative to $1mm^3$. (**C**) Dot plot displaying the number of BrdU-positive cells in sagittal DG sections (40µm thick). Mean and Standard Deviation are shown. Mean and standard deviation are shown. Circles indicate independent biological replicates (n = 6, 8, 9). Asterisks represent p-values obtained by (**A**) unpaired Welch's t-test and (**B, C**) unpaired Student's t-test (****$p < 0.0001$, ***$p < 0.001$, *$p < 0.05$, n.s. ≥ 0.05).

3.2.2 Increase of cycling cells through voluntary physical activity

The initial results from the physically active mice prompted us to investigate whether Pum2 deficient mice exposed to running wheels exhibit a higher retention of cells within the active cell cycle compared to their sedentary counterparts. Therefore, we performed immunostaining for Ki67 in combination with BrdU of the sections obtained from the previous described experiment (**Figure 14**). Compared to control $Pum2^{WT/WT}$ mice, we observed a statistically significant increase in the density of Ki67-positive cells within the DG of $Pum2^{WT/WT}$ mice exposed to running wheels (**Figure 15A**). A similar increase was observed in $Pum2^{WT/WT}$ mice exposed to running wheels when analysing cells positive for both the active cell cycle marker (Ki67) and BrdU (**Figure 15B**). Interestingly, $Pum2^{GT/GT}$ mice exposed to running wheels also exhibited a statistically significant increase in the density of Ki67-positive cells compared to control $Pum2^{WT/WT}$ control mice, showing an increase in cells actively in cell cycle (**Figure 15A**). However, no increase was observed compared to mice without running wheel. At most a downward trend was noted (**Figure 15A**). Unexpectedly, physical activity in $Pum2^{GT/GT}$ mice further elevated the density of cells positive for both Ki67 and BrdU. This increase reached a level comparable to that observed in $Pum2^{WT/WT}$ mice exposed to running wheels (**Figure 15B**). These results highlight a degree of plasticity in the actively cycling cell population within the DG under Pum2 deficiency. The observed increase in actively cycling cells caused by physical activity suggests that exercise may partially compensate for the effects of Pum2 loss in this context.

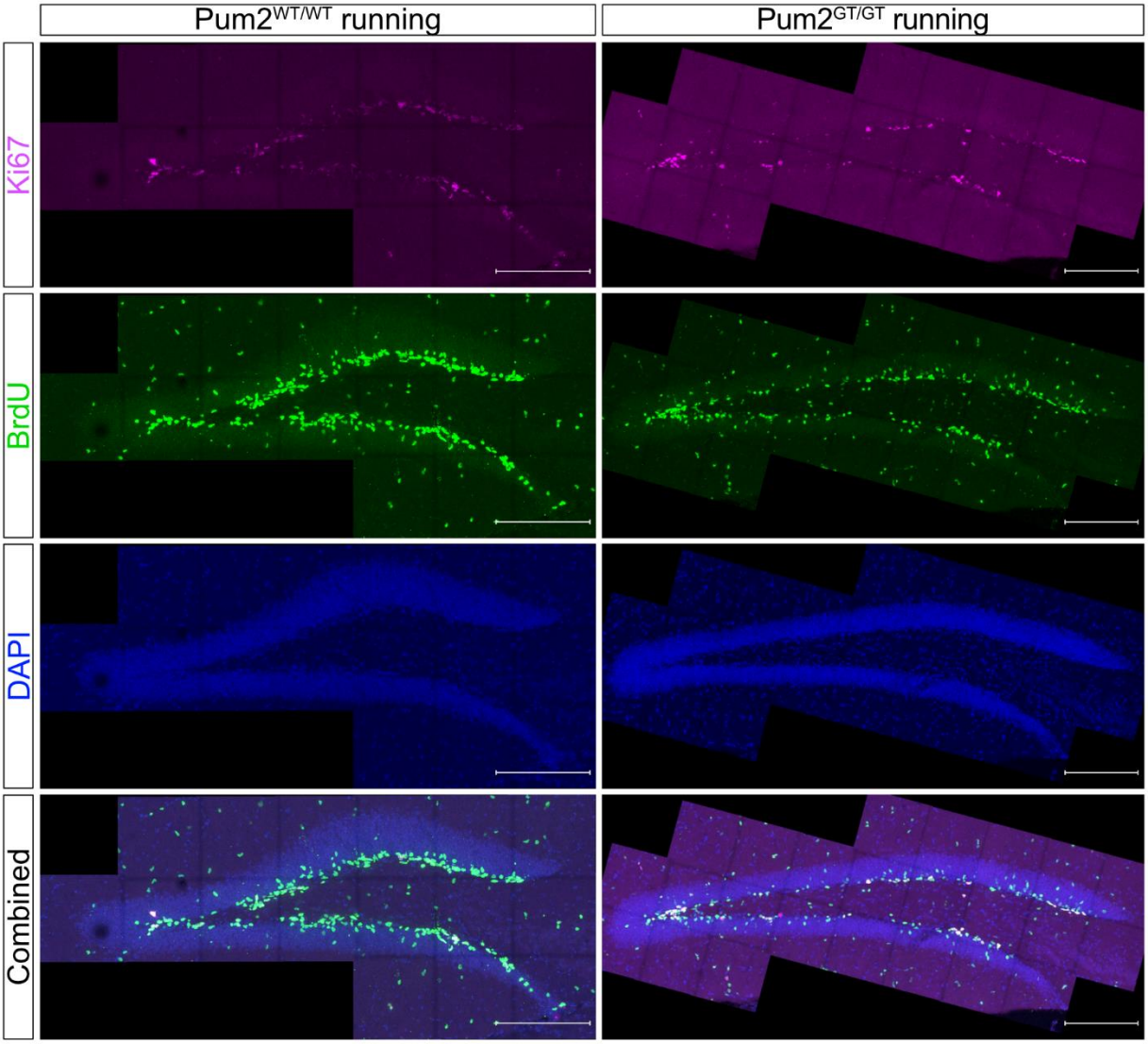

Figure 14: Detection of actively dividing cells in the DG. Representative Z-stack images of Ki67, BrdU and immunostaining on sagittal DG sections (40µm thick) of $Pum2^{WT/WT}$ and $Pum2^{GT/GT}$ mice with voluntary access to a running wheel. Scale bars: 200µm.

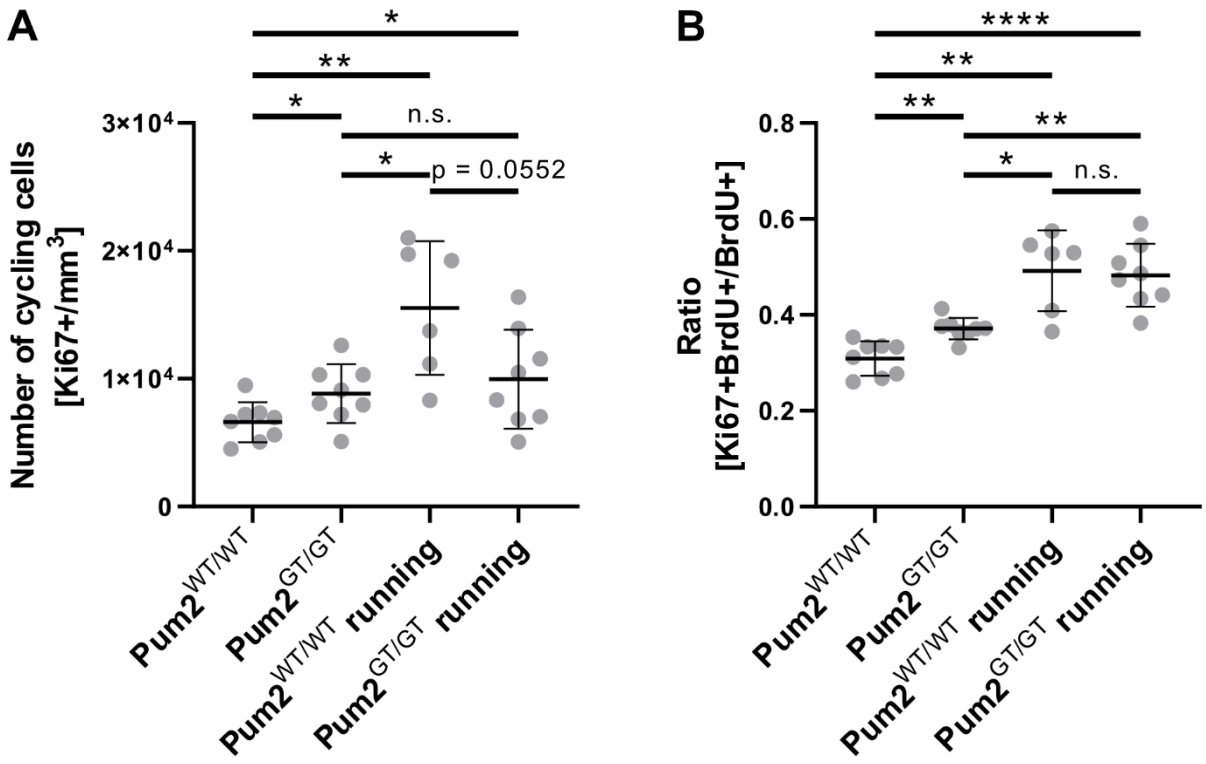

Figure 15: Voluntary physical activity accelerates cell cycle progression. (**A**) Dot plot displaying the number of Ki67-labelled cells relative to 1mm^3. (**B**) Dot plot displaying the ratio of Ki67- and BrdU-labelled cells relative to all BrdU-labelled cells. Mean and standard deviation are shown. Circles indicate independent biological replicates (n = 6, 8). Asterisks represent p-values obtained by (**A, B**) unpaired Welch's t-test (****p < 0.0001, **p < 0.01, *p < 0.05, n.s. ≥ 0.05).

3.2.3 Recovery of newly generated INs through voluntary physical activity under Pum2 deficiency

To gain a better understanding of the previously observed plasticity within the context of adult neurogenesis under Pum2 deficiency, we focused on the cellular marker Dcx, which identifies INs. We utilised immunostaining on sections from our previously described experiment with running wheel exposure (**Figure 12A**). This immunostaining combined the Dcx marker with BrdU, enabling a detailed analysis of changes within the neurogenic lineage induced by voluntary physical activity (**Figure 16**). Intriguingly, my analysis revealed a trend towards an increased cell density of Dcx-positive INs in $Pum2^{WT/WT}$ mice exposed to running wheels compared to control $Pum2^{WT/WT}$ mice (**Figure 17A**). Although not statistically significant, this trend may be influenced by an outlier within the $Pum2^{WT/WT}$ control group. Conversely, $Pum2^{GT/GT}$ mice exposed to running wheels showed no statistically significant change in IN density compared to both control $Pum2^{WT/WT}$ mice and $Pum2^{GT/GT}$ mice without running wheel access (**Figure 17A**). Showing, physical activity has no statistically significant effect on the density of INs in the DG of Pum2-deficient mice. Therefore, we then investigated the proportion of newly proliferated INs. $Pum2^{WT/WT}$ mice exposed to running wheels exhibited a statistically significant increase in this proportion relative to the broader population of newly generated cells, compared to control $Pum2^{WT/WT}$ mice (**Figure 17B**). This finding aligns with the well-documented enhancement of neurogenesis following voluntary physical activity (van Praag et al., 1999). Surprisingly, while $Pum2^{GT/GT}$ mice exposed to running wheels displayed a similar proportion of newly proliferated INs compared to control $Pum2^{WT/WT}$ mice, this proportion did not increase to the same extent observed in $Pum2^{WT/WT}$ mice exposed to running wheels (**Figure 17B**). These findings strongly suggest that voluntary physical activity can partially rescue the impairment of the IN lineage caused by Pum2 deficiency. However, the characteristic boost in neurogenesis observed under WT conditions following physical activity appears to be attenuated in the context of Pum2 deficiency.

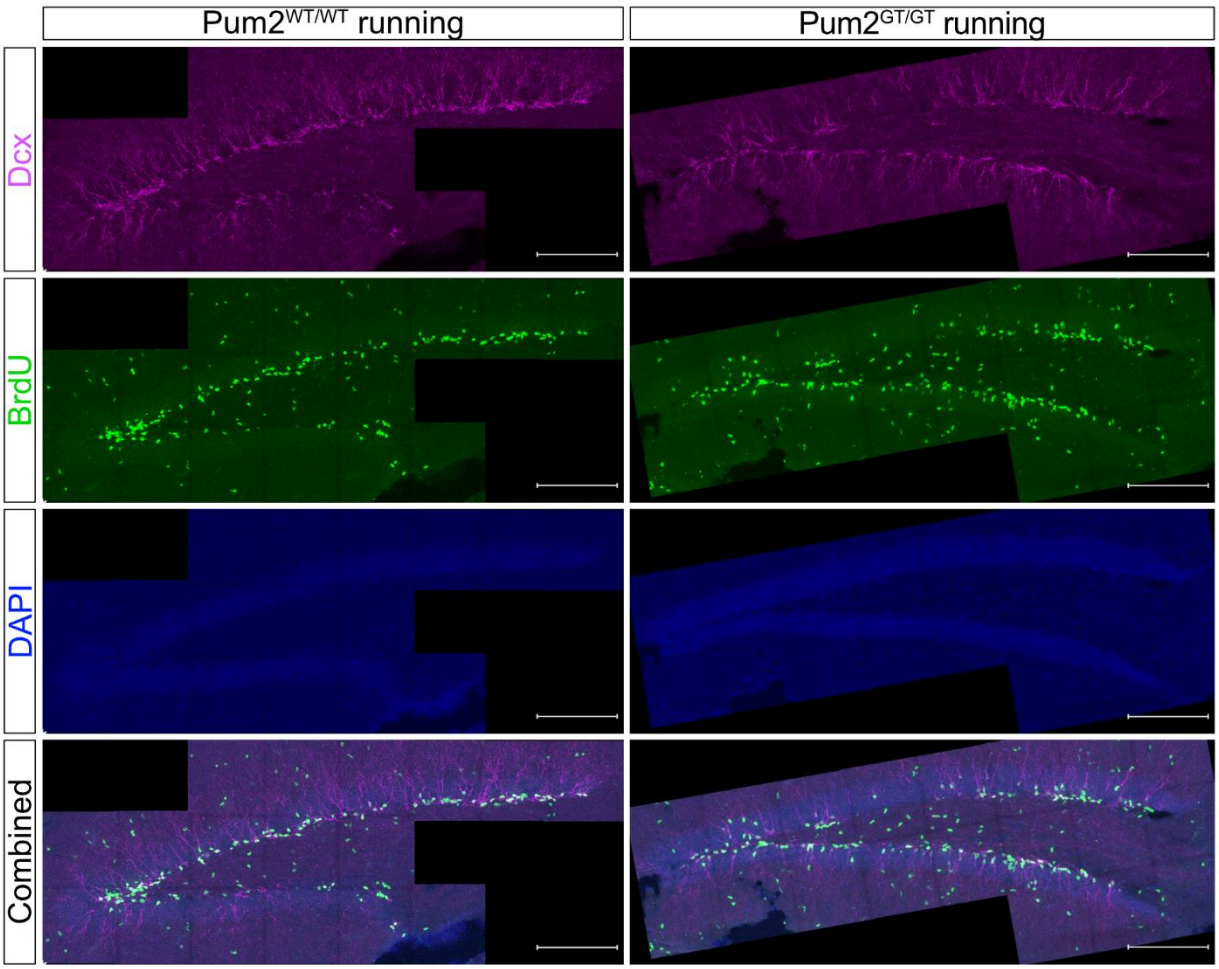

Figure 16: Detection of immature neurons (INs) in the DG. Representative Z-stack images of Dcx, BrdU and DAPI immunostaining on sagittal DG sections (40µm thick) of $Pum2^{WT/WT}$ and $Pum2^{GT/GT}$ mice with voluntary access to a running wheel. Scale bars: 200µm.

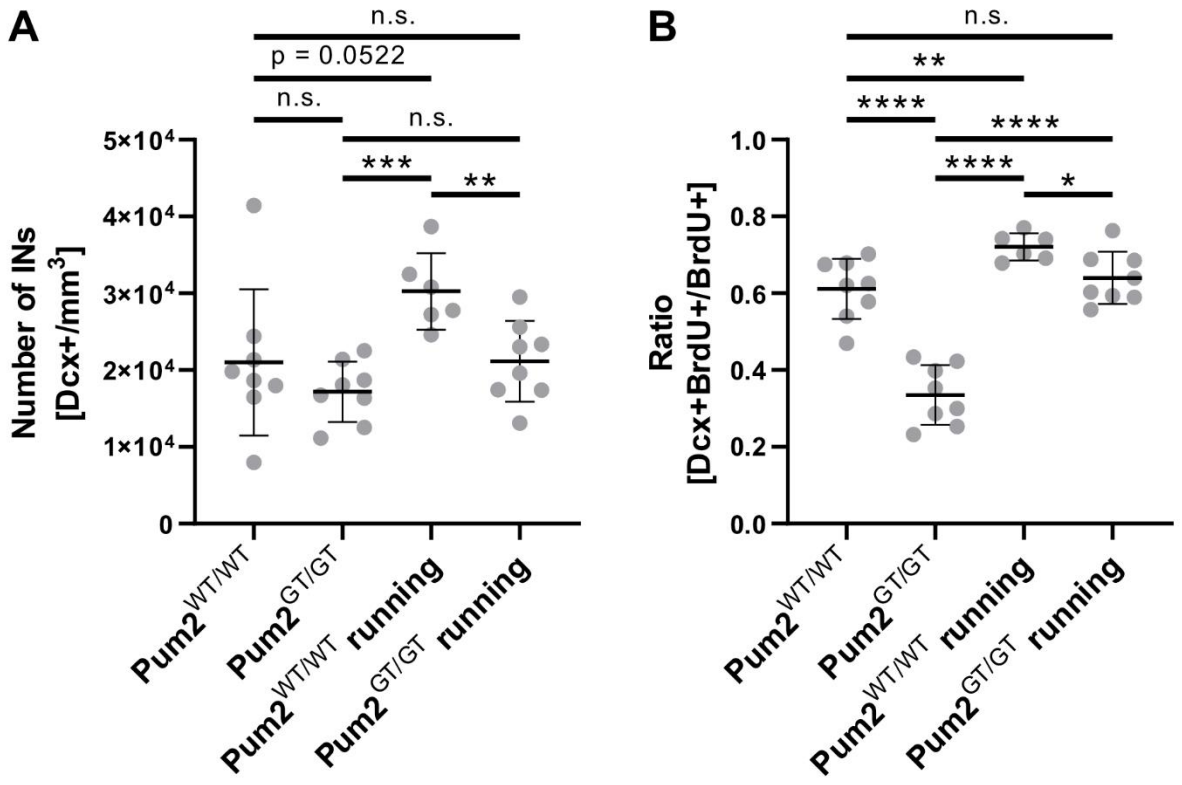

Figure 17: Voluntary physical activity restores proliferation of immature neuron (IN) in Pum2 deficiency. (**A**) Dot plot displaying the number of Dcx-labelled cells relative to 1mm^3. (**B**) Dot plot displaying the ratio of Dcx- and BrdU-labelled cells relative to all BrdU-labelled cells. Mean and standard deviation are shown. Circles indicate independent biological replicates (n = 6, 8). Asterisks represent p-values obtained by (**A, B**) unpaired Student's t-test (****p < 0.0001, ***p < 0.001, **p < 0.01, *p < 0.05, n.s. ≥ 0.05).

3.2.4 Recovery of newly generated intermediate progenitors through voluntary physical activity

To delve into the precise plasticity of adult neurogenesis in Pum2-deficient mice, we focused on a well-established cellular marker of IPCs, Tbr2. Employing sections derived from our previous experiment, we performed immunostaining to visualise these markers (**Figure 12A**). This staining integrated the IPC marker, Tbr2, with BrdU, enabling a thorough evaluation of changes within the neurogenic lineage instigated by voluntary access to a running wheel (**Figure 18**). Intriguingly, my analysis uncovered a substantial increase in the cell density of Tbr2-positive IPCs within $Pum2^{WT/WT}$ mice with physical activity when compared to $Pum2^{WT/WT}$ control mice (**Figure 19A**). Remarkably, this effect was absent in $Pum2^{GT/GT}$ mice with access to a running wheel. These mice exhibited a statistically significant decrease in IPC density compared to both $Pum2^{WT/WT}$ control mice and $Pum2^{GT/GT}$ mice without physical activity (**Figure 19A**). While I observed this drastic increase in $Pum2^{WT/WT}$ mice exposed to the running wheel, it was not reflected in the proportion of newly proliferated IPCs relative to the overall population of newly generated cells when compared to control $Pum2^{WT/WT}$ mice (**Figure 19B**). Furthermore, no statistically significant difference was found in the proportion of newly proliferated IPCs relative to the overall population of newly generated cells between $Pum2^{GT/GT}$ mice with running wheel access and $Pum2^{WT/WT}$ controls without running wheel (**Figure 19B**). These findings imply that voluntary physical activity cannot increase the IPC density in Pum2 deficiency as observed in the control. Nonetheless, it appears to have a restorative effect on the population of newly proliferated IPCs. In conjunction with our previous findings, the voluntary physical activity may stimulate a higher turnover rate of IPCs that differentiate into INs. However, the restoration of the newly generated IPC population may not fully compensate for this increased turnover, leading to a reduction in IPC density.

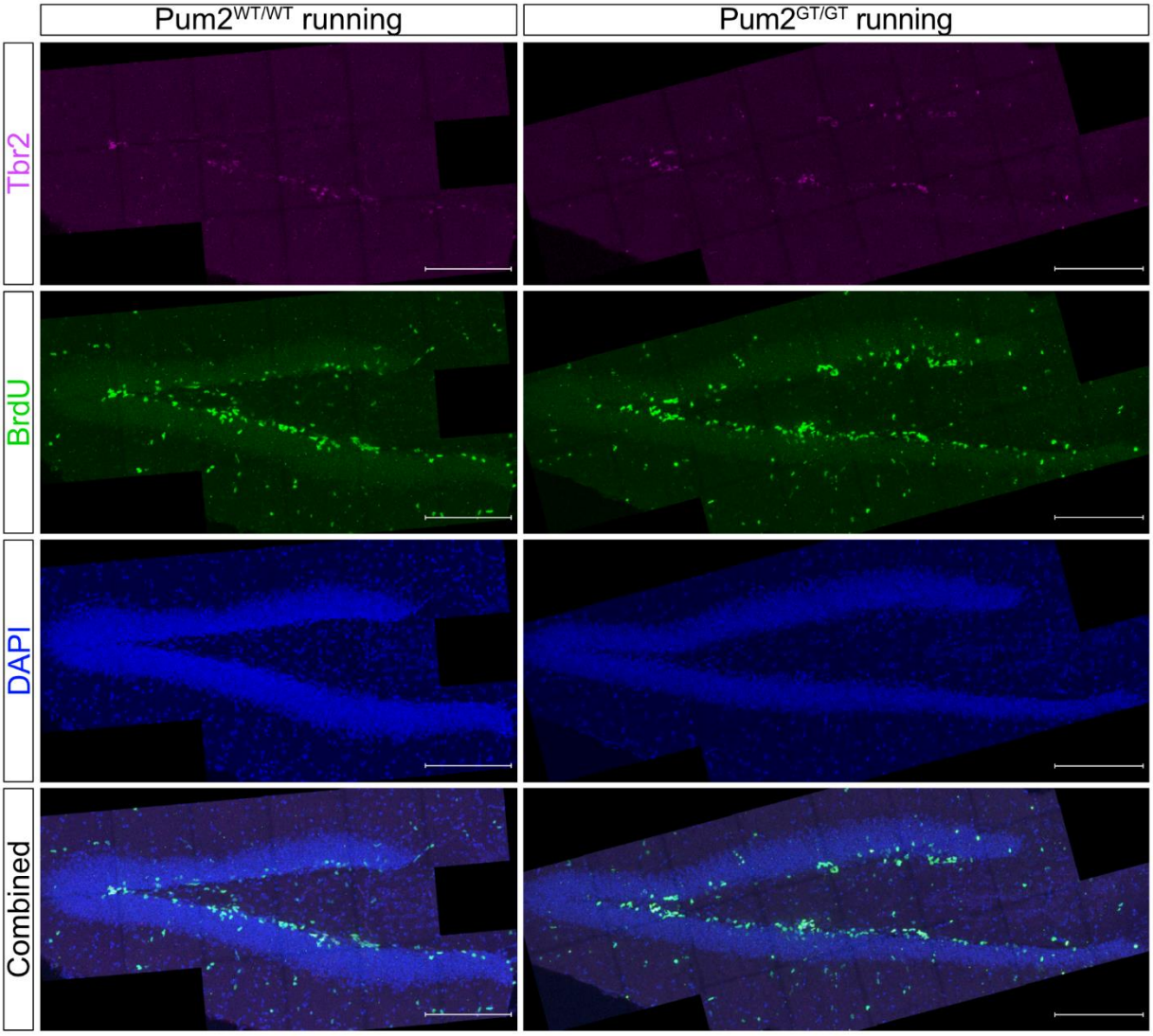

Figure 18: Detection of IPCs in the DG. Representative Z-stack images of Tbr2, BrdU and DAPI immunostaining on sagittal DG sections (40µm thick) of $Pum2^{WT/WT}$ and $Pum2^{GT/GT}$ mice with voluntary access to a running wheel. Scale bars: 200µm.

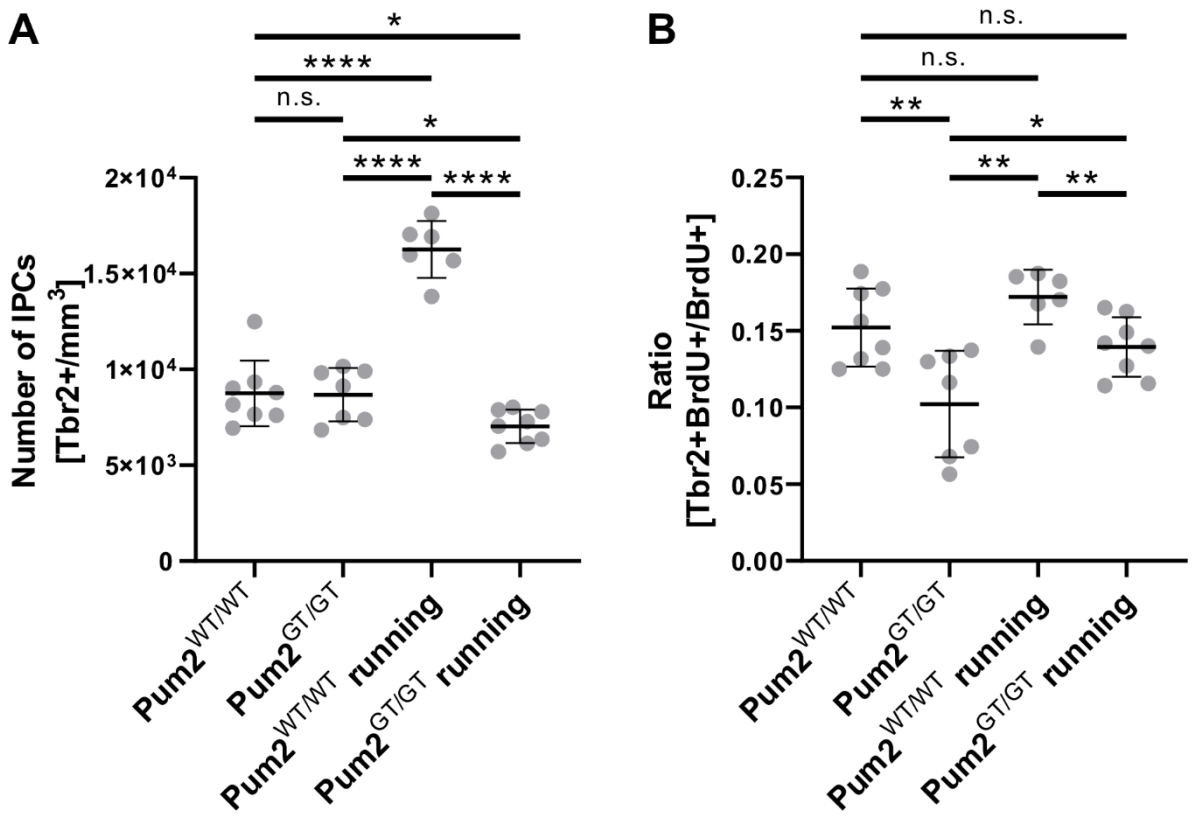

Figure 19: Voluntary exercise restores IPC proliferation in Pum2 deficiency. (**A**) Dot plot displaying the number of Tbr2-labelled cells relative to 1mm^3. (**B**) Dot plot displaying the ratio of Tbr2- and BrdU-labelled cells relative to all BrdU-labelled cells. Mean and standard deviation are shown. Circles indicate independent biological replicates (n = 6, 8). Asterisks represent p-values obtained by (**A, B**) unpaired Student's t-test (****p < 0.0001, **p < 0.01, *p < 0.05, n.s. ≥ 0.05).

3.2.5 Changes in newly generated radial glia cells and mature astrocytes through voluntary physical activity

To explore potential plasticity within glial cells in parallel to the observed plasticity in adult neurogenesis of Pum2-deficient mice, we targeted a well-established cellular marker for RGCs, Hopx. Using sections from the previous experiment, we performed immunostaining to visualise the marker for RGCs (**Figure 12A**). This staining integrated the RGC marker with BrdU, facilitating the meticulous analysis of changes within the glial lineage potentially triggered by voluntary access to a running wheel (**Figure 20**). Unexpectedly by the previous findings, my analysis demonstrated no statistically significant changes in the cell density of Hopx-positive RGCs in $Pum2^{WT/WT}$ mice exposed to physical activity versus $Pum2^{WT/WT}$ control mice (**Figure 21A**). Intriguingly, I discovered a statistically significant reduction in RGC cell density within $Pum2^{GT/GT}$ mice with running wheel access compared to all other conditions, possibly due to the increased size of the DG (**Figure 21A**). Interestingly, both $Pum2^{WT/WT}$ and $Pum2^{GT/GT}$ mice with physical activity exhibited a statistically significant increase in the proportion of newly proliferated RGCs relative to the overall population of newly generated cells, compared to $Pum2^{WT/WT}$ controls (**Figure 21B**). No difference was noted between the two running wheel conditions. Strikingly, the proportion of newly proliferated INs in $Pum2^{GT/GT}$ mice with running wheel access, when compared to control $Pum2^{GT/GT}$ mice, doubled (**Figure 21B**). These results indicate that stem cell self-proliferation can be potentiated under both WT and Pum2-deficient conditions. Consistent with our findings in IPCs, voluntary physical activity appears to stimulate the generation of new RGCs in Pum2-deficient mice. However, this increased generation may not be sufficient to offset the heightened rate at which RGCs differentiate into other cell types, leading to a reduction in overall RGC density.

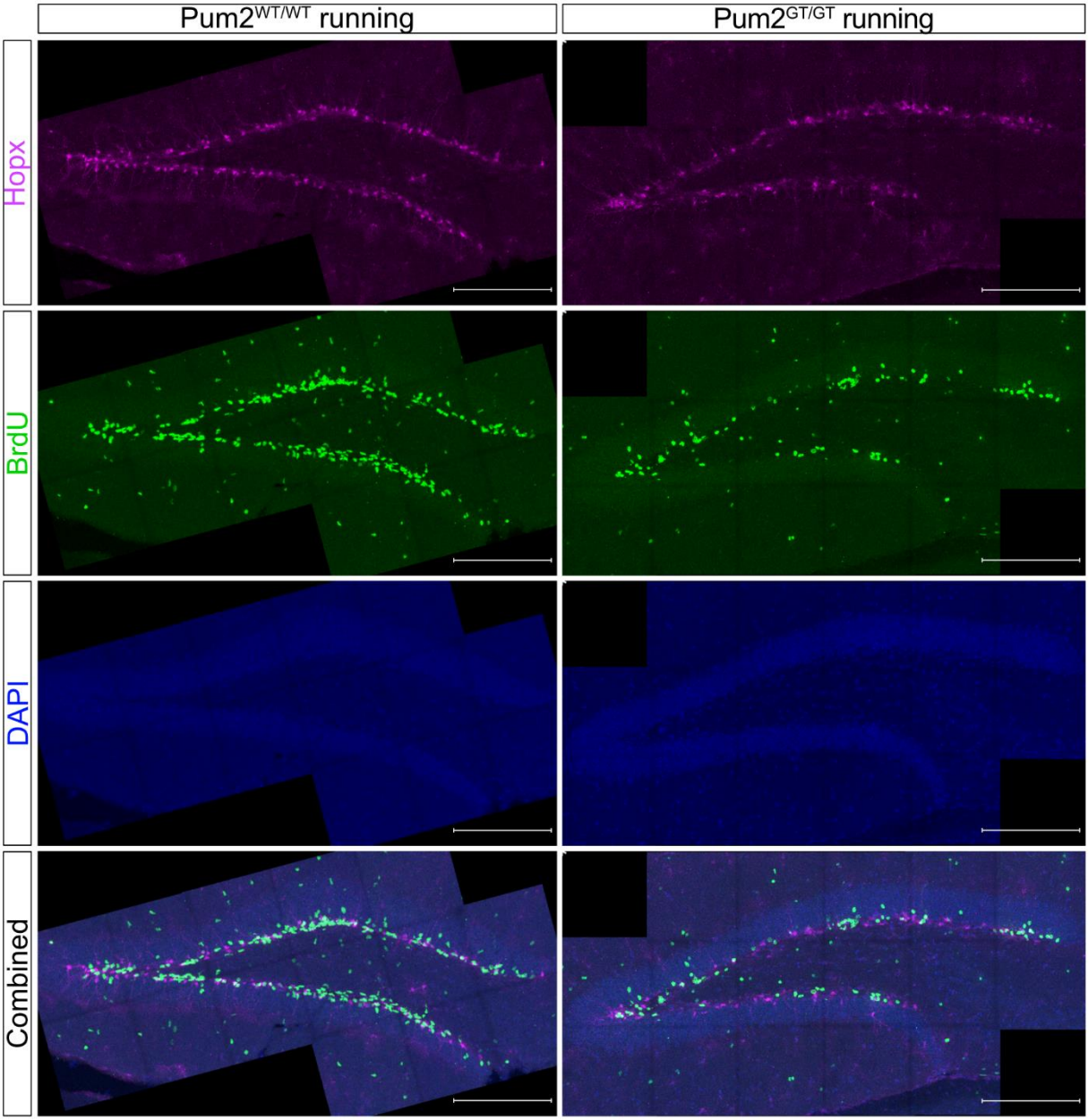

Figure 20: Detection of RGCs in the DG. Representative Z-stack images of Hopx, BrdU and DAPI immunostaining on sagittal DG sections (40µm thick) of $Pum2^{WT/WT}$ and $Pum2^{GT/GT}$ mice with voluntary access to a running wheel. Scale bars: 200µm.

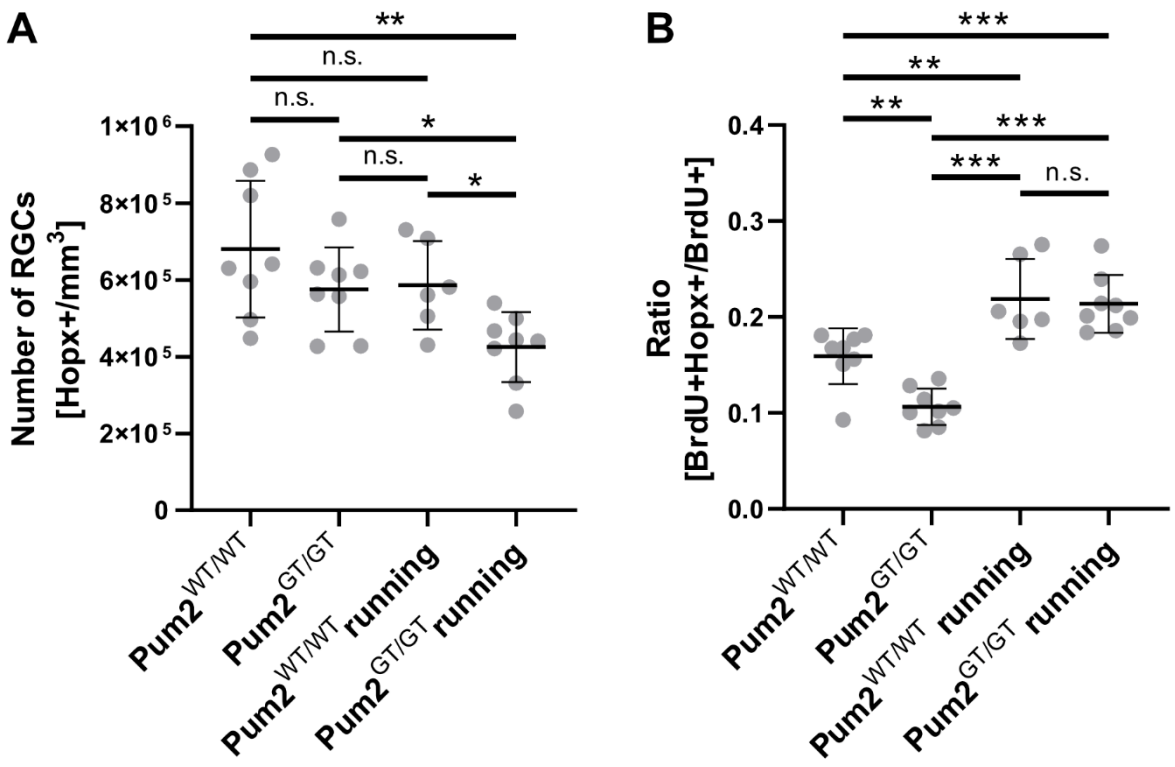

Figure 21: The number of newly proliferated RGCs is increased after voluntary physical activity. (**A**) Dot plot displaying the number of Hopx-labelled cells relative to 1mm^3. (**B**) Dot plot displaying the ratio of Hopx- and BrdU-labelled cells relative to all BrdU-labelled cells. Mean and standard deviation are shown. Circles indicate independent biological replicates (n = 6, 8). Asterisks represent p-values obtained by (**A**) unpaired Student's t-test and (**B**) Mann-Whitney U test (***p < 0.001, **p < 0.01, *p < 0.05, n.s. ≥ 0.05).

3.2.6 Reduction in newly generated mature astrocytes through voluntary physical activity

To investigate potential plasticity exhibited by astrocytes in the context of Pum2 deficiency, I used a well-established cellular marker specific to astrocytes, Sox9. Utilizing sections from the previous experiment, I performed immunostaining to visualise astrocytes (**Figure 12A**). This staining integrated the astrocyte marker with BrdU, facilitating the analysis of changes within the astrocyte population potentially triggered by voluntary access to a running wheel (**Figure 22A**). Intriguingly, my analysis uncovered a substantial decrease in the cell density of Sox9-positive astrocytes within both $Pum2^{WT/WT}$ and $Pum2^{GT/GT}$ mice with physical activity compared to $Pum2^{WT/WT}$ controls (**Figure 22B**). Remarkably, this decrease was even more pronounced in $Pum2^{GT/GT}$ mice exposed to the running wheel versus $Pum2^{GT/GT}$ mice without running wheel access and might be due to the fewer numbers of astrocytes in the DG under Pum2 deficiency. (**Figure 22B**). I observed a reduction in newly proliferated astrocytes within $Pum2^{WT/WT}$ mice exposed to physical activity relative to the overall population of newly generated cells, compared to $Pum2^{WT/WT}$ controls (**Figure 22C**). While newly proliferated astrocytes in $Pum2^{GT/GT}$ mice with running wheel access were not statistically significant different from $Pum2^{WT/WT}$ controls, they exhibited a downward trend. Additionally, they did not differ statistically significant from $Pum2^{WT/WT}$ mice with running wheel access (**Figure 22C**). These findings suggest that voluntary physical activity may both restore and potentially even diminish the astrocyte-favouring bias caused by Pum2 deficiency. This observation warrants further investigation into the complex interplay between Pum2, astrocyte dynamics, and the effects of physical exercise.

The collective findings underscore the multifaceted role of Pum2 in DG neurogenesis. Pum2 appears to influence both cell fate decision of RGCs and cell cycle regulation. In its absence, there is a shift towards astrogenesis without statistically significant changes in the overall cellular composition of the DG, except for a reduction in astrocytes. Notably, voluntary physical activity can partially rescue the neurogenesis deficits caused by Pum2 deficiency, although this may come at the expense of RGC and IPC populations, and a further reduction in astrocyte population.

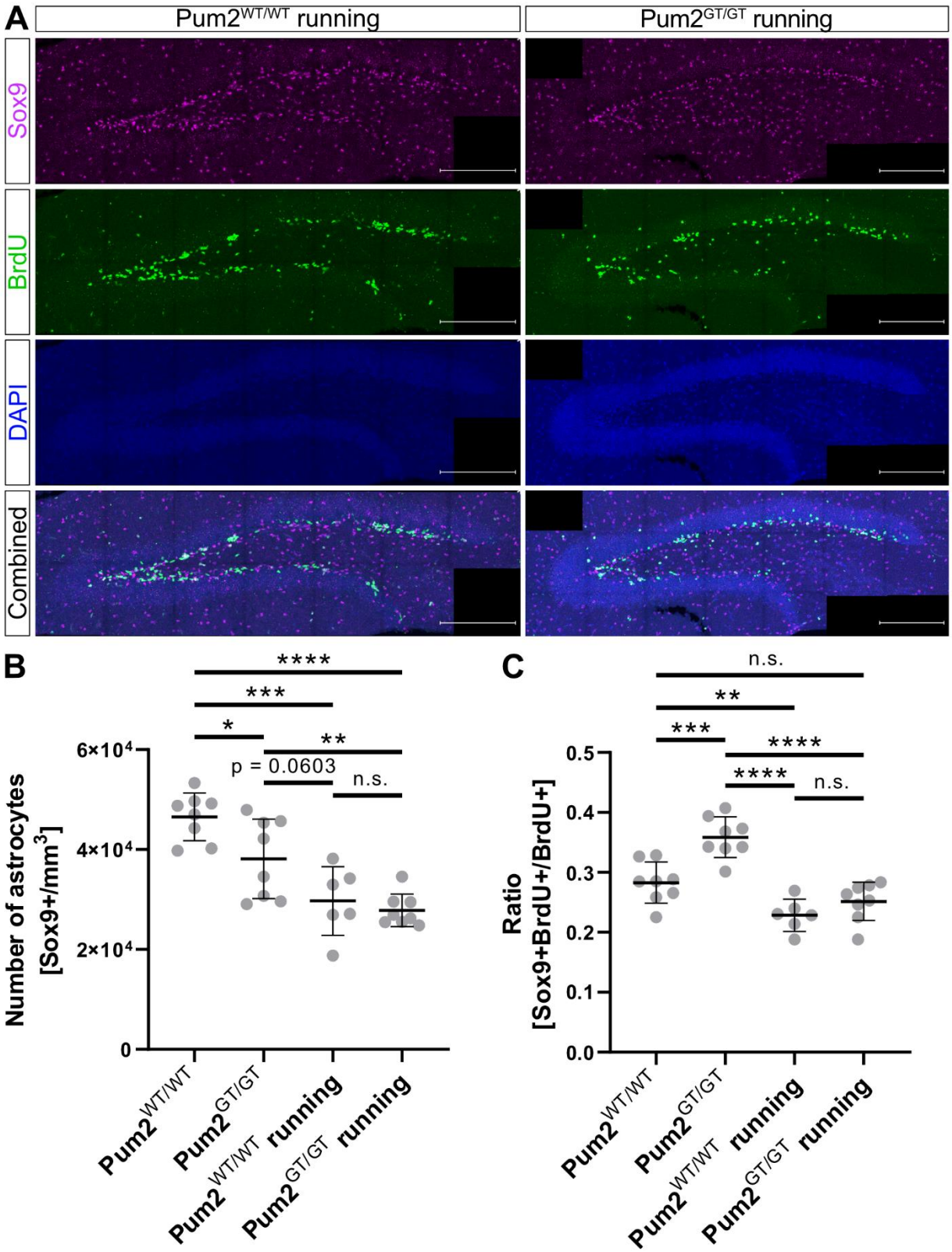

Figure 22: Astrocyte proliferation recovers with physical exercise in Pum2 deficiency. (**A**) Representative Z-stack images of Sox9, BrdU and DAPI immunostaining on sagittal DG sections (40µm thick) of Pum2$^{WT/WT}$ and Pum2$^{GT/GT}$ mice with voluntary access to a running wheel. Scale bars: 200µm. (**B**) Dot plot displaying the number of Sox9-labelled cells relative to 1mm^3. (**C**) Dot plot displaying the ratio of Sox9- and BrdU-labelled cells relative to all BrdU-labelled cells. Mean and standard deviation are shown. Circles indicate independent biological replicates (n = 6, 8). Asterisks represent p-values obtained by (**B, C**) unpaired Student's t-test (****p < 0.0001, ***p < 0.001, **p < 0.01, *p < 0.05, n.s. ≥ 0.05).

3.3 Single-Cell RNA sequencing reveals a novel cell population associated with Pum2 deficiency in the DG

The results so far suggest an important role of Pum2 in adult hippocampal neurogenesis with a shift in cell differentiation towards astrocytes upon depletion of Pum2. To further elucidate the role of Pum2 in adult hippocampal neurogenesis and on the transcriptome, Dr. Christina Koupourtidou, Dr. Stefanie Ohlig, Sabine Thomas together with myself conducted single-cell RNA sequencing (scRNA-seq) on cells isolated from the DG of adult mice. Following established dissection protocols (Hagihara et al., 2009), we minimised contamination from other hippocampal regions. scRNA-seq was performed using a state-of-the-art method optimised for brain cells (Zheng et al., 2017), enabling us to investigate DG cell types with single-cell resolution (**Figure 23A**). The initial analysis revealed diverse cell populations within the DG. Not surprisingly, I identified cell clusters associated with blood vessels, including vascular endothelial cells and pericytes (**Figure 23B**). Additionally, I detected glial cell clusters representing oligodendrocytes and microglia (**Figure 23B**), which are critical for neuronal support, myelin production, and immune function within the brain (Tay et al., 2019). Of particular interest was the finding that I successfully visualised cells related to both astrogenesis and neurogenesis within the hippocampus. Using a tSNE plot for enhanced separation (**Figure 23C**), I identified neuronal lineage clusters: Intermediate Progenitor Cells (IPC)/Immature Neurons (IN), Differentiating Neurons (DN), and Mature Neurons (MN). These cell types were confirmed through characteristic gene expression patterns: Rbfox3 (NeuN) in MN, weaker Rbfox3 expression along with Dcx in DN, and Dcx with Eomes (Tbr2) in IPC/IN (**Figure 24A**). For further confirmation the neuronal identity the expression of Prox1, Neurod1 and Tbr1 was used (**Figure 24B**). Alongside expected neuronal clusters, I observed clusters representing RGC marked by expression of Hopx and Mature Astrocytes (MA) marked by the expression of Sox9, S100β and Aldh1a1 (**Figure 24C, D**). As a general glial marker, Sox2 and Gfap was expressed across all glial cell types (Ellis et al., 2004; Grundmann et al., 2019; Niu et al., 2015). Most interestingly, I discovered a cluster demonstrating mixed lineage characteristics, with partial expression of glia genes and neuron genes. This cluster was termed Transient State Cells (TSC) to suggest its possible intermediate identity (**Figure 23C**). These results offer valuable insights into the effects of Pum2 deficiency and highlight a potentially aberrant cell population associated with this condition.

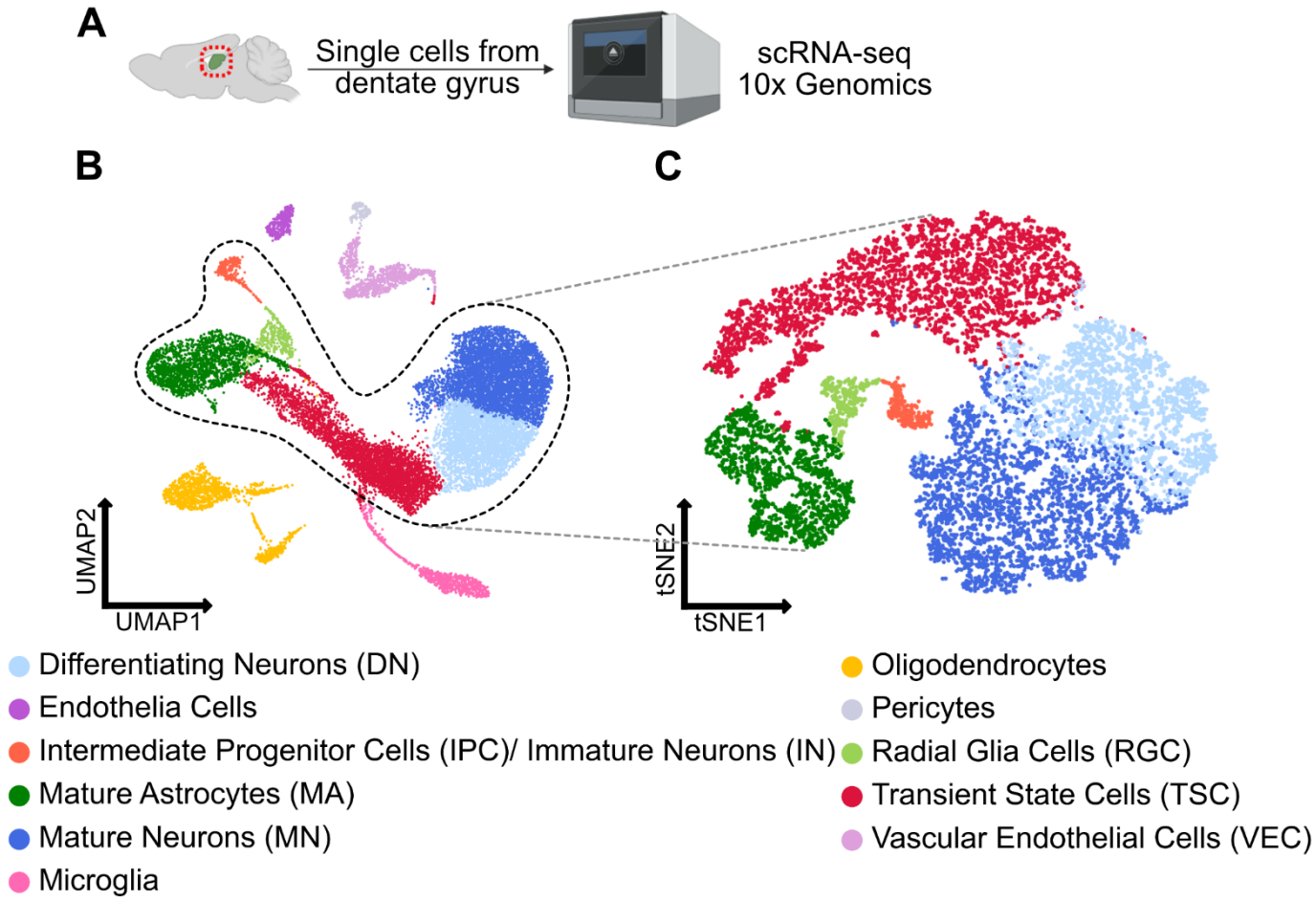

Figure 23: scRNA-seq data of the DG allows a detailed insight into the cellular composition and states comprising the neurogenic niche in Pum2 mice. (**A**) Experimental outline of the scRNA-seq performed by Dr. Christina Koupourtidou with the help of Dr. Stefanie Ohlig, Sabine Thomas and myself. Created with BioRender.com. Agreement number: LZ2759YAYH (**B**) UMAP visualisation of the total dataset and the detected and accordingly annotated cluster from scRNA-seq. (**C**) tSNE visualisation of the neurogenesis and astrogenesis associated cell clusters extracted from the total dataset from scRNA-seq.

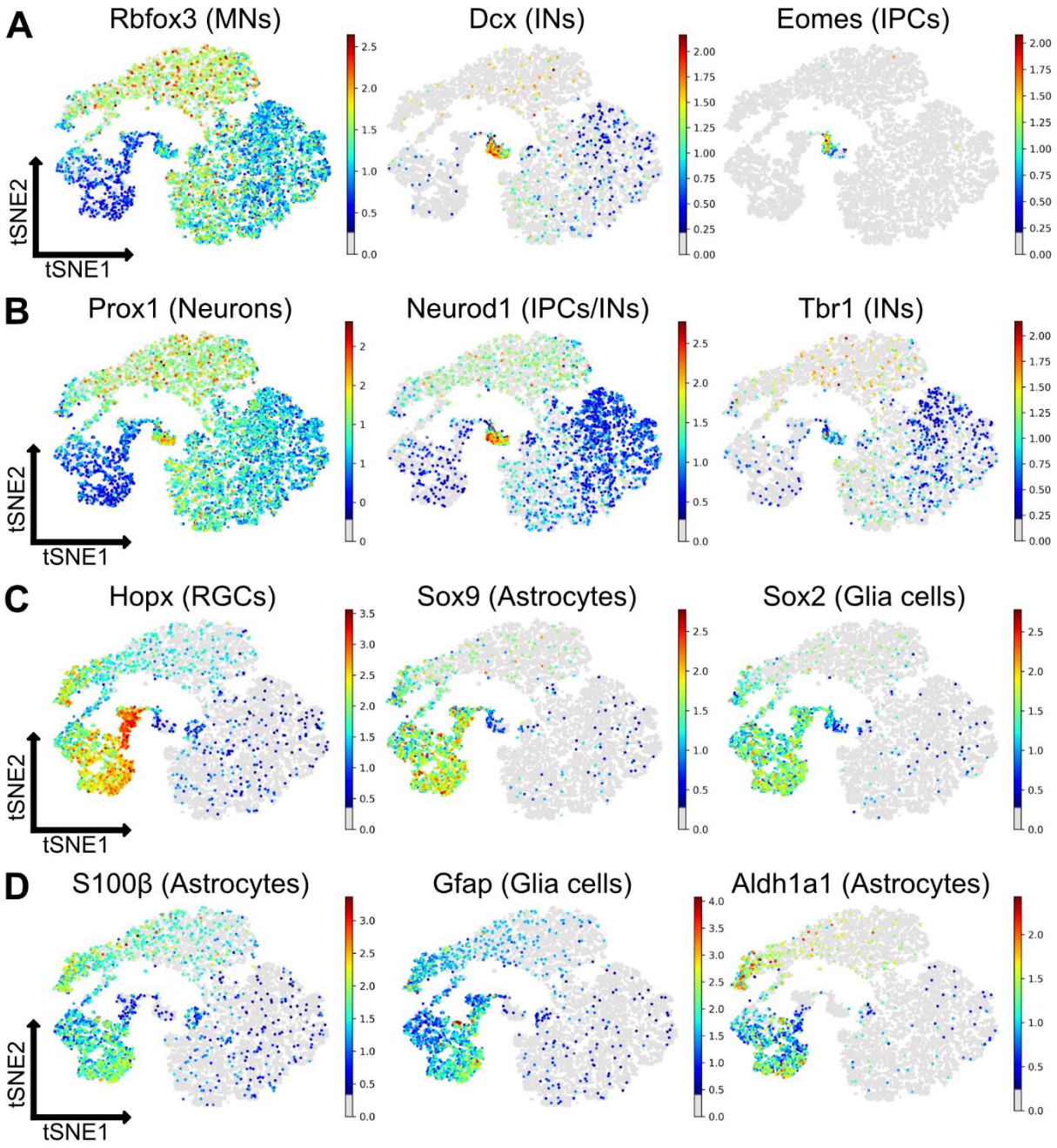

Figure 24: Key markers of the neurogenic and glia lineage display the cell cluster identities. tSNE visualisation of the dataset shown in **Figure 23C** displaying - (**A**) the expression pattern of the genes Rbfox3 (NeuN), Dcx and Eomes (Tbr2) for the identity of the neuronal cells. - (**B**) the expression pattern of the genes Prox1, Neurod1 and Tbr1 for closer identification of neuronal cells. - (**C**) the expression pattern of the genes Hopx, Sox9 and Sox2 for the identity of glia cells. - (**D**) the expression pattern of the genes S100β, Gfap and Aldh1a1 for closer identification of glia cells. Vertical scale on the right side of the graphs represent the relative expression level of the shown genes compared to a common set of housekeeping genes.

3.4 Characterization of the transient state cell cluster

3.4.1 TSC cluster as potential consequence of Pum2 deficiency

My further analysis of the scRNA-seq dataset revealed a compelling association between the previously identified TSC cluster and the $Pum2^{GT/GT}$ mice (**Figure 25A, B**). This cluster, characterised by a mixed expression profile of neuronal and glial markers, was almost exclusively composed of cells derived from Pum2-deficient mice. The striking nature of this observation underscores a potential link between Pum2 deficiency and the emergence of this potentially aberrant cell type. To further visualise this phenomenon, I generated density maps that starkly illustrated the shift in cellular distribution within the $Pum2^{GT/GT}$ DG. These maps highlighted a marked concentration of cells within the TSC cluster, accompanied by a statistically significant reduction in cell density across all other established cell clusters (**Figure 25C, D**). This finding suggests that the TSC cluster may expand at the expense of other cell types within the DG of Pum2-deficient mice. Quantitative cell counts unequivocally supported this interpretation, revealing a substantial seven-fold increase in TSC abundance within the $Pum2^{GT/GT}$ DG compared to WT controls (**Figure 25E**). This dramatic increase raises the intriguing possibility that Pum2 deficiency leads to a specific accumulation of TSCs, potentially disrupting the normal cellular composition and dynamics of the DG. Collectively, these findings point towards a statistically significant role for Pum2 in regulating cell fate and differentiation within the DG. The emergence and expansion of the TSC cluster in Pum2-deficient mice warrant further investigation to determine the precise identity of these cells.

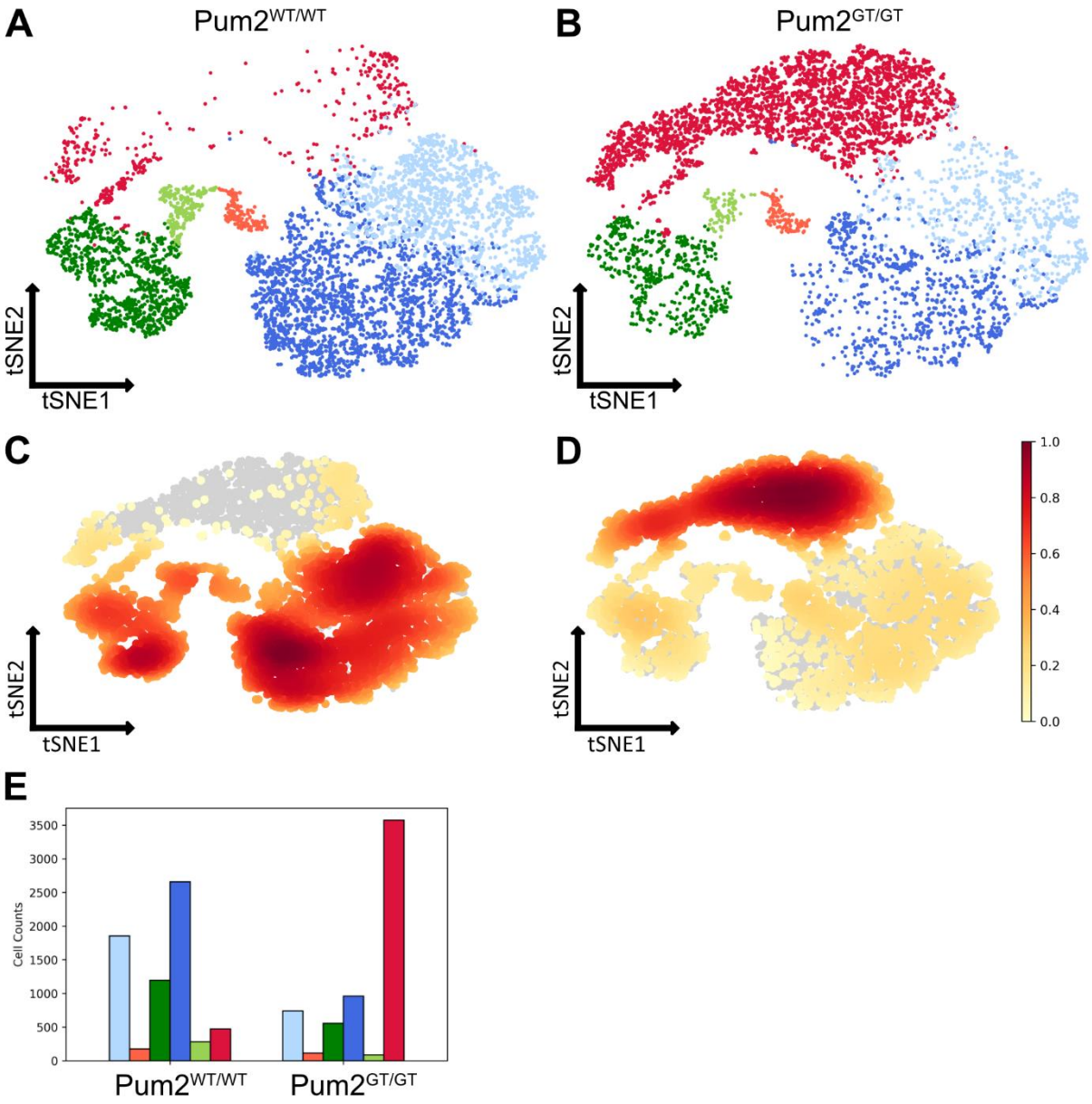

Figure 25: DG scRNA-seq data reveals a massive shift of cells from canonical cell types of the neurogenic lineage towards the TSC cluster upon Pum2 deficiency. (**A, B**) tSNE visualisation of the neurogenesis and astrogenesis associated cell clusters in the $Pum2^{WT/WT}$ and $Pum2^{GT/GT}$ mice. (**C, D**) tSNE visualisation of the density distribution over the cell clusters in the $Pum2^{WT/WT}$ and $Pum2^{GT/GT}$ mice. (**E**) Bar plot visualising the total number of cell in each cluster corresponding to $Pum2^{WT/WT}$ and $Pum2^{GT/GT}$ mice.

3.4.2 TSCs accumulate in the granular cell layer in Pum2 deficiency

The surprising discovery of cells with a mixed expression profile, defying conventional classification within the DG, prompted a deeper investigation of the TSC cluster. My initial goal was to identify genes uniquely expressed by TSCs to definitively establish their existence. Despite the lack of clear-cut markers, I selected three genes with overlapping expression patterns within the TSC cluster. Neurogranin (Nrgn): Primarily expressed in the DN and TSC clusters (**Figure 26A**), Nrgn is involved in synapse formation and neuronal signalling (Zhong et al., 2009). Thymosin beta 4 (Tmsb4x): Primarily expressed in the IPC/IN and TSC clusters (**Figure 26A**), Tmsb4x plays a role in dendritic development (Sun et al., 2018). Aldolase C (Aldoc): Expressed in both MA and TSC clusters (**Figure 26B**), this astrocyte-associated gene is involved in glycolysis and structural organization (Cahoy et al., 2008). The overlap of these genes, particularly within the $Pum2^{GT/GT}$ TSC cluster (**Figure 26D**), provided a means to target these cells specifically. This difference was further underscored by a five-fold increase in TSC abundance within Pum2-deficient mice (**Figure 26C**). Western blot analysis did not reveal mayor changes of the protein expression in the DG between $Pum2^{WT/WT}$ and $Pum2^{GT/GT}$ mice (data not shown). To validate TSCs and examine their spatial distribution, I performed RNA visualisation on 10µm brain sections (**Figure 27A**). By analysing the perinuclear region for triple-positive cells (**Figure 27B**), I confirmed both the existence of TSCs and their statistically significant increase within $Pum2^{GT/GT}$ mice (**Figure 27C**). Furthermore, analysis of TSC localization revealed a preferential accumulation within the granular cell layer of Pum2-deficient mice, with no statistically significant changes observed in the SGZ (**Figure 27D, E**). These findings strongly support the existence of transient state cells within the DG and suggest their potential accumulation within the granular cell layer as a consequence of Pum2 deficiency.

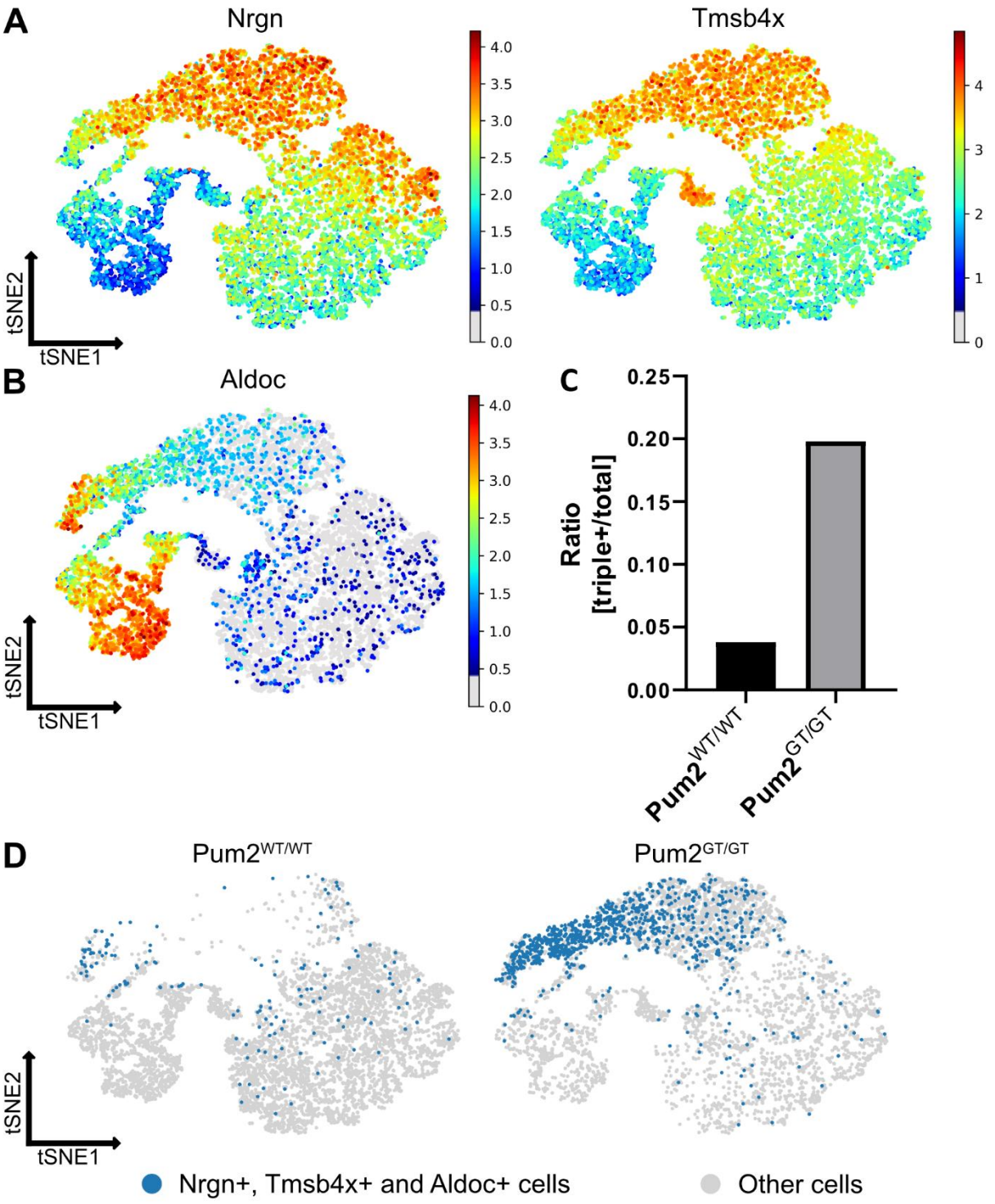

Figure 26: RNA expression of neuronal and glia genes in individual cells offer a potential avenue for visualising TSCs. (**A**) tSNE visualisation of the neuronal associated gene expression pattern of Nrgn and Tmsb4x as well as the glia associated gene Aldoc. (**B**) tSNE visualisation of the strong expression overlap of the corresponding genes within one cell in the colour blue and the other cells in grey. (**C**) Bar plot visualising the ratio of cell positive for the corresponding genes compared to all cells of the scRNA-seq within Pum2$^{WT/WT}$ and Pum2$^{GT/GT}$ mice.

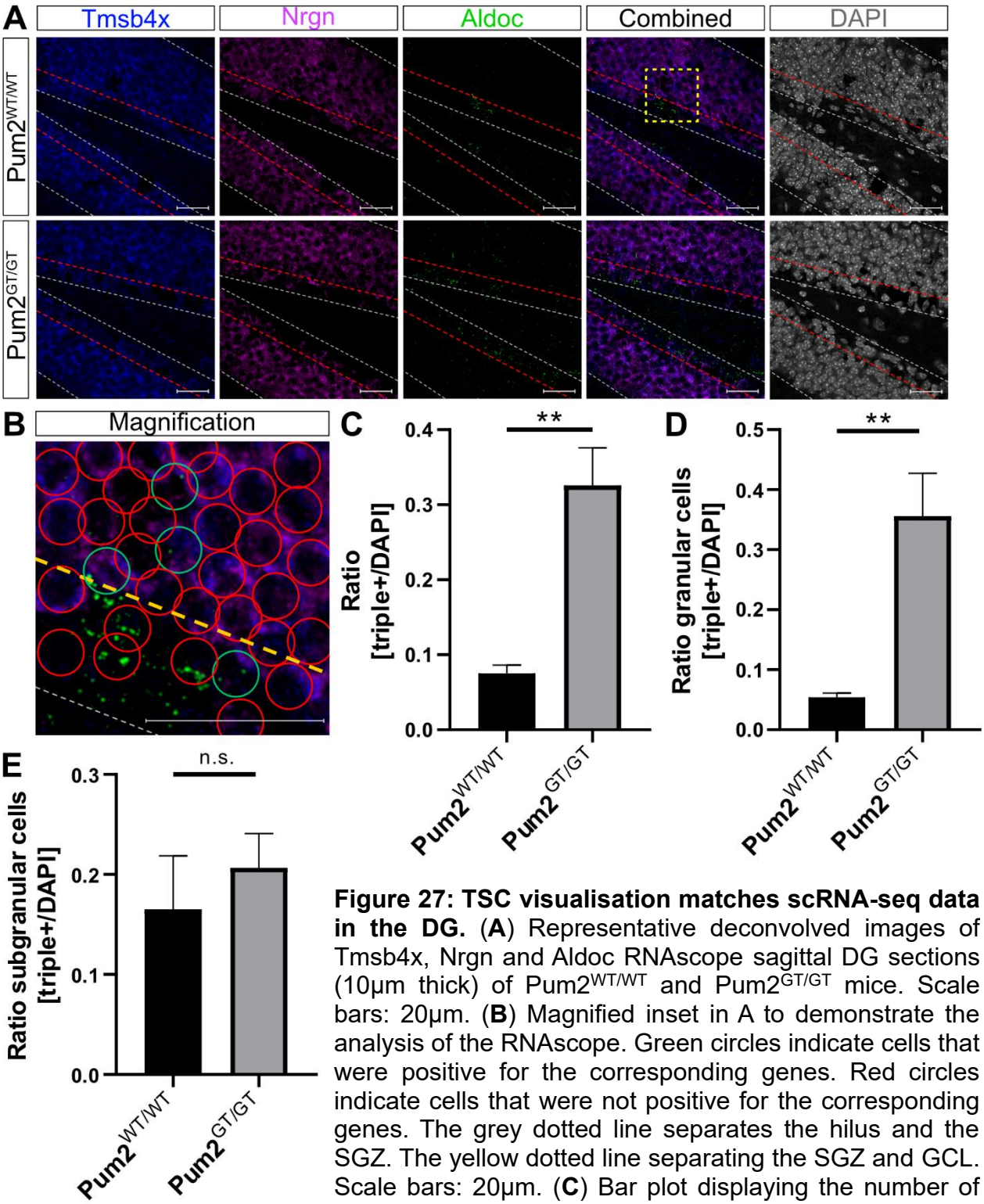

Figure 27: TSC visualisation matches scRNA-seq data in the DG. (**A**) Representative deconvolved images of Tmsb4x, Nrgn and Aldoc RNAscope sagittal DG sections (10µm thick) of $Pum2^{WT/WT}$ and $Pum2^{GT/GT}$ mice. Scale bars: 20µm. (**B**) Magnified inset in A to demonstrate the analysis of the RNAscope. Green circles indicate cells that were positive for the corresponding genes. Red circles indicate cells that were not positive for the corresponding genes. The grey dotted line separates the hilus and the SGZ. The yellow dotted line separating the SGZ and GCL. Scale bars: 20µm. (**C**) Bar plot displaying the number of cells positive for the corresponding genes compared to all cells. (**D**) Bar plot displaying the number of cells positive for the three genes in the GCL compared to all cells in the GCL. (**E**) Bar plot displaying the number of cells positive for the corresponding genes in the SGZ compared to all cells in the SGZ. The graphs consist of 4 independent biological replicates. Asterisks represent p-values obtained by (**C, D, E**) unpaired Welch's t-test (**$p < 0.01$, n.s. ≥ 0.05).

3.4.3 Protein-level validation and morphological analysis of TSCs

Having confirmed the existence of TSCs at the RNA level, I sought to demonstrate their presence at the protein level. I selected well-established markers to visualise the mixed lineage profile of these cells. Thymosin beta 4 (Tmsb4x): A marker of neuronal character, previously identified in RNA analysis (**Figure 28A**). Creatine kinase B-type (Ckb): A glial marker expressed throughout the TSC cluster, crucial for energy metabolism in brain glial cells (**Figure 28B**) (Wong et al., 2012). The combined expression of Tmsb4x and Ckb primarily overlapped within the TSC cluster, with a statistically significant fivefold increase observed in $Pum2^{GT/GT}$ mice (**Figure 28C,D**). Immunostaining for these markers confirmed the existence of double-positive cells in both $Pum2^{GT/GT}$ and $Pum2^{WT/WT}$ mice (**Figure 29A**). Quantification revealed a threefold increase in double-positive cells within the $Pum2^{GT/GT}$ DG, consistent with previous data (**Figure 29B**). Importantly, immunostaining provided initial insights into TSC morphology. Some TSCs displayed radial or immature neuron-like shapes (**Figure 29A**, magnification). Further analysis demonstrated a statistically significant increase in the length of dendritic processes in TSCs from $Pum2^{GT/GT}$ mice compared to controls (**Figure 29C**). Interestingly, the number of TSCs extending into the molecular layer of the hippocampus remained comparable between genotypes (**Figure 29D**). These results establish the existence of TSCs at the protein level, corroborating RNA sequencing and RNAscope findings. Moreover, my observations provide intriguing clues about the morphological characteristics of TSCs and suggest potential alterations in their dendritic development in the context of Pum2 deficiency.

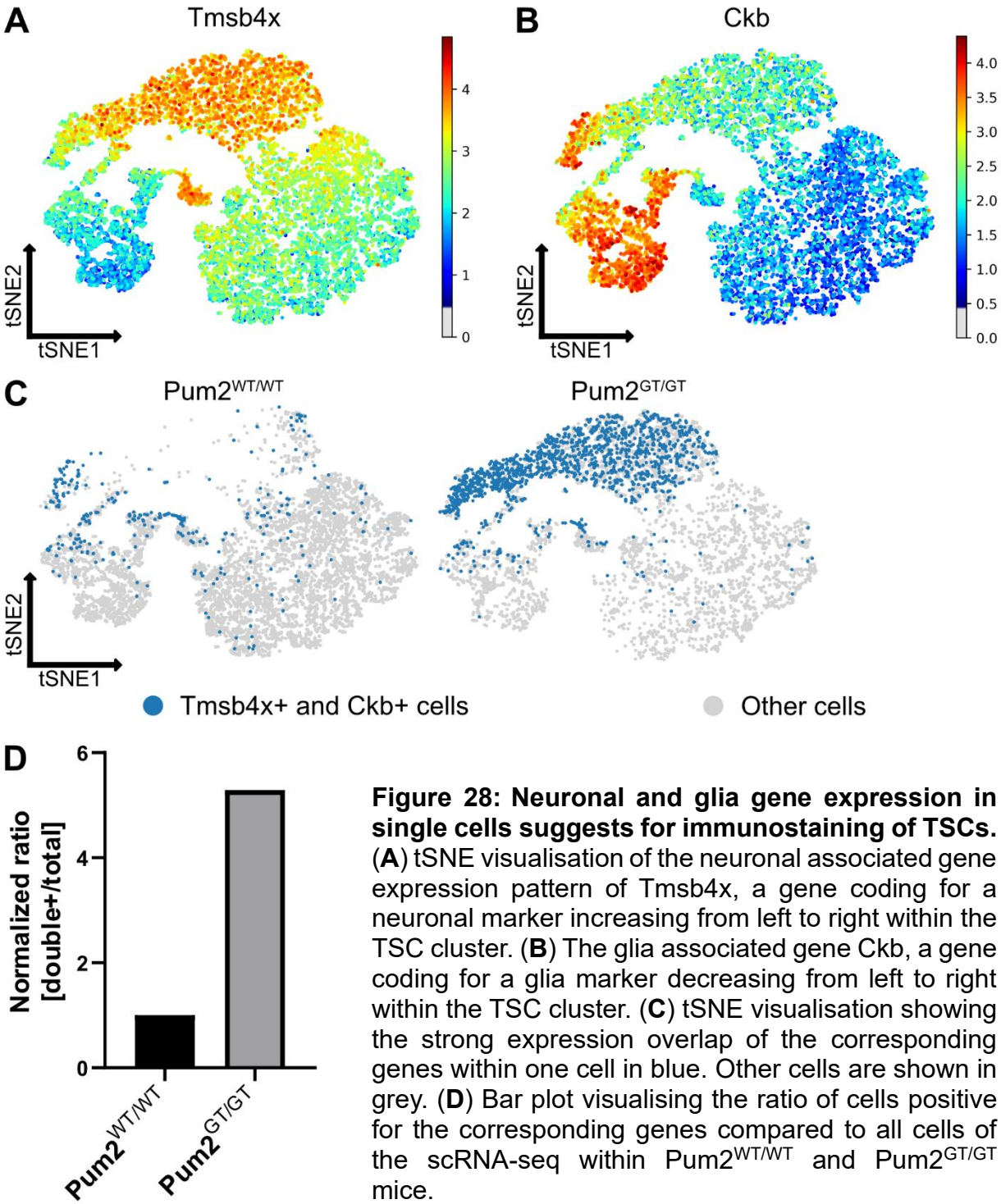

Figure 28: Neuronal and glia gene expression in single cells suggests for immunostaining of TSCs. (**A**) tSNE visualisation of the neuronal associated gene expression pattern of Tmsb4x, a gene coding for a neuronal marker increasing from left to right within the TSC cluster. (**B**) The glia associated gene Ckb, a gene coding for a glia marker decreasing from left to right within the TSC cluster. (**C**) tSNE visualisation showing the strong expression overlap of the corresponding genes within one cell in blue. Other cells are shown in grey. (**D**) Bar plot visualising the ratio of cells positive for the corresponding genes compared to all cells of the scRNA-seq within Pum2$^{WT/WT}$ and Pum2$^{GT/GT}$ mice.

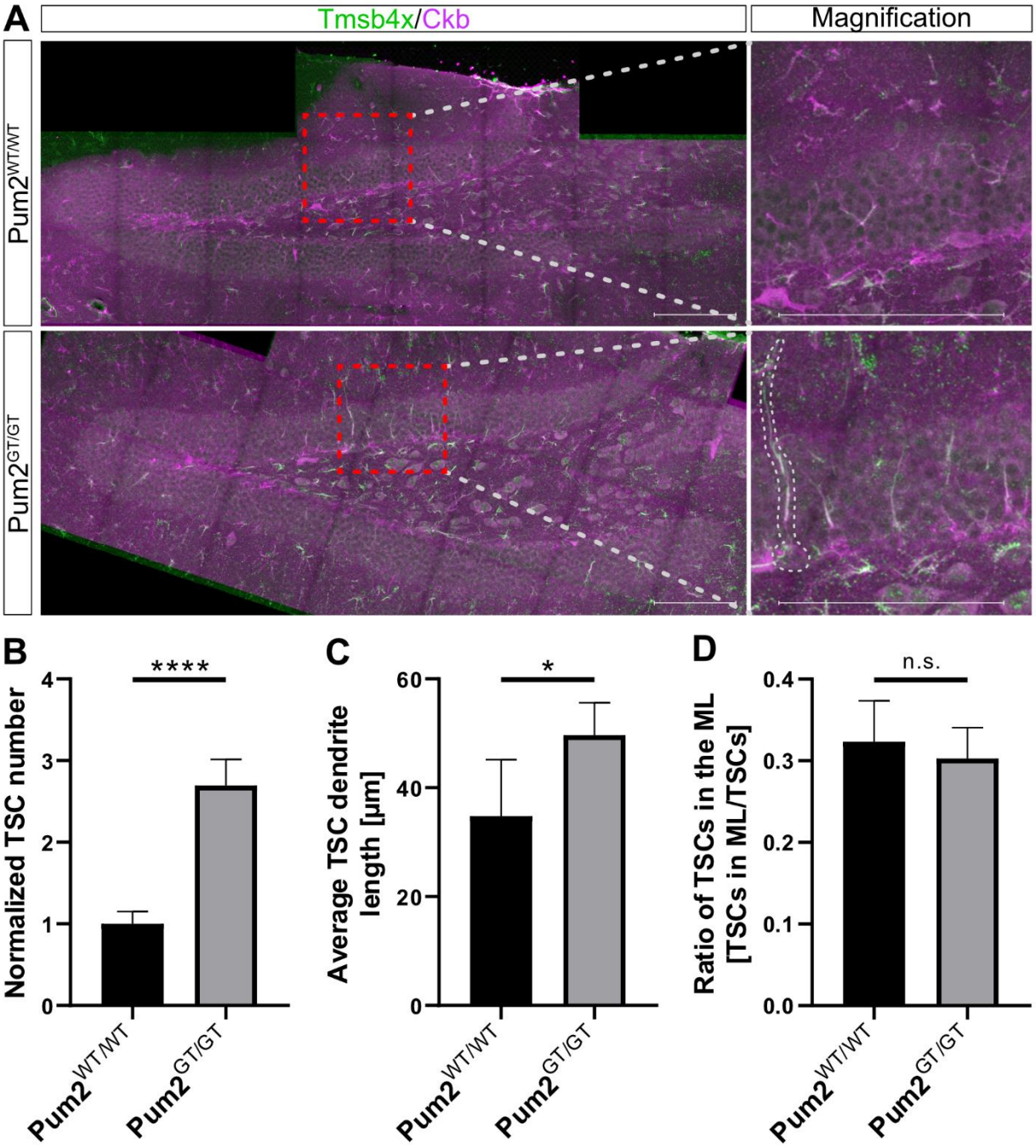

Figure 29: Immunostaining allows the visualisation of TSCs in the DG. (**A**) Representative Z-stack images of Tmsb4x and Ckb immunostaining on sagittal DG sections (40µm thick) of $Pum2^{WT/WT}$ and $Pum2^{GT/GT}$ mice (left side). Cells strongly expressing Ckb and Tmsb4x result in a white signal and therefore will be counted as TSC. Magnification of the red dotted square with indication of the possible morphology indicated by the grey dotted line (right side). Scale bars: 200µm. (**B**) Bar plot displaying the normalised number of cells positive for the two proteins. (**C**) Bar plot displaying the average dendritic length of the cells positive for the two proteins. (**D**) Bar plot displaying the number of cells positive for the two genes that reach into the ML of the DG. The graphs consist of independent biological replicates (n = 4). Asterisks represent p-values obtained by (**B, C, D**) unpaired Student's t-test (****$p < 0.0001$, *$p < 0.01$, n.s. ≥ 0.05).

3.5 Downregulation of Pum2 in the adult hippocampal neurogenic nice

3.5.1 Investigating the origin and dynamics of TSCs

Having established the existence of TSCs, I sought to determine their cellular origin using bioinformatic analysis of my scRNA-seq dataset. Therefore, I employed direct trajectory inference based on the previously visualised tSNE maps of the scRNA-seq dataset. As expected, $Pum2^{WT/WT}$ mice exhibited trajectories consistent with established neuronal differentiation, progressing from the IPC/IN cluster towards DN and MN clusters (**Figure 30A**, left panel). While only one trajectory emerged from the RGC cluster in controls, likely due to the limited number of differentiating RGCs in adulthood, I observed a striking direct trajectory from the RGC cluster to the TSC cluster in $Pum2^{GT/GT}$ mice (**Figure 30A**, right panel). This might indicate for a glial-to-neuron transition. To better understand the dynamics within the TSC cluster, I focused on this part and identified four subclusters based on their position and gene expression: RGC-like TSC, astrocyte-like TSC, mixed Identity cells, and neuron-like TSC. A clear trajectory emerged within these subclusters, progressing from RGC-like TSC through astrocyte-like and mixed Identity cells towards the neuron-like TSC (**Figure 30B**). Refined analysis of the $Pum2^{WT/WT}$ dataset, independent of $Pum2^{GT/GT}$ counterpart, revealed that the TSC cluster separated into two distinct subclusters (**Figure 30C**). One subcluster localized between the IPC/IN and DN clusters, potentially representing an intermediate differentiation state. The other subcluster positioned near the MA cluster, suggesting a possible specialization from mature astrocytes. In collaboration with Dr. Gregor Pilz, I further investigated the role of Pum2 in specifically adult neurogenesis by injecting retroviruses encoding either Pum2-targeting miRNAs (Pum2 miRNA-1/-2) or a control scrambled miRNA (Control miRNA) into the DG of adult WT mice (**Figure 31A**). This approach specifically targeted dividing RGCs and IPCs (Bonaguidi et al., 2011). Additionally, it will allow me to generate TSC as predicted by the direct trajectories and follow their morphology. Preliminary results demonstrated a statistically significant downregulation of Pum2 with Pum2 miRNA-2 compared to the control miRNA (**Figure 31B**). While Pum2 miRNA-1 showed some reduction, it was less pronounced than Pum2 miRNA-2. These initial findings suggest that Pum2 can be successfully downregulated in RGCs/IPCs and their progeny.

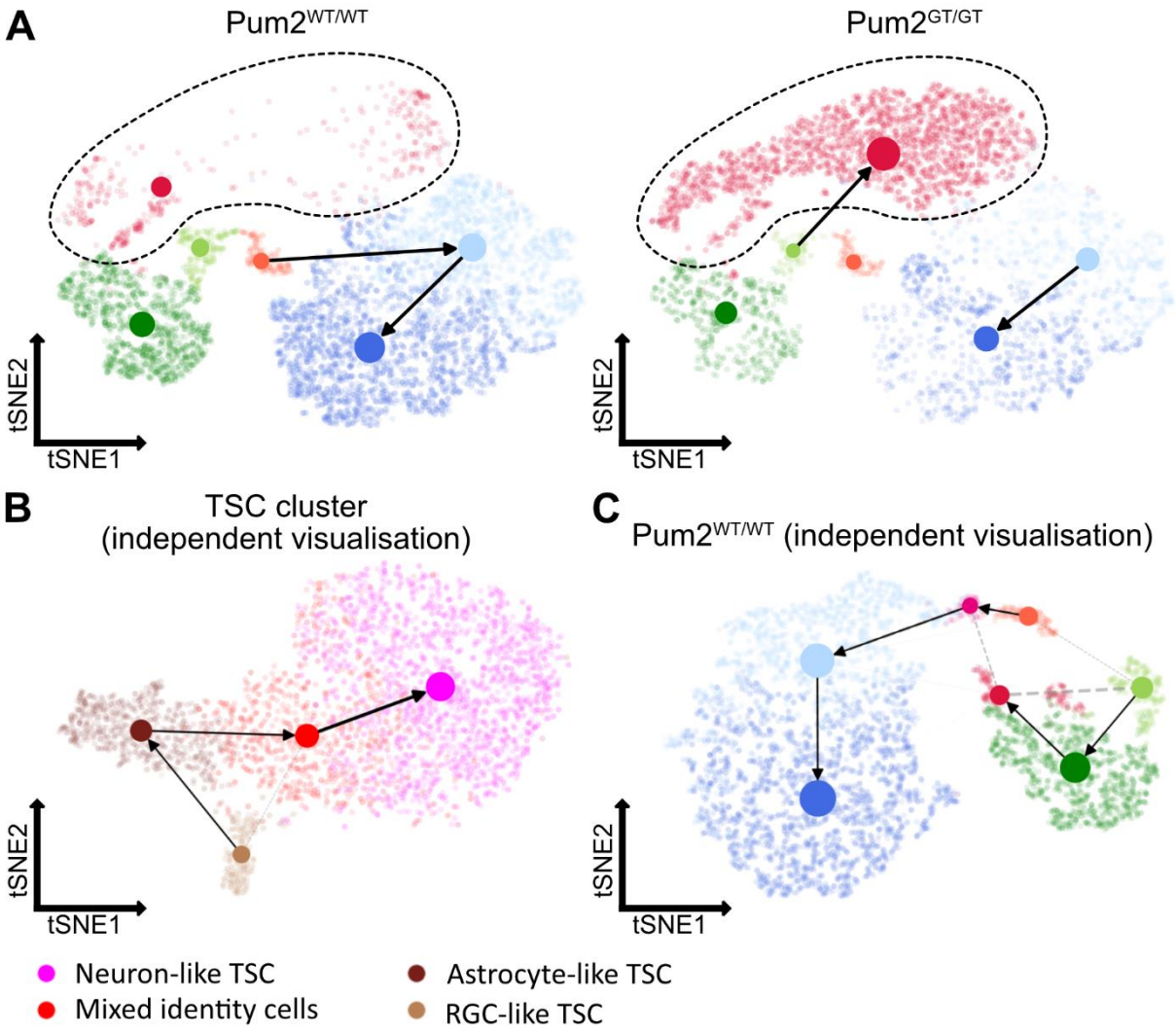

Figure 30: Direct trajectory analysis identifies RGCs as TSC origin. (**A**) tSNE visualisation of the direct trajectories of Pum2$^{WT/WT}$ and Pum2$^{GT/GT}$ scRNA-seq dataset. (**B**) tSNE visualisation of the direct trajectories within the TSC cluster of the combined scRNA-seq dataset of Pum2$^{WT/WT}$ and Pum2$^{GT/GT}$ (dotted line in A). (**C**) tSNE visualisation of the direct trajectories of Pum2$^{WT/WT}$ scRNA-seq dataset that was independently processed from the Pum2$^{GT/GT}$ dataset.

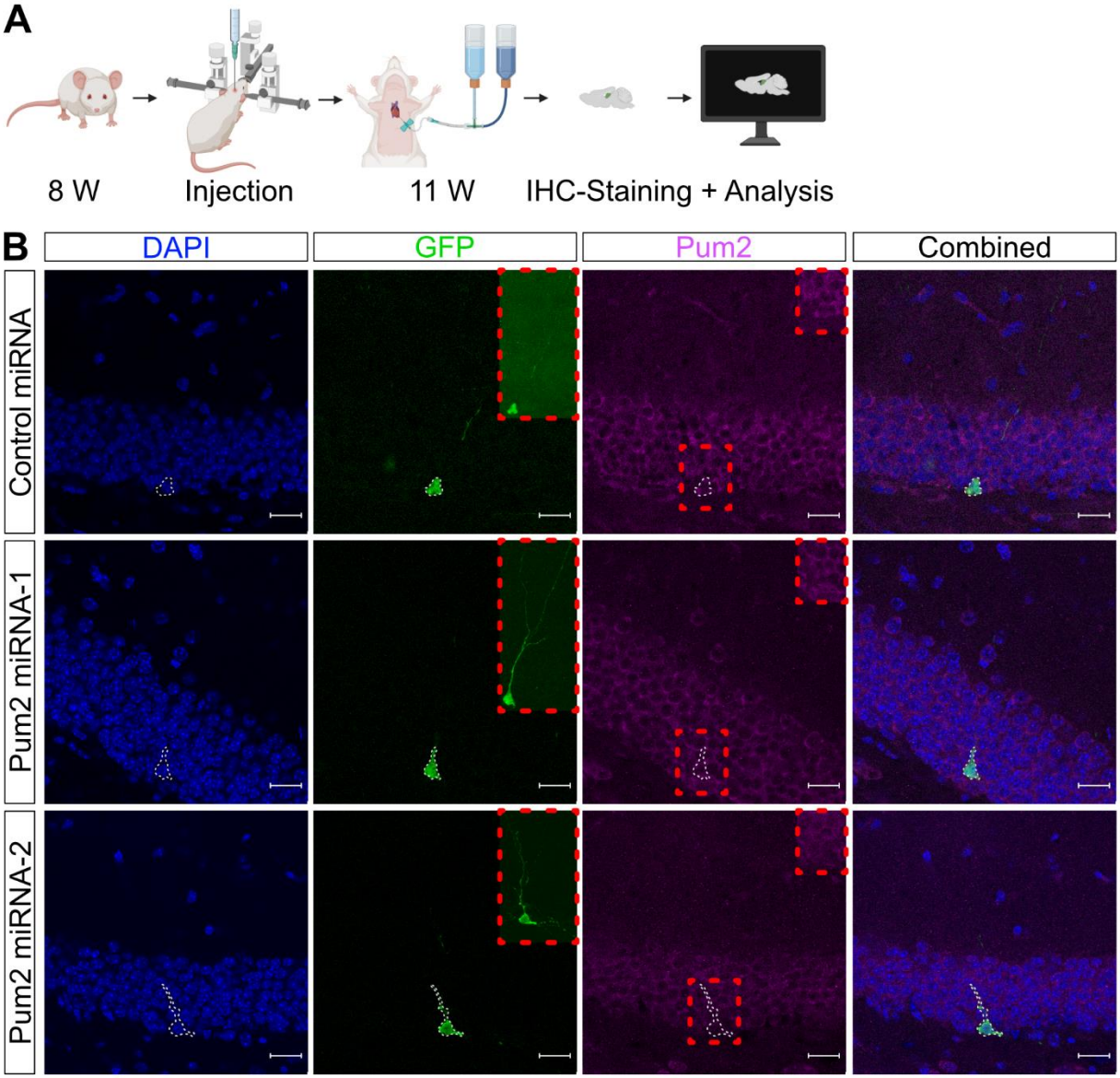

Figure 31: miRNA downregulated Pum2 in the WT DG. (**A**) Experimental outline of the stereotactic injection of the retrovirus encoding GFP together with miRNAs against Pum2 or a control miRNA. Created with BioRender.com. Agreement number: ER2759XYDL (**B**) Representative images of DAPI, GFP and Pum2 immunostaining on sagittal/coronal DG sections (40µm thick) of Pum2 downregulated (Pum2 miRNA-1/2) or control (Control miRNA) cells that were GFP-positive. The white dotted line surrounds the GFP-positive cell body in all channels. The red dotted line shows the Z-projection of the GFP-labelled cells and in the Pum2 channel the signal for Pum2 in the region of GFP-positive cells. Scale bars: 20µm.

3.5.2 Assessing morphological changes and characteristics of Pum2 downregulated cells

Having successfully demonstrated Pum2 downregulation in RGCs/IPCs and their progeny, my focus shifted to investigating the phenotypic consequences of miRNA-mediated Pum2 depletion and the formation of the TSCs. To this end, I first examined the morphology of GFP-positive cells. In all cases, the miRNAs give rise to well-developed neurons (**Figure 32A**). However, in the Pum2 miRNA groups, aberrant or less-developed cells were also observed. Specifically, these aberrant cells were categorised into distinct morphological subtypes, including "Altered Dendrite", "Double Dendrite" and "Large 1° Dendrite" (**Figure 32B**). The "Altered Dendrite" group is characterised by an abnormal dendrite shape, exhibiting uneven thickness and irregular directionality (**Figure 32B**, left panel). The "Double Dendrite" group is defined by the presence of two dendrites originating from the top of the cell body and extending into the GCL (**Figure 32B**, middle panel). The "Large 1° Dendrite" group is distinguished by the presence of a single, large, and short primary dendrite (**Figure 32B**, right panel). In addition to these aberrant morphologies, less-developed cells were also observed and classified into distinct groups. The "Glia-Neuronal Shape" group displays characteristics of both glial cells and neurons, suggesting an incomplete or disrupted differentiation process (**Figure 32C**, left panel). The "Clustered Cells" group consists of multiple cells in close proximity, potentially representing a cluster of very immature cells that have not yet fully separated and migrated to their final positions (**Figure 32C**, middle panel). Finally, the "Curved Dendrite" group exhibits a primary dendrite with an abnormal curvature, a characteristic often associated with immature or developing neurons that have not yet established their mature morphology (**Figure 32C**, right panel). Beyond morphological assessment, I investigated the impact of Pum2 deficiency on cell migration. Analysis of GFP-positive cell positions within the GCL (**Figure 33A**) revealed no statistically significant difference for Pum2 miRNA-1 compared to the control. However, the Pum2 miRNA-2 condition showed a statistically significant higher proportion of cells in the GCL, suggesting that Pum2 depletion, particularly via Pum2 miRNA-2, may accelerate cell migration into this layer. Next, I sought to determine whether the GFP-positive cells exhibited a neuronal phenotype through morphological assessment and immunostaining (**Figure 33B**). While the fraction of neurons in the Pum2 miRNA-1 condition did not statistically significant differ

from the control, a trend towards non-neuronal cells was observed. This effect was more pronounced in the Pum2 miRNA-2 condition, suggesting Pum2 depletion hinders neuronal differentiation. Subsequently, I investigated whether neurons within the GFP-positive population displayed normal or aberrant morphologies. In both Pum2 miRNA conditions, a statistically significant two- to threefold increase in the proportion of neurons with abnormal morphology was observed (**Figure 33C**). This effect was slightly more pronounced in the Pum2 miRNA-2 condition, suggesting a dose-dependent relationship between Pum2 depletion and neuronal morphological abnormalities. Overall, these findings indicate that Pum2 deficiency leads to a decrease in the fraction of normally developed neurons and a concomitant increase in the proportions of glial cells and aberrant neurons within the GFP-positive cell population (**Figure 33D**). This underscores the critical role of Pum2 in regulating neuronal differentiation and maintaining proper neuronal morphology. Concurrent with the observation of aberrant and less-developed neurons, Pum2 deficient neurons exhibited a statistically significant decrease in the length of their primary dendrites (**Figure 34A, B**). In control neurons, the average primary dendrite length was 42 µm after 3 weeks, consistent with previous findings (Cole et al., 2020). Given the stronger effects of Pum2 miRNA-2, subsequent analyses focused on comparing it to the control miRNA. To investigate if RGCs give rise to TSCs, RNAscope was used to assess co-expression of neuronal gene Nrgn and glial gene Aldoc in GFP-positive cells (**Figure 35A**). This revealed a small subset of Pum2 miRNA-2 GFP-positive cells co-expressing both markers, suggesting a potential neuronal-glial transition state. To further support this observation, I performed co-immunostaining for the glial marker Sox9 and the neuronal marker Dcx (**Figure 35B**). Similar to the RNAscope results, only a few cells were detected that co-expressed both markers, further suggesting the presence of a transitional cell population with mixed glial and neuronal characteristics. While preliminary findings suggest the presence of a TSCs, the limited number of identified cells necessitates further replicates to solidify these observations and enable robust statistical analysis. The apparent differences between Pum2 miRNA-1 and Pum2 miRNA-2 regulation are likely attributed to differential Pum2 downregulation efficiencies. Importantly, these results should be interpreted with caution due to the small sample size and may evolve with additional data collection.

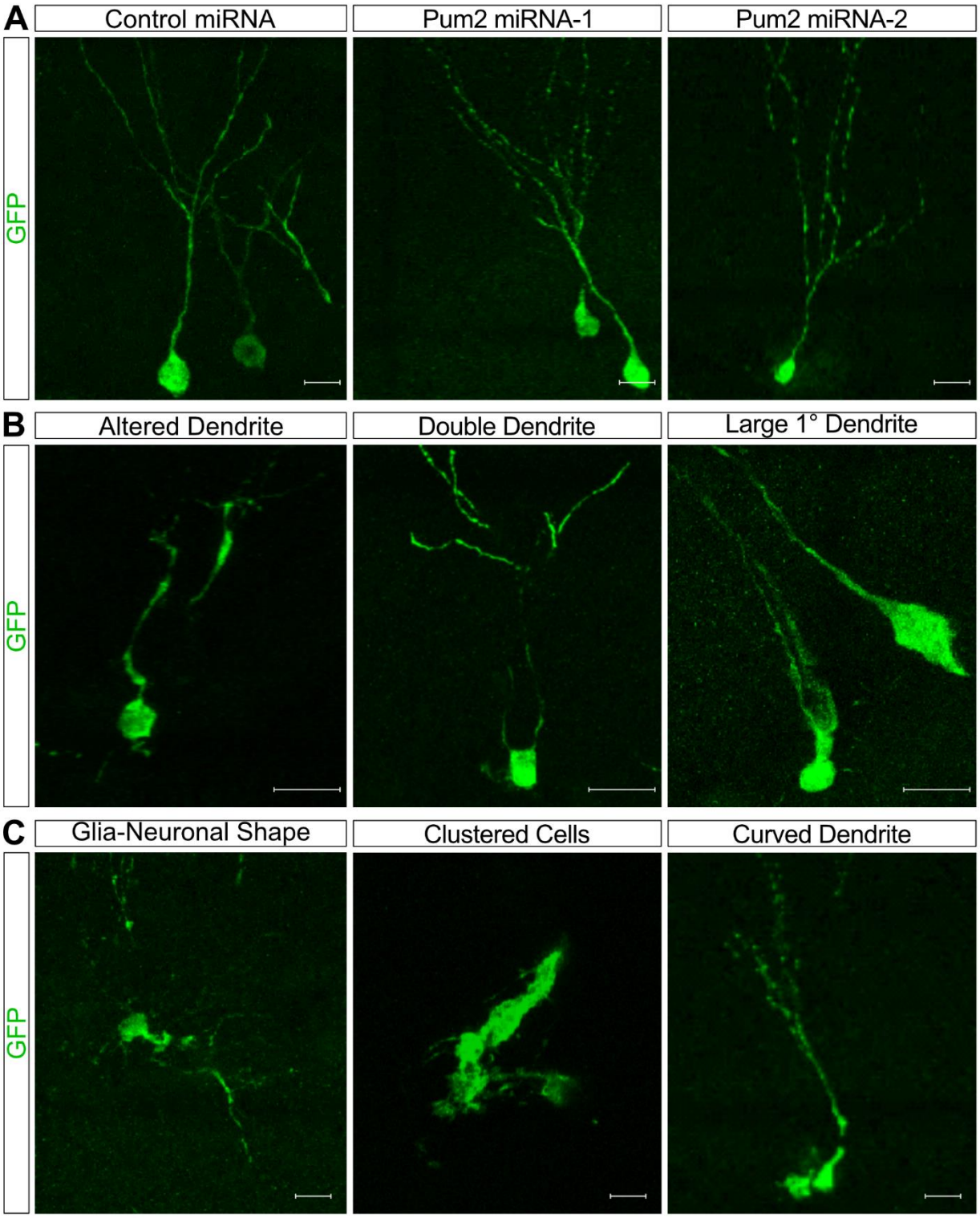

Figure 32: Pum2 depletion in RGCs/IPCs causes aberrant neuronal morphology. (**A**) Representative images of GFP positive well-developed neurons in the sagittal/coronal DG sections (40µm thick) of Pum2 downregulated (Pum2 miRNA-1 & 2) and control (Control miRNA) conditions. Scale bars: 20µm. (**B**) Representative images of GFP positive altered neuronal morphology and astrocytes in the sagittal/coronal DG sections (40µm thick) of Pum2 downregulated (Pum2 miRNA-1 & 2) conditions grouped by "Altered Dendrite", "Double Dendrite" and "Large 1° Dendrite". Scale bars: 20µm. (**C**) Representative images of GFP positive less-developed neuronal morphology in the sagittal/coronal DG sections (40µm thick) of Pum2 downregulated (Pum2 miRNA-1 & 2) conditions grouped by "Glia-Neuronal Shape", "Clustered Cells" and "Curved Dendrite". Scale bars: 20µm.

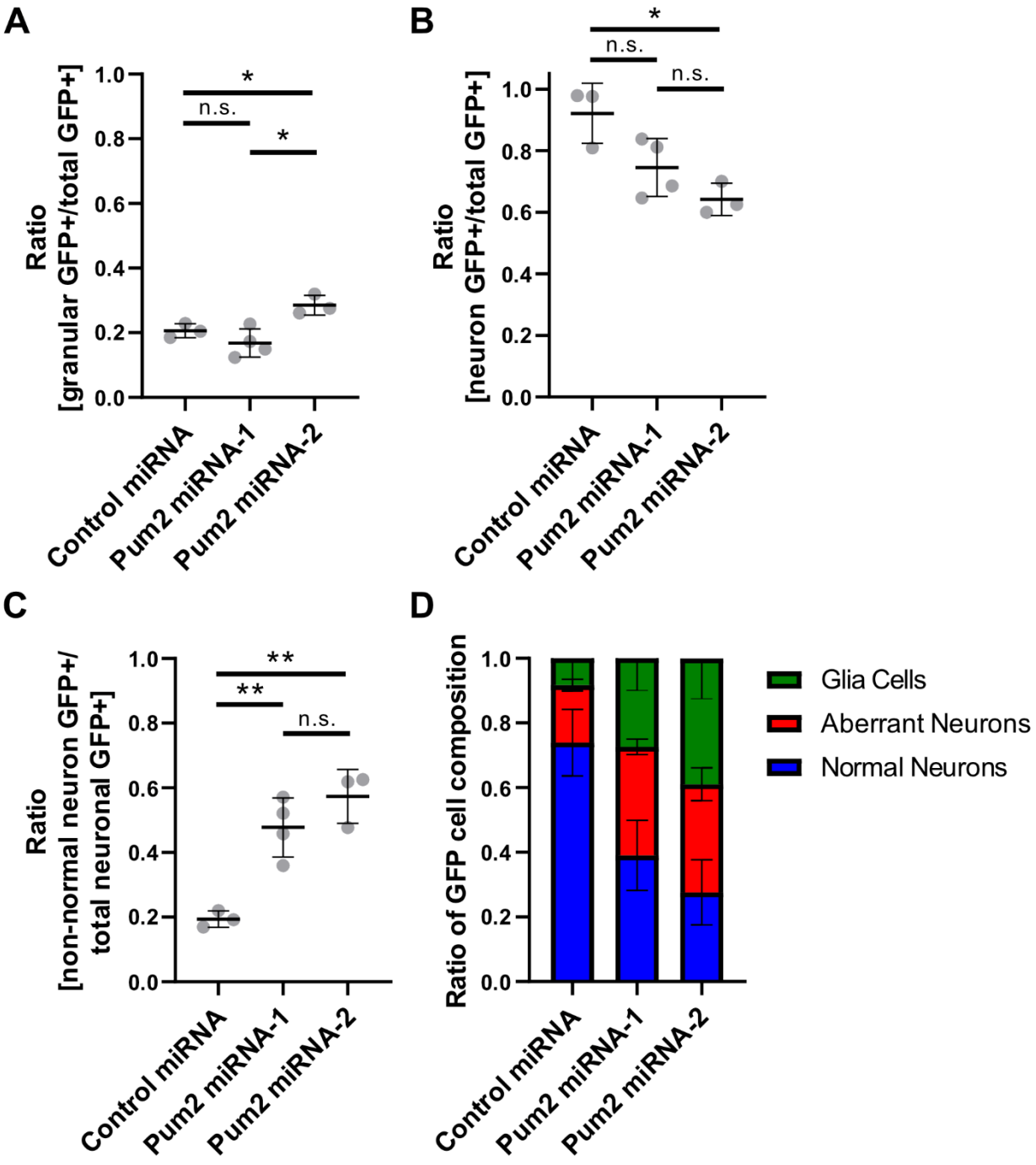

Figure 33: Pum2 deficiency increases aberrant morphology in adult-born DG neurons. (**A**) Dot plot displaying the ratio of GFP positive cells located in the GCL compared to all GFP positive cells in the DG injected with Control miRNA, Pum2 miRNA-1 and Pum2 miRNA-2. (**B**) Dot plot displaying the ratio of GFP positive cells with neuronal morphology compared to all GFP positive cells in the DG. (**C**) Dot plot displaying the ratio of GFP positive with aberrant neuronal morphology compared to all GFP positive neurons in the DG. (**D**) Stacked-bar graph displaying the normalised fraction of cell types classified by "Glia Cells", "Aberrant Neurons" and "Normal Neurons". Mean and standard deviation are shown. Circles indicate independent biological replicates (n = 3, 4). Asterisks represent p-values obtained by (**A, B, C**) unpaired Student's t-test (**p < 0.01, *p < 0.05, n.s. ≥ 0.05).

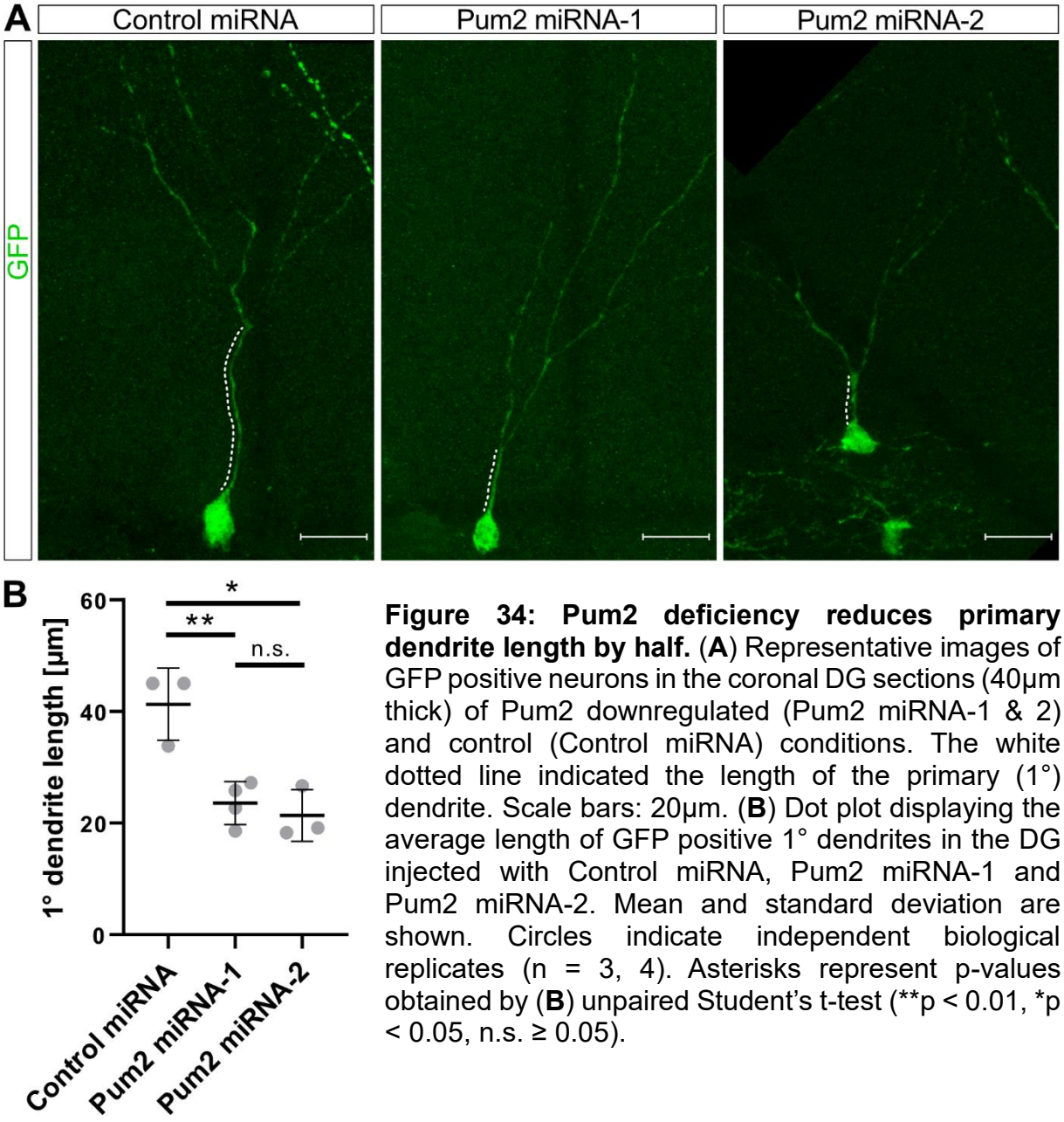

Figure 34: Pum2 deficiency reduces primary dendrite length by half. (**A**) Representative images of GFP positive neurons in the coronal DG sections (40µm thick) of Pum2 downregulated (Pum2 miRNA-1 & 2) and control (Control miRNA) conditions. The white dotted line indicated the length of the primary (1°) dendrite. Scale bars: 20µm. (**B**) Dot plot displaying the average length of GFP positive 1° dendrites in the DG injected with Control miRNA, Pum2 miRNA-1 and Pum2 miRNA-2. Mean and standard deviation are shown. Circles indicate independent biological replicates (n = 3, 4). Asterisks represent p-values obtained by (**B**) unpaired Student's t-test (**p < 0.01, *p < 0.05, n.s. ≥ 0.05).

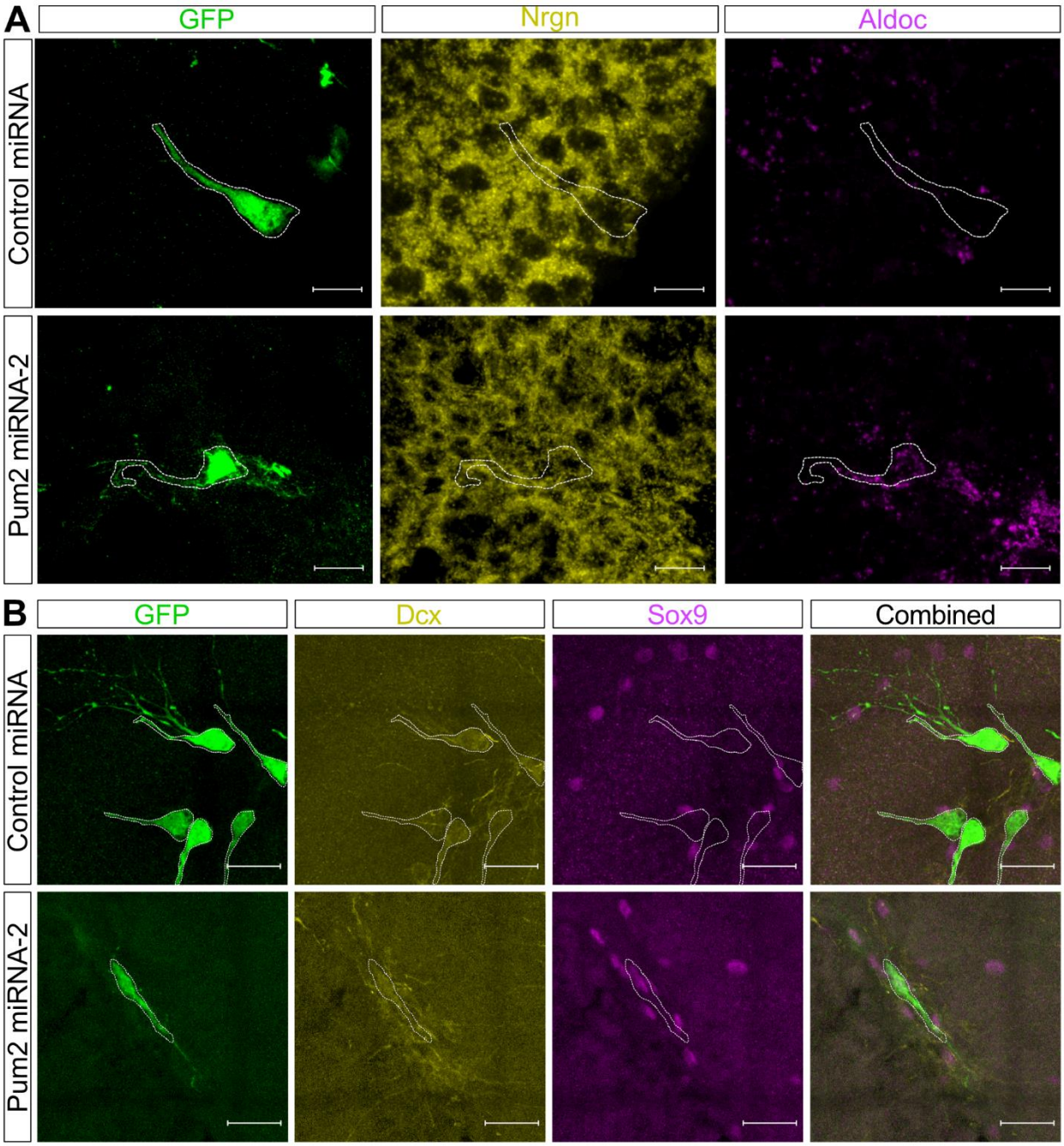

Figure 35: Pum2 deficient cells exhibit characteristics of TSCs. (**A**) Representative deconvolved images of Nrgn and Aldoc mRNA detected by RNAscope on coronal DG sections (10µm thick) and GFP immunostaining of Pum2 downregulated (Pum2 miRNA-2) and control (Control miRNA) conditions. The white dotted line surrounds the GFP positive cell body in all channels. Scale bars: 20µm. (**B**) Representative images of an immunostaining for GFP, Dcx and Sox9 on coronal DG sections (40µm thick) of Pum2 downregulated (Pum2 miRNA-2) and control (Control miRNA) conditions. The white dotted line surrounds the GFP positive cell bodies in all channels. Scale bars: 20µm.

3.6 TSC cluster shows an increase in translation and deficits in neuronal development

To gain deeper insights into the characteristics of the TSC cluster, I performed additional bioinformatic analyses. Differential gene expression analysis, followed by Gene Ontology (GO) (Ashburner et al., 2000; Gene Ontology et al., 2023) and Kyoto Encyclopedia of Genes and Genomes (KEGG) (Kanehisa, 2019; Kanehisa et al., 2023; Kanehisa & Goto, 2000) pathway analyses, revealed specific biological processes and pathways altered within the TSC cluster. GO analysis of upregulated processes highlighted a statistically significant enrichment of translation-associated processes and mitochondrial electron transport (**Figure 36A**). KEGG analysis corroborated this finding, with a marked increase in ribosomal proteins, suggesting a potential upregulation of the translational machinery in $Pum2^{GT/GT}$ mice (**Figure 37A**). As the TSC cluster is predominantly observed in Pum2-deficient mice, this suggests a possible link between Pum2 depletion and increased translation. To investigate this further, I performed polysome profiling of DG tissue from five-month-old mice. Analysis revealed a small but consistent and statistically significant higher polysome to monosome ratio in $Pum2^{GT/GT}$ mice compared to controls (**Figure 38**). This indicates a possible altered translational activity in the DG of Pum2-deficient mice. Intriguingly, GO analysis also revealed a downregulation of processes associated with axogenesis, axon guidance, nervous system development, and synapse organization within the TSC cluster (**Figure 36B**). Consistent with this, KEGG analysis indicated decreased axon guidance pathways and an enrichment of genes associated with neurodegenerative diseases, including Parkinson's, Alzheimer's, and Huntington's disease (**Figure 37B**). Collectively, these findings suggest that Pum2 deficiency may lead to dysregulated translation and an accumulation of genes linked to neurodegeneration. Concurrently, TSCs appear to exhibit potential developmental deficits, with downregulation of genes crucial for neuronal development and synapse formation.

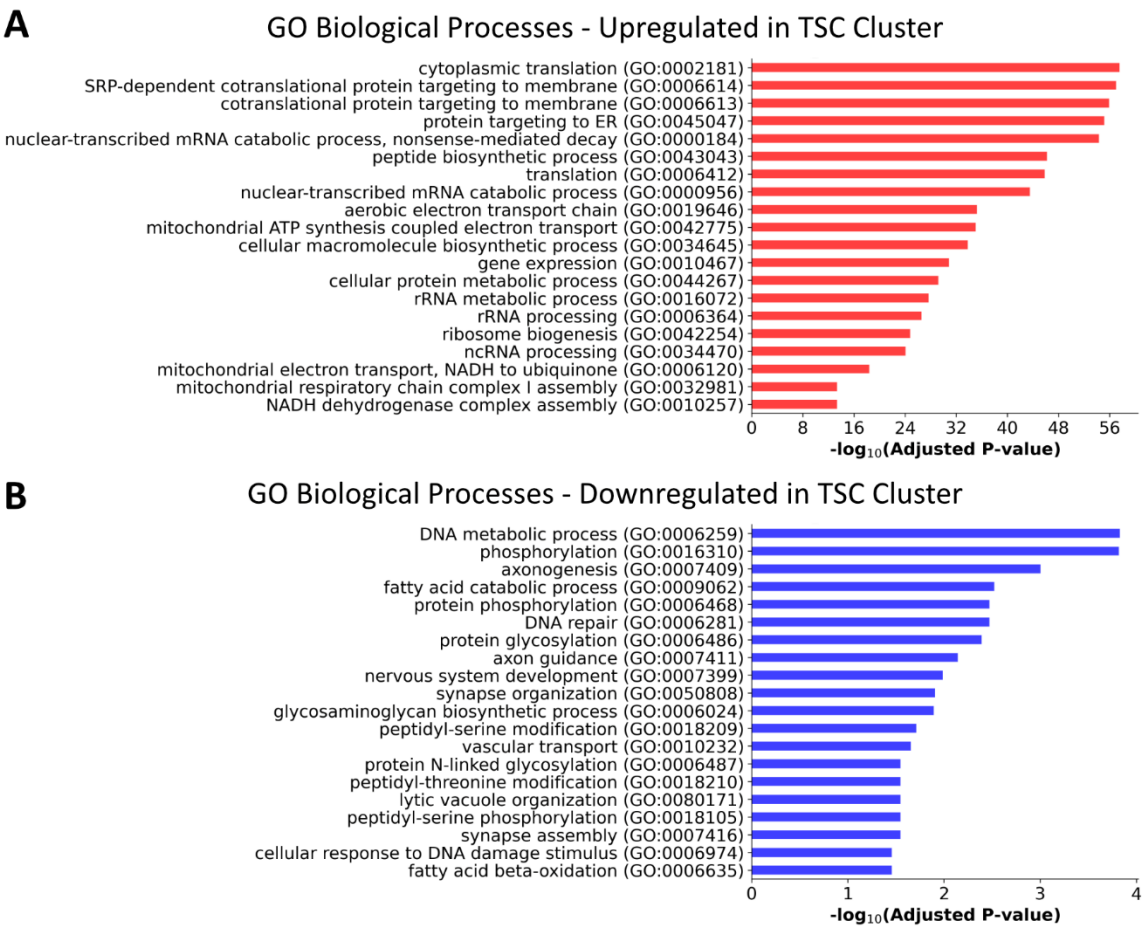

Figure 36: GO term biological analysis of the TSC cluster. (**A**) The graph shows GO term biological processes downregulated in the TSC cluster compared to the rest of the scRNA-seq dataset. (**B**) The graph shows GO term biological Processes downregulated in the TSC cluster compared to the rest of the scRNA-seq dataset.

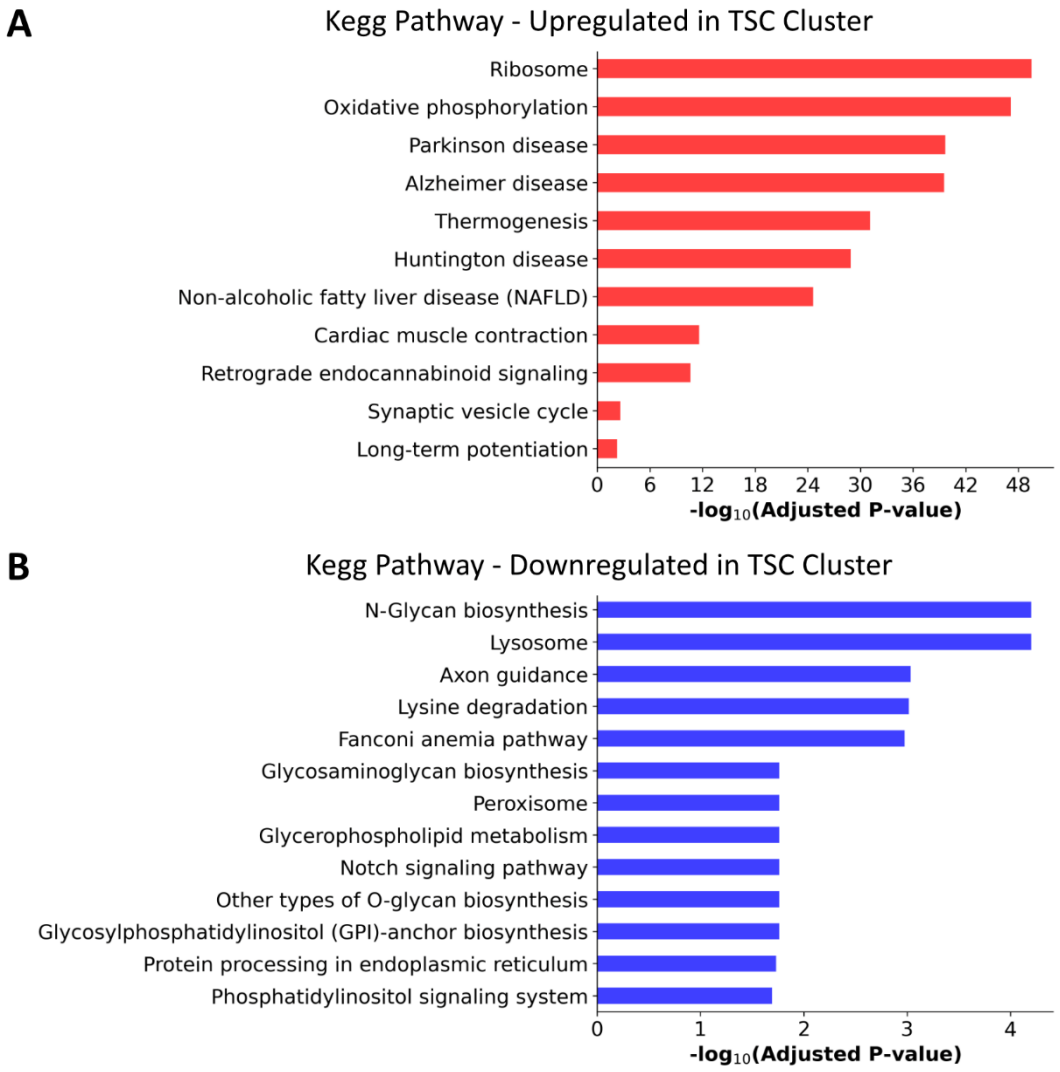

Figure 37: KEGG pathway analysis of the TSC cluster to address biological processes. (**A**) The graph shows Kegg pathway upregulated cellular processes the TSC cluster compared to the rest of the scRNA-seq dataset. (**B**) Kegg pathway shows downregulated cellular processes in the TSC cluster compared to the rest of the scRNA-seq dataset.

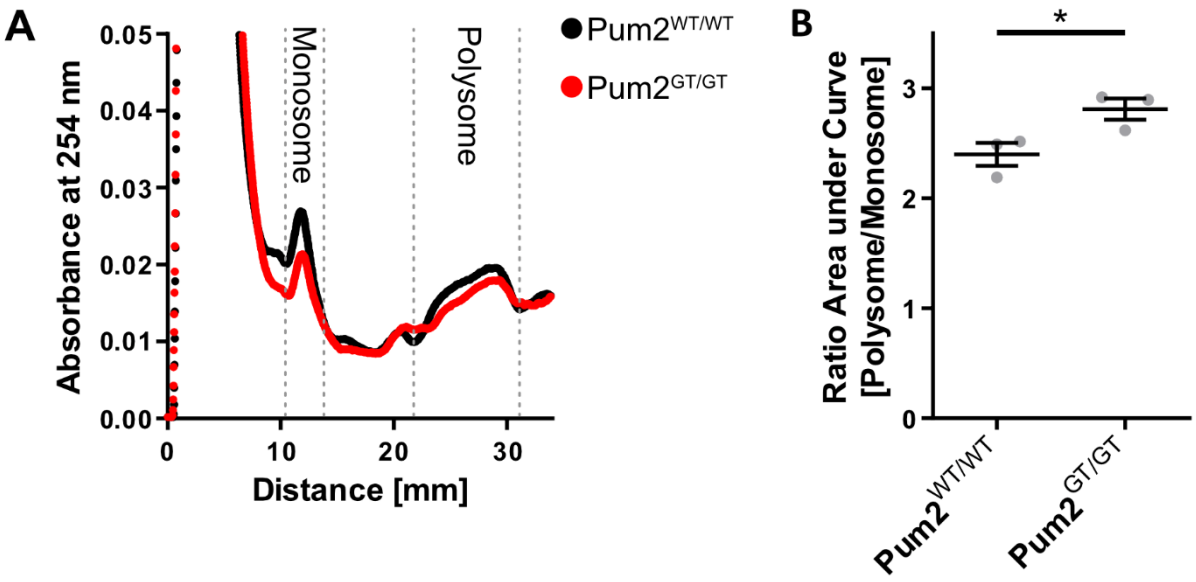

Figure 38: Pum2 deficiency appears to affect translation. (**A**) Graph displaying polysome profiling with the absorbance at 254nm on the Y axis and the distance in mm on the X axis of five months old mice. (**B**) Mean and standard deviation are shown. Dot plot displaying the polysome to monosome ratio of the graph shown in A. The graphs consist of 3 independent biological replicates. Asterisks represent p-values obtained by (**B**) unpaired Student's t-test (*p < 0.05).

4 Discussion

Adult neurogenesis is known to critically contribute to learning and memory formation. It is a highly regulated process. One important group of proteins – in addition to transcription factors (Beckervordersandforth et al., 2015) – that is known to have a regulatory function in this process are RBPs as they regulate every step of a RNA's life cycle. The Pumilio gene family encodes RBPs with significant roles in development, particularly within the CNS. Growing evidence indicates the importance of Pum family proteins for proper adult neurogenesis within the hippocampus (Zhang et al., 2017). Depletion of Pum2, has been associated with maladaptation to environmental challenges and abnormal cortical excitability (Siemen et al., 2011). The specific contributions of Pum2 to neurogenesis, however, remain unknown. This motivated my investigation of Pum2's potential role in adult hippocampal neurogenesis. To my knowledge, this study provides the first comprehensive analysis of a Pum2-deficient mouse line and an *in vivo* downregulation of Pum2 in the adult DG, to unravel the specific contribution of Pum2 to adult neurogenesis in higher eukaryotes.

4.1 Defective neurogenesis in Pum2 deficient DG

In this thesis, I aimed at exploring the function of Pum2 in neurogenesis and its role in the adult neurogenic lineage and the maturation of neurons, given prior evidence of its importance in neurogenesis. My results highlight a role of Pum2 within several steps in the adult neurogenic lineage, such as cell fate decision of RGCs and maturation. I observed an early impact on stem cell proliferation and a bias towards astrocyte fate commitment (**Figure 39A**). This leads to a shift in the DG balance towards an increased astrocyte/glial output in Pum2-deficient mice (**Figure 39B**). This altered lineage composition does not appear to disrupt the localization of proliferating cells. They demonstrate a migration pattern into the GCL over time, like WT cells. This migration is essential for proper functional integration into the hippocampal circuit (Morgenstern et al., 2008). In addition, my findings revealed a significant size reduction of the DG in Pum2-deficient mice, with a constant density of proliferating cells and no increased apoptosis. This reduction in size is consistent with the published phenotype observed in Pum1/Pum2 double KD mice (Zhang et al., 2017). There could be several possible explanations for this. Pum2 is implicated to influence signalling pathways that regulate overall cell body size, leading to reduced growth in Pum2-deficient mice (Lin et al., 2019). An additional possibility is that Pum2 may be involved in the regulation of

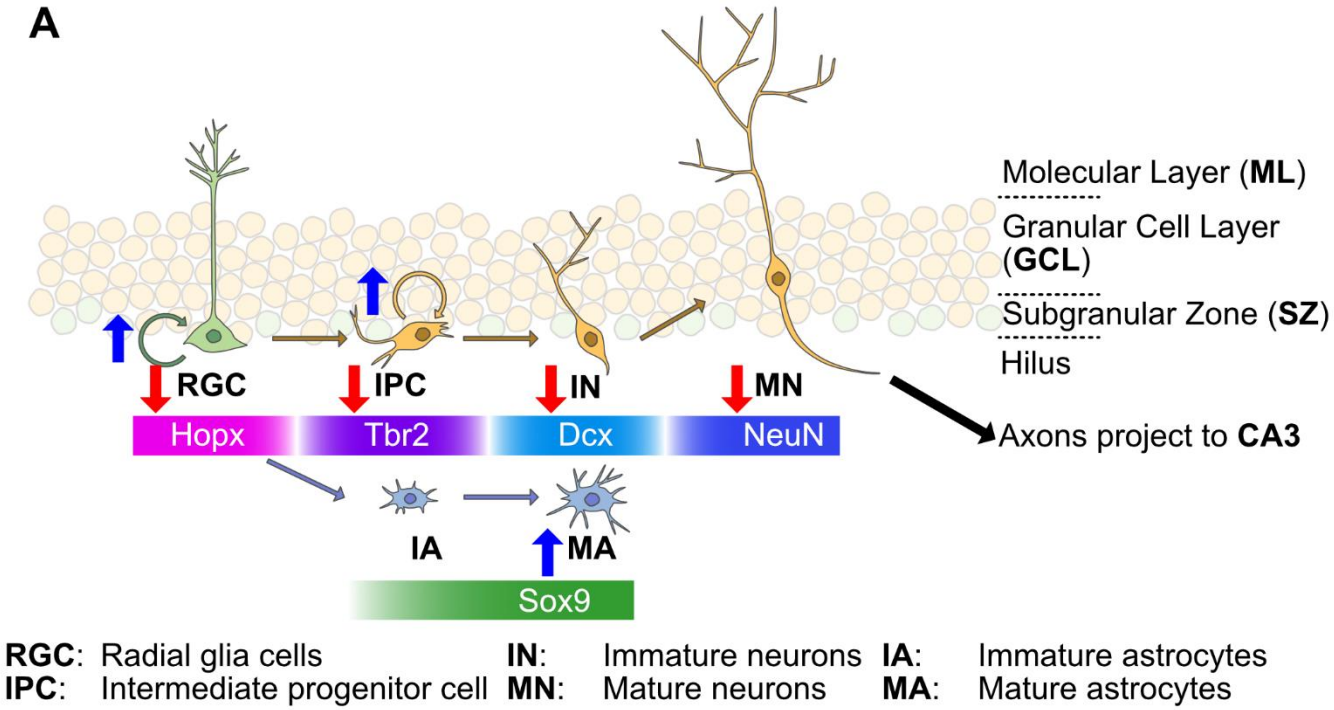

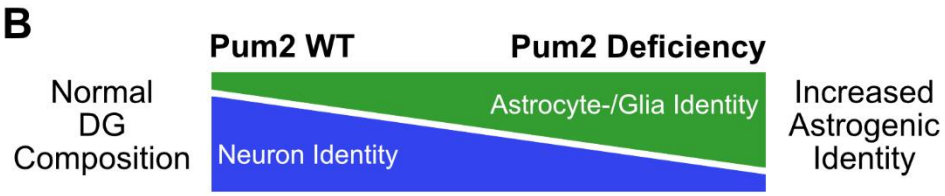

Figure 39: Reduction of neurogenesis favours astrogenesis in Pum2 deficiency. (**A**) A lack of Pum2 leads to a decreased neurogenesis rate and stem cell self-renewal including all cell types as RGCs, IPCs, INs and MNs. The cycling capabilities of RGCs and IPCs are increased. Furthermore, the astrogenic lineage is favoured upon Pum2 deficiency. Arrows indicate increase (blue) and decrease (red) of the corresponding cell type. (**B**) Scheme shows the potential change in DG upon lack of Pum2 towards a more glia like identity. Adapted with the help of Dr. Barbara Nitz.

extracellular matrix (ECM) component production. The absence of Pum2 could result in an altered generation of ECM, possibly hindering tissue expansion by preventing proper cell migration despite normal cell division. Other RBPs, like members of the ELAV/Hu family, are known to regulate target mRNAs that encode cell cycle proteins, which could explain the reduced proliferation (Blackinton & Keene, 2014). Similarly, previous research suggests Pum2's involvement in cell cycle progression through its interaction with the Aurora-A kinase, promoting mitotic entry (Huang et al., 2011). My findings demonstrate an increase in actively cycling cells within the DG of Pum2-deficient mice. This increase, without a corresponding increase in apoptosis rates, suggests that it is not a simple replacement of dead cells. These observations point towards a significant role for Pum2 in cell cycle regulation, likely through its control of mRNAs or interaction with cell cycle-related proteins, such as FOXP1 or Aurora-A kinase (Huang et al., 2011; Smialek et al., 2021). On the other hand, my findings reveal

a reduction in the generation of several cell types in the neurogenic lineage, such as MNs and INs in Pum2-deficient mice. However, only the total number of IPCs was reduced. This suggests a potential compensatory/regulatory mechanism to maintain the density of INs, in which the IPC pool differentiates without additional cell division for self-proliferation and therefore reducing the total number of IPCs. The precise composition of cell types within the DG is essential for its proper function (Kesner, 2018). A disruption in this delicate balance can contribute to various neurological deficits (Hagihara et al., 2013). While not yet published, similar findings have been partially observed in a recent study of a MD thesis (Demleitner, 2021). This MD thesis explored the effect of the downregulation of two RBPs, including Pum2, on behaviour and memory in mice. This work offers support for my hypothesis that Pum2 plays a key role in adult neurogenesis as well as for my related observations of an increase astrogenesis and the cell cycle regulation. These results suggest a broader impact of Pum2 on cell fate regulation and therefore for neurological function in adulthood. The reduced maintenance of radial stem cells is consistent with the evolutionary conserved role of Pum proteins, which support stem cell proliferation and self-renewal (Crittenden et al., 2002; Nolde et al., 2007; Wickens et al., 2002). This suggests that mammalian Pumilio orthologs, like Pum2, could regulate asymmetric division and cell fate specification across various lineages, including stem cell maintenance (Spassov & Jurecic, 2003). Recent findings point towards a potential role for Pum2 as an inhibitor of stem cell differentiation, simply modulating lineage specification (Lee et al., 2020). Further investigation is therefore needed to dissect Pum2's precise function within this complex process. Despite the observed reduction in RGC maintenance, the density of RGCs remained surprisingly stable. This suggests a dual role for Pum2 in RGCs. It appears to be essential for their maintenance and self-proliferation. Pum2 might therefore participate in pathways that promote RGC survival by preventing premature terminal division. Changes in signalling mechanisms or cell support structures could protect the existing RGC population. Alternatively, the impact of reduced radial stem cell maintenance on RGC density might be delayed. It is possible that young adults maintain a stable RGC population, but a decline could occur later if the stem cell maintenance issue persists. Another possibility is that RGCs could prematurely adopt an astrocytic fate as previously reported (Miranda-Negron & Garcia-Arraras, 2022). This would align with the observed reduction in radial stem cell maintenance and

decreased neurogenesis while potentially explaining the stable RGC density. In support of this hypothesis is an increased generation of new astrocytes that was observed. However, the observed decrease in astrocytic cell density within the DG appears to contradict this potential mechanism. The seemingly contradictory findings could be reconciled by two mechanisms. Firstly, newly formed astrocytes might migrate away from the DG (Brunne et al., 2010). This would explain increased astrocyte production while simultaneously accounting for their decreased local density within the DG. An alternative hypothesis is that the astrocytic marker Sox9 may also be present in an intermediate stage of cell development. It has been reported that Sox9 is an astrocyte-specific marker, except for the neurogenic niche, where it can also be expressed by progenitor cells (Sun et al., 2017). This may be the case in the TSC cluster, as shown in **Figure 24** representing the sc-RNAseq data. In the TSC cluster, several glial genes are gradually expressed, such as S100β and Gfap. Under Pum2-deficient conditions, these cells could further differentiate and lose their astrocytic characteristics, a process not typically observed in WT conditions. Traditional tissue analysis is focusing on cell type proportions within a given volume. The analysis of cells within the Pum2-deficient DG, regardless of the volume, revealed an overall reduction of cell populations. This aligns with the observed size reduction of the DG. However, analysing sheer cell counts irrespective of volume presents an intriguing anomaly: a notable increase in actively cycling cells. Ki67, expressed throughout active phases of the cell cycle (G1, S, G2, and mitosis), serves as a reliable proliferation marker (Sun & Kaufman, 2018). Yet, its presence does not warrant cell division. Cells lacking essential signals may stall in the cycle despite expressing Ki67 (Sobecki et al., 2017). Furthermore, senescent cells, while permanently growth-arrested, can express certain cell cycle markers like Ki67 without actively dividing (Alessio et al., 2021). The true proliferative status of the increased Ki67-positive cells is therefore questionable and might need to be confirmed by confirmed by other cell cycle markers that stain for late G2 phase or mitosis, such as phosphor-histone H3 (Kim et al., 2017).

4.2 Plasticity capability of the Pum2 deficient DG

The brain's remarkable plasticity allows the adaption of neural pathways in response to experiences (Draganski et al., 2004). As demonstrated in the preceding analysis, physical activity has been shown to stimulate adult neurogenesis (van Praag et al., 1999). While this effect is well-documented in WT DG, its implications for the Pum2-

deficient DG remained unexplored. I hypothesised that physical activity could rescue the Pum2-deficient phenotype. Interestingly, I observed an increase in DG size with physical activity in both WT and Pum2-deficient mice, aligning with previous findings (Nauer et al., 2020). While the size increases, the density of proliferating cells is decreasing, and their total number remained unchanged. My findings suggest that despite differences in proliferation dynamics, the overall DG cell count in Pum2-deficient mice eventually reaches levels like WT mice under physical activity. This raises questions about the mechanisms driving DG expansion under Pum2 deficiency. A potential explanation is an increased number of directly generated neurons entering a postmitotic, non-proliferative state, a pathway detected at low levels in adult hippocampal neurogenesis (Pilz et al., 2018). However, the observed increase in actively cycling cells appears to challenge this hypothesis. As previously discussed, Ki67 expression does not warrant actual cell division (Alessio et al., 2021). Consistent with the reported exercise-induced boost in neurogenesis, I observed a similar increase in total IN density, along with newly generated INs and IPCs, in the WT DG. This expected increase was absent in Pum2-deficient mice. However, I indeed detected a partial recovery towards basal WT neurogenesis levels. This could be explained by a predicted lower expression of Pum2 specifically within exercise-induced neurogenesis (Nishanth & Jha, 2022). The partial recovery of neurogenesis under physical activity in Pum2-deficient mice suggests compensatory mechanisms. Other RBPs known for their neurogenic roles, such as Stau2, might partially compensate for Pum2's absence, particularly because Pum2 expression is predicted to be naturally lower in exercise-induced neurogenesis (Nishanth & Jha, 2022). The observed decrease in IPC density might be due to the reduced self-renewal and increased differentiation towards an IN fate. This aligns with the reduced RGC density in Pum2 deficiency, and a similar trend observed in WT mice under exercise, further supporting the idea of enhanced differentiation. Importantly, my results indicate that neither proliferation nor maintenance of RGCs appears to be disrupted, suggesting a potential preference for differentiation in both WT and Pum2-deficient conditions (**Figure 40A**). This increased neurogenesis aligns with the observed reduction in astrocyte density (**Figure 40B**). Interestingly, the reduction in newly proliferated astrocytes within the Pum2-deficient DG is less pronounced than in WT condition. This aligns with the observed recovery of neurogenesis, suggesting a dynamic adaptation of astrogenesis

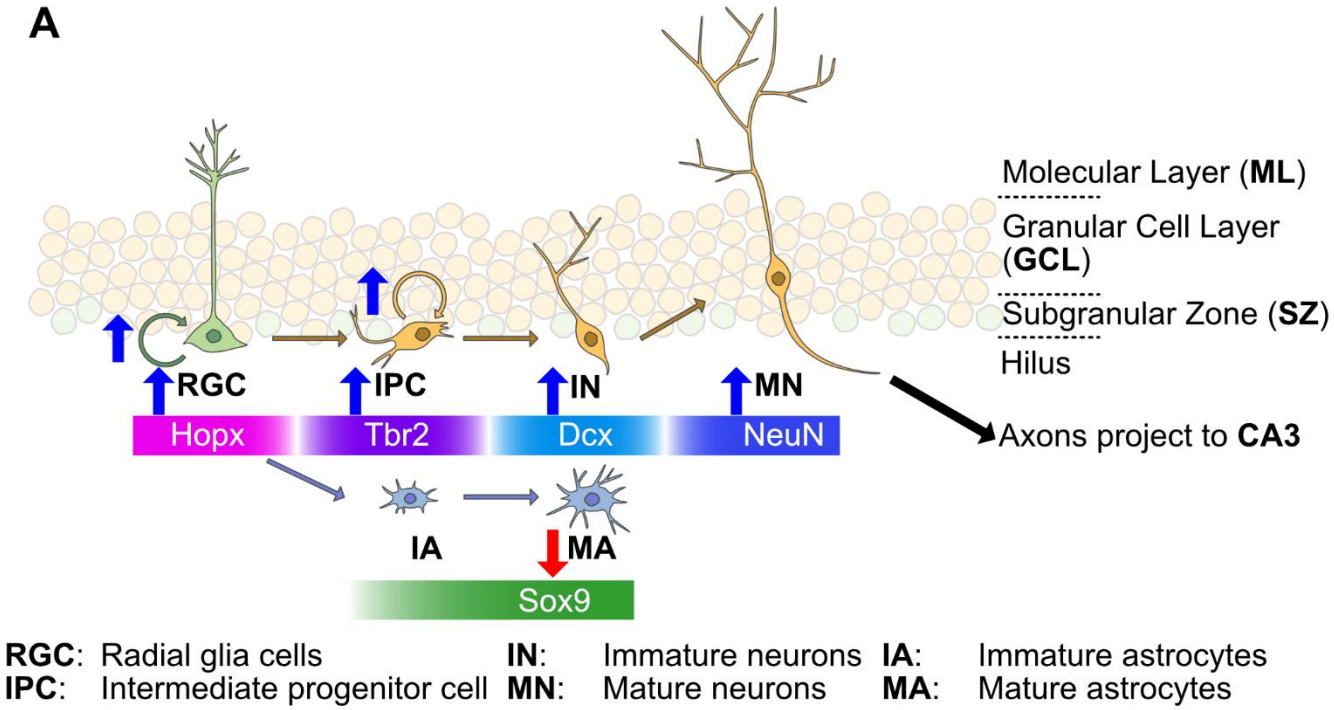

Figure 40: Recovery of the neurogenic lineage upon physical activity in Pum2 deficiency. (**A**) The previously reported deficiency of Pum2 could be recovered by physical activity. The neurogenesis rate and stem cell self-renewal including all cell types as RGCs, IPCs, INs and MNs are increased compared to the basal Pum2 deficiency. The cycling capabilities of RGCs and IPCs are further increased. The astrogenic lineage seems not to be favoured in Pum2 deficiency upon physical activity. Arrows indicate increase (blue) and decrease (red) of the corresponding cell type. (**B**) Scheme shows the potential recovery of exercise induced neurogenesis in the Pum2 deficient DG towards a WT like composition. Adapted with the help of Dr. Barbara Nitz.

to maintain a balanced cellular composition within the DG (Drew et al., 2013). One potential explanation for the increased DG size is that while the absolute number of neurons might increase with exercise, the overall cell density may remain relatively stable. New neurons extend dendrites and axons, leading to a denser network of connections and an expansion of DG volume (Nauer et al., 2020). Additionally, exercise could alter the proportion of neurons to supporting cells. Changes in other cell types might contribute to the increased size, potentially offsetting the effects of increased neuronal density (Maugeri et al., 2023). My findings suggest a potential

explanation for the increased DG size, elevated actively cycling cell density and reduced proliferating cell density observed in Pum2 deficiency. The potential explanation could be, while overall cell density may be decreasing, the total cell number remains relatively stable. This may be a consequence of a combined effect, namely the expansion of the neuronal connections and a change in the composition of supporting cell types, such as oligodendrocytes. Importantly, these results demonstrate the remarkable plasticity of the Pum2-deficient brain, highlighting its ability to partially recover and achieve a DG state closer to WT conditions. While physical activity induces a recovery of neurogenesis in Pum2 deficiency, the long-term stability of this effect remains unknown. Even in WT conditions, the long-term consequences of increased neurogenesis through physical activity are complex and under ongoing investigation. Furthermore, it is unclear whether newly generated neurons in Pum2-deficient mice integrate properly into existing neural circuits and achieve full functionality. Previous studies have indicated impaired neuronal development in Pum2 deficiency (Vessey et al., 2010). Thus, while neurogenesis may recover with exercise, it might not lead to properly developed or fully functional neurons. This is because Pum2 plays a critical role in proper development, the cell fate decisions of RGCs and IPCs can also be modulated through other processes (Kriegstein & Gotz, 2003). My results indicate a reduced importance of Pum2 specifically in exercise-induced neurogenesis as its functions may be naturally compensated for by other RBPs or key genes such as BDNF. This, together with the observed recovery, highlights the remarkable plasticity of the Pum2-deficient brain in overcoming its limitations.

4.3 TSC as novel aberrant cell type in Pum2 deficiency

To investigate the transcriptional changes associated with Pum2 deficiency, we employed a 10x scRNA-seq approach. I successfully identified all major DG cell types, consistent with previous literature (Hochgerner et al., 2018). Additionally, I observed the neurogenic lineage, spanning from IPCs to MNs. A connection between RGCs and IPCs is known to exist (Hochgerner et al., 2018). However, limited cell numbers, data characteristics and methodological assumptions in the transition between RGCs and IPCs may have hindered its detection in my analysis. This aligns with the computational requirements for reliable connection identification as there is no single optimal method and a better approach might be a combination of complementary techniques (Saelens

et al., 2019). Most strikingly, I discovered a significant increase in a novel cell population termed TSCs, with a gradual expression of both glial and neuronal genes from opposing sides in the tSNE visualisation of the TSC cluster. TSCs were found predominantly in the Pum2-deficient DG, with only a small fraction present in WT conditions. However, this small fraction is only present when clustered together with the dataset from Pum2-deficient DG, potentially explaining that it was not discovered so far in previous studies. Interestingly, the accumulation of TSCs in Pum2 deficiency coincides with a reduction in all other cell types associated with neurogenesis and astrogenesis. In addition, the existence of TSCs is demonstrated within tissue slices, using both RNA detection via RNAscope and immunostaining. This complements the scRNA-seq data and confirms the reduction of other cell types commonly found within the DG. While TSCs in Pum2-deficient mice appear to localize preferentially within the granular cell layer, I could not detect mayor morphological differences compared to WT TSCs. In the dataset of WT mice, TSCs cluster near the neuronal and astrocytic regions as two separated cell populations, suggesting that a full transition within WT cells may rare or even absent. Intriguingly, my data indicate that TSCs likely originate from RGCs. This potential shift in lineage in Pum2 deficiency could explain both the observed reduction in astrocytes and the increase in Sox9-positive proliferating cells possibly representing an intermediate cell state. Interestingly, separate clustering of the WT dataset reveals TSCs positioned between IPCs and DNs, with another part of the TSC along the normal MA trajectory. Their rarity may explain why these cells have not been described before (Hochgerner et al., 2018). The differentiation of RGCs into TSCs raises the question of how the TSC cluster might emerge (**Figure 41**). Recent results also support the ability of RGCs to directly giving rise to neurons, bypassing the IPC state (Huilgol et al., 2023; Pilz et al., 2018). Pum2 deficiency might promote this direct neurogenic pathway. However, rather than maturing into neurons, these cells appear to become stalled and accumulate in the TSC cluster as Pum2 plays an important role in proper neuronal development and maturation (Schieweck, Schoneweiss, et al., 2021; Vessey et al., 2010). In its absence, direct neurogenesis might initiate, but the process may become arrested, leading to the observed TSC buildup (**Figure 41**). However, the lack of Dcx expression contradicts the direct neurogenesis pathway, as these cells would express Dcx after the bypassing the IPC state. The expression of Rbfox3, Prox1 and Neurod1 clearly supports the idea that the

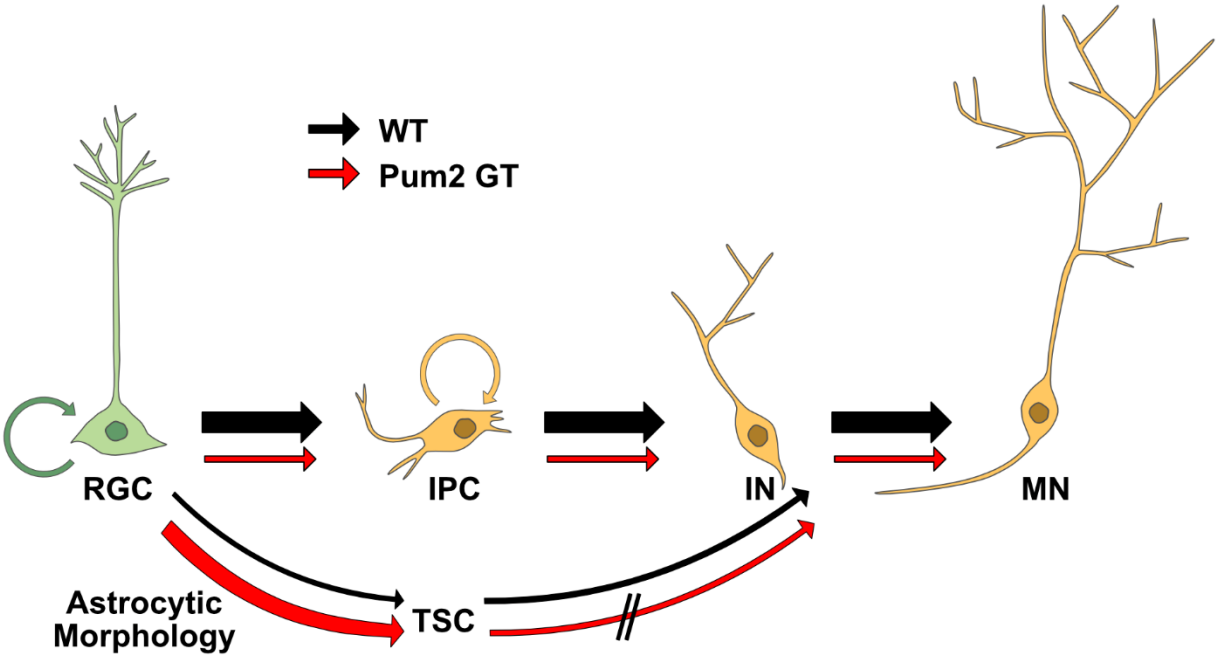

Figure 41: Pum2 deficiency disrupts adult neurogenesis and leads to an abnormal accumulation of TSCs. The working model illustrates the potential consequences of Pum2 loss on DG neurogenesis and cell fate progeny. Adapted with the help of Dr. Barbara Nitz.

cells develop into neurons, possibly via an altered direct neurogenesis pathway. These findings underscore the possibility that Pum2 regulate the differentiation and maturation process of adult-born granule cells. An alternative explanation is that TSCs represent a novel, dysregulated cell type arising specifically due to Pum2 deficiency. Since they might also exist in WT mice, understanding their true nature and potential impact on the DG will therefore be essential. The increase in proliferating astrocytes within Pum2-deficient mice aligns with the hypothesis of altered RGC fate decisions. However, the observed decrease in astrocyte proliferation and the partial recovery of neurogenesis under physical activity suggest two potential explanations. No TSC cluster builds up as physical activity might overcome the formation of TSCs in Pum2 deficiency, allowing RGCs to follow regular differentiation pathways. Alternatively, TSCs might mature. Physical activity is likely to induce factors that promote the maturation of TSCs into neurons. Known growth factors play a supportive role in neuronal maturation during physical activity (Fabel & Kempermann, 2008). It is worth investigating whether these factors could potentially overcome the stalled state of TSCs in Pum2 deficiency even without physical activity. Analysis of differentially expressed genes within the TSC cluster reveals intriguing insights by GO and KEGG analysis. It revealed an enrichment of genes that are associated with pathways linked

to neurological diseases, including a decreased regulation of axonal guidance. The observed dysregulation of axonal guidance aligns with previous findings on Pum2's role in axon and dendrite formation (Martinez et al., 2019; Vessey et al., 2010). Additionally, the increase in translation-associated genes and pathways was expected, given Pum2's known role in translational regulation (Van Etten et al., 2012). Initial polysome profiling indicates an altered translational activity. This experiment will be repeated with young adult mice for confirmation. A translational dysregulation, even small changes, might therefore have significant implications for the emergence of TSCs. The mixed cellular identity of TSCs suggests that an increase in translation might drive the expression of diverse cellular proteins. This could impede a clear differentiation trajectory, resulting in a stalled intermediate state. While the direct link between translational dysregulation and a mixed-identity state remains to be demonstrated, the phenomenon of mixed identities is proposed in other research areas, particularly within cancer studies (Pan et al., 2022). My findings raise the intriguing possibility that a similar mechanism, potentially influenced by Pum2, could affect cell fate decisions within the neurogenic lineage. The disease association aligns with the proposed role of Pum2 in neurological disorders and its demonstrated enrichment of mRNAs associated with Parkinson's disease (Siemen et al., 2011). The emergence of the TSC and their possible importance for neurological disorders might be the cause for the reported spontaneous epileptic seizures in Pum2 deficient mice (Follwaczny et al., 2017; Siemen et al., 2011). However, while research suggests potential links, a molecular role of Pum2 in diseases such as Alzheimer's or Huntington's is currently unknown.

4.4 Pum2 in an adult specific role

A possible limitation of my study is the use of the Pum2 gene-trap mouse line as Pum2 is absent from birth on, effects during the development and alterations in the neurogenic nice cannot be excluded. Therefore, we employed a retroviral approach targeting only dividing cells within the DG, primarily IPCs (Miranda-Negron & Garcia-Arraras, 2022), to analyse the cell-specific impact on adult neurogenesis. The downregulation of Pum2 was achieved via miRNA targeting specifically Pum2. While Pum2 miRNA-2 demonstrated an efficient KD, the Pum2 miRNA-1 achieved only partial suppression. Both Pum2 miRNAs showed a phenotype of less developed neurons and more aberrant neurons together with an increase in glia cells. The

phenotype was even more prominent for the Pum2 miRNA-2. The scrambled miRNA produced mainly well-developed neurons and few astrocytes. This observation for the control miRNA is in line with my WT scRNA-seq data and previous literature (Deshpande et al., 2013; Pilz et al., 2018; Tashiro et al., 2006; Vivar et al., 2012), raising intriguing questions about the relationship between Pum2 levels and neuronal development and cell fate commitment *in vivo*. I was largely able to reproduce the TSC phenotype. The presence of underdeveloped neurons with processes that resemble those of astrocytes introduces a novel element to the hypothesis that RGCs give rise to TSCs over an intermediate cell state with characteristics of an astrocytic morphology (**Figure 41**). This suggests a conversion process from an astrocyte-like intermediate state towards neuronal differentiation. Such a mechanism aligns with observations from reprogramming research, where astrocytes are artificially converted into a neuron by the expression of neuronal transcription factors such as Ascl1 or Ngn2 (Chanda et al., 2014; Zhou et al., 2021). However, a major limitation of this retroviral approach is that it primarily targets dividing cells, which are predominantly IPCs, making it difficult to specifically target RGCs as they divide at a much lower rate (Morales & Mira, 2019). This might explain the challenges in demonstrating TSC derivation from Pum2-downregulated RGCs. However, these initial findings offer promising insights. The observed phenotype of an increase of less-developed neurons and neurons with an aberrant morphology upon Pum2 KD, along with the overlap in genes representing the TSCs, strengthens the hypothesis of an impaired lineage commitment. This approach holds the high potential for investigating Pum2's distinct role in adult neurogenesis beyond the RGC differentiation stage.

4.5 Conclusion and future perspectives

In conclusion, I demonstrated an important role for Pum2 in adult neurogenesis, specifically in regulating the cell fate decision of RGCs. Furthermore, through scRNA-seq, immunostaining, and RNA detection via RNAscope, I discovered a novel cell type that is predominant in Pum2 KD tissue, but also appears in WT, however with much less incidence. Due to its properties, this cluster was termed TSCs. While the adult-specific downregulation of Pum2 in RGCs and IPCs appears promising and demonstrates a distinct phenotype, the primary target of the retrovirus is the IPCs. This results in the emergence of the TSCs being a rare occurrence with this approach, as the TSCs are predicted to derive from RGCs. Importantly, my results showcase the

remarkable plasticity of the Pum2-deficient brain upon exercise. I could demonstrate its ability to recover and achieve a state closer to WT conditions. Although the precise role of Pum2 or the adaption mechanism of the brain in this recovery process remains unclear, my findings open many promising avenues for further investigation.

It is important to acknowledge the limitations of this study. The global Pum2 knockout mouse model, while physiologically relevant as disease model, cannot isolate effects specifically arising from adult-onset Pum2 deficiency. The observed results might be influenced by potential embryonic and/or developmental deficits due to this lifelong downregulation. However, despite the limitation, the study provides valuable insights into the impact of Pum2 deficiency on the adult DG.

To further characterise TSCs, I'm pursuing two complementary approaches. First, I am increasing the replicates of the viral approach to generate a larger amount of TSCs specifically in adult mice. Additionally, I would like to include the Pum2-deficient mice for the injection of the control miRNA. This will allow me to investigate their development within the intact and the Pum2 deficient nervous system.

To address the challenge of targeting RGCs, I propose two strategies. Constructing a virus that incorporates the Gli1 promoter would enable specific Pum2 downregulation in RGCs. As research indicates that Gli1-CreER^{T2} mouse lines can effectively label RGCs in both the SVZ and DG (Ahn & Joyner, 2005; Bottes & Jessberger, 2021; Guo et al., 2022), combining the promotor from these mouse lines with Pum2 miRNAs would allow precise tracking of RGC differentiation and TSC generation *in vivo*. Another possibility would be the combination of the inducible Gli1-CreER^{T2} mouseline with floxed Pum2 mice (Uyhazi et al., 2020) which would enable timely controlled downregulation of Pum2 in adult RGCs and their progeny. This offers the most reliable approach for studying adult specific Pum2 function in RGCs. Both strategies could enable the use of *ex vivo* slices to investigate the electrophysiological properties of TSCs, providing valuable insights into their functional maturation state and possibly explore epileptic seizures.

In parallel, an *in vitro* cell culture model using human neural progenitor cells (hNPCs) can be employed. These cells are characterised by an RGC-like transcriptomic profile (Masjosthusmann et al., 2018) and thus offer an appropriate model system to study hNPC differentiation under Pum2 deficiency. Importantly, these cells differentiate into

electrophysiological active neuronal-like cells within several weeks (Gunhanlar et al., 2018). This combined approach will allow me to study the biochemical, morphological, and potentially electrophysiological features of TSCs *in vitro* and gain insights into their functional properties.

Further in-depth analysis of the TSCs' transcriptomic profile, cell-cell interactions, and functional properties within the existing neuronal network are likely to unravel their specific role within the demonstrated Pum2-related changes to adult hippocampal neurogenesis. In this line, the strong disease association suggested by KEGG pathway analysis of genes specifically regulated in the TSC cluster warrants further experimental exploration. Despite the lack of an immediate, severe phenotype in young adult Pum2 deficient mice, the findings presenting in this thesis pave the way for understanding the long-term consequences of Pum2 deficiency and therefore the presence of TSC and their potential implications for an altered brain function and seizure susceptibility.

Literature

Adermark, L., Lagstrom, O., Loften, A., Licheri, V., Havenang, A., Loi, E. A., Stomberg, R., Soderpalm, B., Domi, A., & Ericson, M. (2022). Astrocytes modulate extracellular neurotransmitter levels and excitatory neurotransmission in dorsolateral striatum via dopamine D2 receptor signaling. *Neuropsychopharmacology*, *47*(8), 1493-1502. https://doi.org/10.1038/s41386-021-01232-x

Ahn, S., & Joyner, A. L. (2005). In vivo analysis of quiescent adult neural stem cells responding to Sonic hedgehog. *Nature*, *437*(7060), 894-897. https://doi.org/10.1038/nature03994

Aimone, J. B., Wiles, J., & Gage, F. H. (2009). Computational influence of adult neurogenesis on memory encoding. *Neuron*, *61*(2), 187-202. https://doi.org/10.1016/j.neuron.2008.11.026

Alessio, N., Aprile, D., Cappabianca, S., Peluso, G., Di Bernardo, G., & Galderisi, U. (2021). Different Stages of Quiescence, Senescence, and Cell Stress Identified by Molecular Algorithm Based on the Expression of Ki67, RPS6, and Beta-Galactosidase Activity. *Int J Mol Sci*, *22*(6), 3102. https://doi.org/10.3390/ijms22063102

Allen, N. J., & Eroglu, C. (2017). Cell Biology of Astrocyte-Synapse Interactions. *Neuron*, *96*(3), 697-708. https://doi.org/10.1016/j.neuron.2017.09.056

Allen, W. E., Blosser, T. R., Sullivan, Z. A., Dulac, C., & Zhuang, X. (2023). Molecular and spatial signatures of mouse brain aging at single-cell resolution. *Cell*, *186*(1), 194-208 e118. https://doi.org/10.1016/j.cell.2022.12.010

Altman, J., & Das, G. D. (1965). Autoradiographic and histological evidence of postnatal hippocampal neurogenesis in rats. *J Comp Neurol*, *124*(3), 319-335. https://doi.org/10.1002/cne.901240303

Angevine, J. B., Jr., & Sidman, R. L. (1961). Autoradiographic study of cell migration during histogenesis of cerebral cortex in the mouse. *Nature*, *192*, 766-768. https://doi.org/10.1038/192766b0

Ashburner, M., Ball, C. A., Blake, J. A., Botstein, D., Butler, H., Cherry, J. M., Davis, A. P., Dolinski, K., Dwight, S. S., Eppig, J. T., Harris, M. A., Hill, D. P., Issel-Tarver, L., Kasarskis, A., Lewis, S., Matese, J. C., Richardson, J. E., Ringwald, M., Rubin, G. M., & Sherlock, G. (2000). Gene ontology: tool for the unification of biology. The Gene Ontology Consortium. *Nat Genet*, *25*(1), 25-29. https://doi.org/10.1038/75556

Azevedo, F. A., Carvalho, L. R., Grinberg, L. T., Farfel, J. M., Ferretti, R. E., Leite, R. E., Jacob Filho, W., Lent, R., & Herculano-Houzel, S. (2009). Equal numbers of neuronal and nonneuronal cells make the human brain an isometrically scaled-up primate brain. *J Comp Neurol*, *513*(5), 532-541. https://doi.org/10.1002/cne.21974

Barkovich, A. J., Guerrini, R., Kuzniecky, R. I., Jackson, G. D., & Dobyns, W. B. (2012). A developmental and genetic classification for malformations of cortical development: update 2012. *Brain*, *135*(Pt 5), 1348-1369. https://doi.org/10.1093/brain/aws019

Bauer, K. E., Bargenda, N., Schieweck, R., Illig, C., Segura, I., Harner, M., & Kiebler, M. A. (2022). RNA supply drives physiological granule assembly in neurons. *Nat Commun*, *13*(1), 2781. https://doi.org/10.1038/s41467-022-30067-3

Bauer, K. E., Segura, I., Gaspar, I., Scheuss, V., Illig, C., Ammer, G., Hutten, S., Basyuk, E., Fernandez-Moya, S. M., Ehses, J., Bertrand, E., & Kiebler, M. A.

(2019). Live cell imaging reveals 3'-UTR dependent mRNA sorting to synapses. *Nat Commun*, *10*(1), 3178. https://doi.org/10.1038/s41467-019-11123-x

Bazargani, N., & Attwell, D. (2016). Astrocyte calcium signaling: the third wave. *Nat Neurosci*, *19*(2), 182-189. https://doi.org/10.1038/nn.4201

Beauchamp, A., Yee, Y., Darwin, B. C., Raznahan, A., Mars, R. B., & Lerch, J. P. (2022). Whole-brain comparison of rodent and human brains using spatial transcriptomics. *Elife*, *11*. https://doi.org/10.7554/eLife.79418

Beckervordersandforth, R., Zhang, C. L., & Lie, D. C. (2015). Transcription-Factor-Dependent Control of Adult Hippocampal Neurogenesis. *Cold Spring Harb Perspect Biol*, *7*(10), a018879. https://doi.org/10.1101/cshperspect.a018879

Berg, D. A., Bond, A. M., Ming, G. L., & Song, H. (2018). Radial glial cells in the adult dentate gyrus: what are they and where do they come from? *F1000Res*, *7*, 277. https://doi.org/10.12688/f1000research.12684.1

Berg, D. A., Su, Y., Jimenez-Cyrus, D., Patel, A., Huang, N., Morizet, D., Lee, S., Shah, R., Ringeling, F. R., Jain, R., Epstein, J. A., Wu, Q. F., Canzar, S., Ming, G. L., Song, H., & Bond, A. M. (2019). A Common Embryonic Origin of Stem Cells Drives Developmental and Adult Neurogenesis. *Cell*, *177*(3), 654-668 e615. https://doi.org/10.1016/j.cell.2019.02.010

Bergami, M., & Berninger, B. (2012). A fight for survival: the challenges faced by a newborn neuron integrating in the adult hippocampus. *Dev Neurobiol*, *72*(7), 1016-1031. https://doi.org/10.1002/dneu.22025

Berninger, B., Hack, M. A., & Gotz, M. (2006). Neural stem cells: on where they hide, in which disguise, and how we may lure them out. *Handb Exp Pharmacol*, *174*, 319-360. https://www.ncbi.nlm.nih.gov/pubmed/16370334

Bertrand, N., & Dahmane, N. (2006). Sonic hedgehog signaling in forebrain development and its interactions with pathways that modify its effects. *Trends Cell Biol*, *16*(11), 597-605. https://doi.org/10.1016/j.tcb.2006.09.007

Blackinton, J. G., & Keene, J. D. (2014). Post-transcriptional RNA regulons affecting cell cycle and proliferation. *Semin Cell Dev Biol*, *34*, 44-54. https://doi.org/10.1016/j.semcdb.2014.05.014

Blanchard, M. G., Willemsen, M. H., Walker, J. B., Dib-Hajj, S. D., Waxman, S. G., Jongmans, M. C., Kleefstra, T., van de Warrenburg, B. P., Praamstra, P., Nicolai, J., Yntema, H. G., Bindels, R. J., Meisler, M. H., & Kamsteeg, E. J. (2015). De novo gain-of-function and loss-of-function mutations of SCN8A in patients with intellectual disabilities and epilepsy. *J Med Genet*, *52*(5), 330-337. https://doi.org/10.1136/jmedgenet-2014-102813

Boczonadi, V., Muller, J. S., Pyle, A., Munkley, J., Dor, T., Quartararo, J., Ferrero, I., Karcagi, V., Giunta, M., Polvikoski, T., Birchall, D., Princzinger, A., Cinnamon, Y., Lutzkendorf, S., Piko, H., Reza, M., Florez, L., Santibanez-Koref, M., Griffin, H., . . . Horvath, R. (2014). EXOSC8 mutations alter mRNA metabolism and cause hypomyelination with spinal muscular atrophy and cerebellar hypoplasia. *Nat Commun*, *5*, 4287. https://doi.org/10.1038/ncomms5287

Bonaguidi, M. A., Wheeler, M. A., Shapiro, J. S., Stadel, R. P., Sun, G. J., Ming, G. L., & Song, H. (2011). In vivo clonal analysis reveals self-renewing and multipotent adult neural stem cell characteristics. *Cell*, *145*(7), 1142-1155. https://doi.org/10.1016/j.cell.2011.05.024

Bottes, S., & Jessberger, S. (2021). Live imaging of remyelination in the adult mouse corpus callosum. *Proc Natl Acad Sci U S A*, *118*(28), 442-454. https://doi.org/10.1073/pnas.2025795118

Bradl, M., & Lassmann, H. (2010). Oligodendrocytes: biology and pathology. *Acta Neuropathol*, *119*(1), 37-53. https://doi.org/10.1007/s00401-009-0601-5
Brunne, B., Zhao, S., Derouiche, A., Herz, J., May, P., Frotscher, M., & Bock, H. H. (2010). Origin, maturation, and astroglial transformation of secondary radial glial cells in the developing dentate gyrus. *Glia*, *58*(13), 1553-1569. https://doi.org/10.1002/glia.21029
Bullmore, E., & Sporns, O. (2009). Complex brain networks: graph theoretical analysis of structural and functional systems. *Nat Rev Neurosci*, *10*(3), 186-198. https://doi.org/10.1038/nrn2575
Buxbaum, A. R., Haimovich, G., & Singer, R. H. (2015). In the right place at the right time: visualizing and understanding mRNA localization. *Nat Rev Mol Cell Biol*, *16*(2), 95-109. https://doi.org/10.1038/nrm3918
Buxbaum, A. R., Wu, B., & Singer, R. H. (2014). Single beta-actin mRNA detection in neurons reveals a mechanism for regulating its translatability. *Science*, *343*(6169), 419-422. https://doi.org/10.1126/science.1242939
Bystron, I., Blakemore, C., & Rakic, P. (2008). Development of the human cerebral cortex: Boulder Committee revisited. *Nat Rev Neurosci*, *9*(2), 110-122. https://doi.org/10.1038/nrn2252
Cahoy, J. D., Emery, B., Kaushal, A., Foo, L. C., Zamanian, J. L., Christopherson, K. S., Xing, Y., Lubischer, J. L., Krieg, P. A., Krupenko, S. A., Thompson, W. J., & Barres, B. A. (2008). A transcriptome database for astrocytes, neurons, and oligodendrocytes: a new resource for understanding brain development and function. *J Neurosci*, *28*(1), 264-278. https://doi.org/10.1523/JNEUROSCI.4178-07.2008
Cao, Q., Padmanabhan, K., & Richter, J. D. (2010). Pumilio 2 controls translation by competing with eIF4E for 7-methyl guanosine cap recognition. *RNA*, *16*(1), 221-227. https://doi.org/10.1261/rna.1884610
Chalmers, N., Masouti, E., & Beckervordersandforth, R. (2024). Astrocytes in the adult dentate gyrus-balance between adult and developmental tasks. *Mol Psychiatry*, *29*(4), 982-991. https://doi.org/10.1038/s41380-023-02386-4
Chanda, S., Ang, C. E., Davila, J., Pak, C., Mall, M., Lee, Q. Y., Ahlenius, H., Jung, S. W., Sudhof, T. C., & Wernig, M. (2014). Generation of induced neuronal cells by the single reprogramming factor ASCL1. *Stem Cell Reports*, *3*(2), 282-296. https://doi.org/10.1016/j.stemcr.2014.05.020
Cheng, X., Li, Y., Huang, Y., Feng, X., Feng, G., & Xiong, Z. Q. (2011). Pulse labeling and long-term tracing of newborn neurons in the adult subgranular zone. *Cell Res*, *21*(2), 338-349. https://doi.org/10.1038/cr.2010.141
Chizhikov, V. V., Iskusnykh, I. Y., Steshina, E. Y., Fattakhov, N., Lindgren, A. G., Shetty, A. S., Roy, A., Tole, S., & Millen, K. J. (2019). Early dorsomedial tissue interactions regulate gyrification of distal neocortex. *Nat Commun*, *10*(1), 5192. https://doi.org/10.1038/s41467-019-12913-z
Christian, K. M., Song, H., & Ming, G. L. (2014). Functions and dysfunctions of adult hippocampal neurogenesis. *Annu Rev Neurosci*, *37*, 243-262. https://doi.org/10.1146/annurev-neuro-071013-014134
Clarke, L. E., & Barres, B. A. (2013). Emerging roles of astrocytes in neural circuit development. *Nat Rev Neurosci*, *14*(5), 311-321. https://doi.org/10.1038/nrn3484
Clelland, C. D., Choi, M., Romberg, C., Clemenson, G. D., Jr., Fragniere, A., Tyers, P., Jessberger, S., Saksida, L. M., Barker, R. A., Gage, F. H., & Bussey, T. J. (2009). A functional role for adult hippocampal neurogenesis in spatial pattern

separation. *Science*, *325*(5937), 210-213. https://doi.org/10.1126/science.1173215
Cole, J. D., Espinueva, D. F., Seib, D. R., Ash, A. M., Cooke, M. B., Cahill, S. P., O'Leary, T. P., Kwan, S. S., & Snyder, J. S. (2020). Adult-Born Hippocampal Neurons Undergo Extended Development and Are Morphologically Distinct from Neonatally-Born Neurons. *J Neurosci*, *40*(30), 5740-5756. https://doi.org/10.1523/JNEUROSCI.1665-19.2020
Copp, A. J., Greene, N. D., & Murdoch, J. N. (2003). The genetic basis of mammalian neurulation. *Nat Rev Genet*, *4*(10), 784-793. https://doi.org/10.1038/nrg1181
Crittenden, S. L., Bernstein, D. S., Bachorik, J. L., Thompson, B. E., Gallegos, M., Petcherski, A. G., Moulder, G., Barstead, R., Wickens, M., & Kimble, J. (2002). A conserved RNA-binding protein controls germline stem cells in Caenorhabditis elegans. *Nature*, *417*(6889), 660-663. https://doi.org/10.1038/nature754
D'Arcangelo, G., Miao, G. G., Chen, S. C., Soares, H. D., Morgan, J. I., & Curran, T. (1995). A protein related to extracellular matrix proteins deleted in the mouse mutant reeler. *Nature*, *374*(6524), 719-723. https://doi.org/10.1038/374719a0
Dahm, R., & Kiebler, M. (2005). Cell biology: silenced RNA on the move. *Nature*, *438*(7067), 432-435. https://doi.org/10.1038/438432a
Darnell, R. B. (2013). RNA protein interaction in neurons. *Annu Rev Neurosci*, *36*, 243-270. https://doi.org/10.1146/annurev-neuro-062912-114322
Dawson, T. M., Golde, T. E., & Lagier-Tourenne, C. (2018). Animal models of neurodegenerative diseases. *Nat Neurosci*, *21*(10), 1370-1379. https://doi.org/10.1038/s41593-018-0236-8
De Conti, L., Baralle, M., & Buratti, E. (2017). Neurodegeneration and RNA-binding proteins. *Wiley Interdiscip Rev RNA*, *8*(2), e1394. https://doi.org/10.1002/wrna.1394
DeepL Write. (2024). https://www.deepl.com/de/write
Demleitner, A. F. (2021). *THE ROLE OF STAUFEN 2 AND PUMILIO 2 IN HIPPOCAMPUS BASED LEARNING* [Dissertation, Ludwig-Maximilians-Universität]. https://edoc.ub.uni-muenchen.de/28387/
Deng, W., Aimone, J. B., & Gage, F. H. (2010). New neurons and new memories: how does adult hippocampal neurogenesis affect learning and memory? *Nat Rev Neurosci*, *11*(5), 339-350. https://doi.org/10.1038/nrn2822
Deshpande, A., Bergami, M., Ghanem, A., Conzelmann, K. K., Lepier, A., Gotz, M., & Berninger, B. (2013). Retrograde monosynaptic tracing reveals the temporal evolution of inputs onto new neurons in the adult dentate gyrus and olfactory bulb. *Proc Natl Acad Sci U S A*, *110*(12), E1152-1161. https://doi.org/10.1073/pnas.1218991110
Doetsch, F., Caille, I., Lim, D. A., Garcia-Verdugo, J. M., & Alvarez-Buylla, A. (1999). Subventricular zone astrocytes are neural stem cells in the adult mammalian brain. *Cell*, *97*(6), 703-716. https://doi.org/10.1016/s0092-8674(00)80783-7
Doetsch, F., Garcia-Verdugo, J. M., & Alvarez-Buylla, A. (1997). Cellular composition and three-dimensional organization of the subventricular germinal zone in the adult mammalian brain. *J Neurosci*, *17*(13), 5046-5061. https://doi.org/10.1523/JNEUROSCI.17-13-05046.1997
Dong, H., Zhu, M., Meng, L., Ding, Y., Yang, D., Zhang, S., Qiang, W., Fisher, D. W., & Xu, E. Y. (2018). Pumilio2 regulates synaptic plasticity via translational repression of synaptic receptors in mice. *Oncotarget*, *9*(63), 32134-32148. https://doi.org/10.18632/oncotarget.24345

Doyle, M., & Kiebler, M. A. (2011). Mechanisms of dendritic mRNA transport and its role in synaptic tagging. *EMBO J*, *30*(17), 3540-3552. https://doi.org/10.1038/emboj.2011.278

Draganski, B., Gaser, C., Busch, V., Schuierer, G., Bogdahn, U., & May, A. (2004). Neuroplasticity: changes in grey matter induced by training. *Nature*, *427*(6972), 311-312. https://doi.org/10.1038/427311a

Dranovsky, A., & Hen, R. (2006). Hippocampal neurogenesis: regulation by stress and antidepressants. *Biol Psychiatry*, *59*(12), 1136-1143. https://doi.org/10.1016/j.biopsych.2006.03.082

Drapeau, E., Mayo, W., Aurousseau, C., Le Moal, M., Piazza, P. V., & Abrous, D. N. (2003). Spatial memory performances of aged rats in the water maze predict levels of hippocampal neurogenesis. *Proc Natl Acad Sci U S A*, *100*(24), 14385-14390. https://doi.org/10.1073/pnas.2334169100

Drew, L. J., Fusi, S., & Hen, R. (2013). Adult neurogenesis in the mammalian hippocampus: why the dentate gyrus? *Learn Mem*, *20*(12), 710-729. https://doi.org/10.1101/lm.026542.112

Dreyfuss, G., Kim, V. N., & Kataoka, N. (2002). Messenger-RNA-binding proteins and the messages they carry. *Nat Rev Mol Cell Biol*, *3*(3), 195-205. https://doi.org/10.1038/nrm760

Driscoll, H. E., Muraro, N. I., He, M., & Baines, R. A. (2013). Pumilio-2 regulates translation of Nav1.6 to mediate homeostasis of membrane excitability. *J Neurosci*, *33*(23), 9644-9654. https://doi.org/10.1523/JNEUROSCI.0921-13.2013

Dubnau, J., Chiang, A. S., Grady, L., Barditch, J., Gossweiler, S., McNeil, J., Smith, P., Buldoc, F., Scott, R., Certa, U., Broger, C., & Tully, T. (2003). The staufen/pumilio pathway is involved in Drosophila long-term memory. *Curr Biol*, *13*(4), 286-296. https://doi.org/10.1016/s0960-9822(03)00064-2

Ellis, P., Fagan, B. M., Magness, S. T., Hutton, S., Taranova, O., Hayashi, S., McMahon, A., Rao, M., & Pevny, L. (2004). SOX2, a persistent marker for multipotential neural stem cells derived from embryonic stem cells, the embryo or the adult. *Dev Neurosci*, *26*(2-4), 148-165. https://doi.org/10.1159/000082134

Eriksson, P. S., Perfilieva, E., Bjork-Eriksson, T., Alborn, A. M., Nordborg, C., Peterson, D. A., & Gage, F. H. (1998). Neurogenesis in the adult human hippocampus. *Nat Med*, *4*(11), 1313-1317. https://doi.org/10.1038/3305

Fabel, K., & Kempermann, G. (2008). Physical activity and the regulation of neurogenesis in the adult and aging brain. *Neuromolecular Med*, *10*(2), 59-66. https://doi.org/10.1007/s12017-008-8031-4

Fernandez-Moya, S. M., Bauer, K. E., & Kiebler, M. A. (2014). Meet the players: local translation at the synapse. *Front Mol Neurosci*, *7*, 84. https://doi.org/10.3389/fnmol.2014.00084

Fernandez-Moya, S. M., Ehses, J., Bauer, K. E., Schieweck, R., Chakrabarti, A. M., Lee, F. C. Y., Illig, C., Luscombe, N. M., Harner, M., Ule, J., & Kiebler, M. A. (2021). RGS4 RNA Secondary Structure Mediates Staufen2 RNP Assembly in Neurons. *Int J Mol Sci*, *22*(23), 13021. https://doi.org/10.3390/ijms222313021

Finch, C. E., & Tanzi, R. E. (1997). Genetics of aging. *Science*, *278*(5337), 407-411. https://doi.org/10.1126/science.278.5337.407

Florio, M., & Huttner, W. B. (2014). Neural progenitors, neurogenesis and the evolution of the neocortex. *Development*, *141*(11), 2182-2194. https://doi.org/10.1242/dev.090571

Follwaczny, P., Schieweck, R., Riedemann, T., Demleitner, A., Straub, T., Klemm, A. H., Bilban, M., Sutor, B., Popper, B., & Kiebler, M. A. (2017). Pumilio2-deficient mice show a predisposition for epilepsy. *Dis Model Mech*, *10*(11), 1333-1342. https://doi.org/10.1242/dmm.029678

Fox, M., Urano, J., & Reijo Pera, R. A. (2005). Identification and characterization of RNA sequences to which human PUMILIO-2 (PUM2) and deleted in Azoospermia-like (DAZL) bind. *Genomics*, *85*(1), 92-105. https://doi.org/10.1016/j.ygeno.2004.10.003

Friend, K., Campbell, Z. T., Cooke, A., Kroll-Conner, P., Wickens, M. P., & Kimble, J. (2012). A conserved PUF-Ago-eEF1A complex attenuates translation elongation. *Nat Struct Mol Biol*, *19*(2), 176-183. https://doi.org/10.1038/nsmb.2214

Fritzsche, R., Karra, D., Bennett, K. L., Ang, F. Y., Heraud-Farlow, J. E., Tolino, M., Doyle, M., Bauer, K. E., Thomas, S., Planyavsky, M., Arn, E., Bakosova, A., Jungwirth, K., Hormann, A., Palfi, Z., Sandholzer, J., Schwarz, M., Macchi, P., Colinge, J., . . . Kiebler, M. A. (2013). Interactome of two diverse RNA granules links mRNA localization to translational repression in neurons. *Cell Rep*, *5*(6), 1749-1762. https://doi.org/10.1016/j.celrep.2013.11.023

Gage, F. H. (2000). Mammalian neural stem cells. *Science*, *287*(5457), 1433-1438. https://doi.org/10.1126/science.287.5457.1433

Ge, S., Yang, C. H., Hsu, K. S., Ming, G. L., & Song, H. (2007). A critical period for enhanced synaptic plasticity in newly generated neurons of the adult brain. *Neuron*, *54*(4), 559-566. https://doi.org/10.1016/j.neuron.2007.05.002

Ge, W. P., Miyawaki, A., Gage, F. H., Jan, Y. N., & Jan, L. Y. (2012). Local generation of glia is a major astrocyte source in postnatal cortex. *Nature*, *484*(7394), 376-380. https://doi.org/10.1038/nature10959

Gebauer, F., Schwarzl, T., Valcarcel, J., & Hentze, M. W. (2021). RNA-binding proteins in human genetic disease. *Nat Rev Genet*, *22*(3), 185-198. https://doi.org/10.1038/s41576-020-00302-y

Gebicke-Haerter, P. J. (2023). The computational power of the human brain. *Front Cell Neurosci*, *17*, 1220030. https://doi.org/10.3389/fncel.2023.1220030

Gene Ontology, C., Aleksander, S. A., Balhoff, J., Carbon, S., Cherry, J. M., Drabkin, H. J., Ebert, D., Feuermann, M., Gaudet, P., Harris, N. L., Hill, D. P., Lee, R., Mi, H., Moxon, S., Mungall, C. J., Muruganugan, A., Mushayahama, T., Sternberg, P. W., Thomas, P. D., . . . Westerfield, M. (2023). The Gene Ontology knowledgebase in 2023. *Genetics*, *224*(1). https://daoi.org/10.1093/genetics/iyad031

Gerstberger, S., Hafner, M., & Tuschl, T. (2014). A census of human RNA-binding proteins. *Nat Rev Genet*, *15*(12), 829-845. https://doi.org/10.1038/nrg3813

Geschwind, D. H., & Rakic, P. (2013). Cortical evolution: judge the brain by its cover. *Neuron*, *80*(3), 633-647. https://doi.org/10.1016/j.neuron.2013.10.045

Goetze, B., Grunewald, B., Baldassa, S., & Kiebler, M. (2004). Chemically controlled formation of a DNA/calcium phosphate coprecipitate: application for transfection of mature hippocampal neurons. *J Neurobiol*, *60*(4), 517-525. https://doi.org/10.1002/neu.20073

Goldstrohm, A. C., Hall, T. M. T., & McKenney, K. M. (2018). Post-transcriptional Regulatory Functions of Mammalian Pumilio Proteins. *Trends Genet*, *34*(12), 972-990. https://doi.org/10.1016/j.tig.2018.09.006

Goldstrohm, A. C., Seay, D. J., Hook, B. A., & Wickens, M. (2007). PUF protein-mediated deadenylation is catalyzed by Ccr4p. *J Biol Chem*, *282*(1), 109-114. https://doi.org/10.1074/jbc.M609413200

Goncalves, J. T., Schafer, S. T., & Gage, F. H. (2016). Adult Neurogenesis in the Hippocampus: From Stem Cells to Behavior. *Cell*, *167*(4), 897-914. https://doi.org/10.1016/j.cell.2016.10.021

Google Gemini. (2024). https://gemini.google.com/app

Gotz, M., & Huttner, W. B. (2005). The cell biology of neurogenesis. *Nat Rev Mol Cell Biol*, *6*(10), 777-788. https://doi.org/10.1038/nrm1739

Gratzner, H. G. (1982). Monoclonal antibody to 5-bromo- and 5-iododeoxyuridine: A new reagent for detection of DNA replication. *Science*, *218*(4571), 474-475. https://doi.org/10.1126/science.7123245

Grundmann, D., Loris, E., Maas-Omlor, S., Huang, W., Scheller, A., Kirchhoff, F., & Schafer, K. H. (2019). Enteric Glia: S100, GFAP, and Beyond. *Anat Rec (Hoboken)*, *302*(8), 1333-1344. https://doi.org/10.1002/ar.24128

Guillemot, F. (2007). Spatial and temporal specification of neural fates by transcription factor codes. *Development*, *134*(21), 3771-3780. https://doi.org/10.1242/dev.006379

Gumy, L. F., Katrukha, E. A., Kapitein, L. C., & Hoogenraad, C. C. (2014). New insights into mRNA trafficking in axons. *Dev Neurobiol*, *74*(3), 233-244. https://doi.org/10.1002/dneu.22121

Gunhanlar, N., Shpak, G., van der Kroeg, M., Gouty-Colomer, L. A., Munshi, S. T., Lendemeijer, B., Ghazvini, M., Dupont, C., Hoogendijk, W. J. G., Gribnau, J., de Vrij, F. M. S., & Kushner, S. A. (2018). A simplified protocol for differentiation of electrophysiologically mature neuronal networks from human induced pluripotent stem cells. *Mol Psychiatry*, *23*(5), 1336-1344. https://doi.org/10.1038/mp.2017.56

Guo, N., McDermott, K. D., Shih, Y. T., Zanga, H., Ghosh, D., Herber, C., Meara, W. R., Coleman, J., Zagouras, A., Wong, L. P., Sadreyev, R., Goncalves, J. T., & Sahay, A. (2022). Transcriptional regulation of neural stem cell expansion in the adult hippocampus. *Elife*, *11*, e72195. https://doi.org/10.7554/eLife.72195

Hagihara, H., Takao, K., Walton, N. M., Matsumoto, M., & Miyakawa, T. (2013). Immature dentate gyrus: an endophenotype of neuropsychiatric disorders. *Neural Plast*, *2013*, 318596. https://doi.org/10.1155/2013/318596

Hagihara, H., Toyama, K., Yamasaki, N., & Miyakawa, T. (2009). Dissection of hippocampal dentate gyrus from adult mouse. *J Vis Exp*, *33*, e1543. https://doi.org/10.3791/1543

Hansen, D. V., Lui, J. H., Parker, P. R., & Kriegstein, A. R. (2010). Neurogenic radial glia in the outer subventricular zone of human neocortex. *Nature*, *464*(7288), 554-561. https://doi.org/10.1038/nature08845

Haubensak, W., Attardo, A., Denk, W., & Huttner, W. B. (2004). Neurons arise in the basal neuroepithelium of the early mammalian telencephalon: a major site of neurogenesis. *Proc Natl Acad Sci U S A*, *101*(9), 3196-3201. https://doi.org/10.1073/pnas.0308600100

Hentze, M. W., Castello, A., Schwarzl, T., & Preiss, T. (2018). A brave new world of RNA-binding proteins. *Nat Rev Mol Cell Biol*, *19*(5), 327-341. https://doi.org/10.1038/nrm.2017.130

Heraud-Farlow, J. E., & Kiebler, M. A. (2014). The multifunctional Staufen proteins: conserved roles from neurogenesis to synaptic plasticity. *Trends Neurosci*, *37*(9), 470-479. https://doi.org/10.1016/j.tins.2014.05.009

Herculano-Houzel, S. (2009). The human brain in numbers: a linearly scaled-up primate brain. *Front Hum Neurosci*, *3*, 31. https://doi.org/10.3389/neuro.09.031.2009
Hochgerner, H., Zeisel, A., Lonnerberg, P., & Linnarsson, S. (2018). Conserved properties of dentate gyrus neurogenesis across postnatal development revealed by single-cell RNA sequencing. *Nat Neurosci*, *21*(2), 290-299. https://doi.org/10.1038/s41593-017-0056-2
Hodge, R. D., Nelson, B. R., Kahoud, R. J., Yang, R., Mussar, K. E., Reiner, S. L., & Hevner, R. F. (2012). Tbr2 is essential for hippocampal lineage progression from neural stem cells to intermediate progenitors and neurons. *J Neurosci*, *32*(18), 6275-6287. https://doi.org/10.1523/JNEUROSCI.0532-12.2012
Hofman, M. A. (1989). On the evolution and geometry of the brain in mammals. *Prog Neurobiol*, *32*(2), 137-158. https://doi.org/10.1016/0301-0082(89)90013-0
Holt, C. E., & Schuman, E. M. (2013). The central dogma decentralized: new perspectives on RNA function and local translation in neurons. *Neuron*, *80*(3), 648-657. https://doi.org/10.1016/j.neuron.2013.10.036
Holtmaat, A., & Svoboda, K. (2009). Experience-dependent structural synaptic plasticity in the mammalian brain. *Nat Rev Neurosci*, *10*(9), 647-658. https://doi.org/10.1038/nrn2699
Hotz, M., & Nelson, W. J. (2017). Pumilio-dependent localization of mRNAs at the cell front coordinates multiple pathways required for chemotaxis. *Nat Commun*, *8*(1), 1366. https://doi.org/10.1038/s41467-017-01536-x
Huang, Y. H., Wu, C. C., Chou, C. K., & Huang, C. Y. (2011). A translational regulator, PUM2, promotes both protein stability and kinase activity of Aurora-A. *PLoS One*, *6*(5), e19718. https://doi.org/10.1371/journal.pone.0019718
Huilgol, D., Levine, J. M., Galbavy, W., Wang, B. S., He, M., Suryanarayana, S. M., & Huang, Z. J. (2023). Direct and indirect neurogenesis generate a mosaic of distinct glutamatergic projection neuron types in cerebral cortex. *Neuron*, *111*(16), 2557-2569 e2554. https://doi.org/10.1016/j.neuron.2023.05.021
Huttner, W. B., & Kosodo, Y. (2005). Symmetric versus asymmetric cell division during neurogenesis in the developing vertebrate central nervous system. *Curr Opin Cell Biol*, *17*(6), 648-657. https://doi.org/10.1016/j.ceb.2005.10.005
Jacobs, B., Driscoll, L., & Schall, M. (1997). Life-span dendritic and spine changes in areas 10 and 18 of human cortex: a quantitative Golgi study. *J Comp Neurol*, *386*(4), 661-680. https://www.ncbi.nlm.nih.gov/pubmed/9378859
Jerison, H. J., & Count, E. W. (1955). On brain ratios and the evolution of intelligence. *Science*, *122*(3171), 647-648. https://doi.org/10.1126/science.122.3171.647
Jessberger, S., Clark, R. E., Broadbent, N. J., Clemenson, G. D., Jr., Consiglio, A., Lie, D. C., Squire, L. R., & Gage, F. H. (2009). Dentate gyrus-specific knockdown of adult neurogenesis impairs spatial and object recognition memory in adult rats. *Learn Mem*, *16*(2), 147-154. https://doi.org/10.1101/lm.1172609
Jessell, T. M. (2000). Neuronal specification in the spinal cord: inductive signals and transcriptional codes. *Nat Rev Genet*, *1*(1), 20-29. https://doi.org/10.1038/35049541
Kanehisa, M. (2019). Toward understanding the origin and evolution of cellular organisms. *Protein Sci*, *28*(11), 1947-1951. https://doi.org/10.1002/pro.3715

Kanehisa, M., Furumichi, M., Sato, Y., Kawashima, M., & Ishiguro-Watanabe, M. (2023). KEGG for taxonomy-based analysis of pathways and genomes. *Nucleic Acids Res*, *51*(D1), D587-D592. https://doi.org/10.1093/nar/gkac963
Kanehisa, M., & Goto, S. (2000). KEGG: kyoto encyclopedia of genes and genomes. *Nucleic Acids Res*, *28*(1), 27-30. https://doi.org/10.1093/nar/28.1.27
Kempermann, G., Gage, F. H., Aigner, L., Song, H., Curtis, M. A., Thuret, S., Kuhn, H. G., Jessberger, S., Frankland, P. W., Cameron, H. A., Gould, E., Hen, R., Abrous, D. N., Toni, N., Schinder, A. F., Zhao, X., Lucassen, P. J., & Frisen, J. (2018). Human Adult Neurogenesis: Evidence and Remaining Questions. *Cell Stem Cell*, *23*(1), 25-30. https://doi.org/10.1016/j.stem.2018.04.004
Kempermann, G., Jessberger, S., Steiner, B., & Kronenberg, G. (2004). Milestones of neuronal development in the adult hippocampus. *Trends Neurosci*, *27*(8), 447-452. https://doi.org/10.1016/j.tins.2004.05.013
Kempermann, G., Song, H., & Gage, F. H. (2015). Neurogenesis in the Adult Hippocampus. *Cold Spring Harb Perspect Biol*, *7*(9), a018812. https://doi.org/10.1101/cshperspect.a018812
Kesner, R. P. (2018). An analysis of dentate gyrus function (an update). *Behav Brain Res*, *354*, 84-91. https://doi.org/10.1016/j.bbr.2017.07.033
Khakh, B. S., & Deneen, B. (2019). The Emerging Nature of Astrocyte Diversity. *Annu Rev Neurosci*, *42*, 187-207. https://doi.org/10.1146/annurev-neuro-070918-050443
Kiebler, M. A., & Bassell, G. J. (2006). Neuronal RNA granules: movers and makers. *Neuron*, *51*(6), 685-690. https://doi.org/10.1016/j.neuron.2006.08.021
Kim, J. Y., Jeong, H. S., Chung, T., Kim, M., Lee, J. H., Jung, W. H., & Koo, J. S. (2017). The value of phosphohistone H3 as a proliferation marker for evaluating invasive breast cancers: A comparative study with Ki67. *Oncotarget*, *8*(39), 65064-65076. https://doi.org/10.18632/oncotarget.17775
Klann, E., & Dever, T. E. (2004). Biochemical mechanisms for translational regulation in synaptic plasticity. *Nat Rev Neurosci*, *5*(12), 931-942. https://doi.org/10.1038/nrn1557
Klum, S., Zaouter, C., Alekseenko, Z., Bjorklund, A. K., Hagey, D. W., Ericson, J., Muhr, J., & Bergsland, M. (2018). Sequentially acting SOX proteins orchestrate astrocyte- and oligodendrocyte-specific gene expression. *EMBO Rep*, *19*(11). https://doi.org/10.15252/embr.201846635
Knobloch, M., & Jessberger, S. (2017). Metabolism and neurogenesis. *Curr Opin Neurobiol*, *42*, 45-52. https://doi.org/10.1016/j.conb.2016.11.006
Knoth, R., Singec, I., Ditter, M., Pantazis, G., Capetian, P., Meyer, R. P., Horvat, V., Volk, B., & Kempermann, G. (2010). Murine features of neurogenesis in the human hippocampus across the lifespan from 0 to 100 years. *PLoS One*, *5*(1), e8809. https://doi.org/10.1371/journal.pone.0008809
Kohler, A., & Hurt, E. (2007). Exporting RNA from the nucleus to the cytoplasm. *Nat Rev Mol Cell Biol*, *8*(10), 761-773. https://doi.org/10.1038/nrm2255
Kriegstein, A. R., & Gotz, M. (2003). Radial glia diversity: a matter of cell fate. *Glia*, *43*(1), 37-43. https://doi.org/10.1002/glia.10250
Kuan, C. Y., Roth, K. A., Flavell, R. A., & Rakic, P. (2000). Mechanisms of programmed cell death in the developing brain. *Trends Neurosci*, *23*(7), 291-297. https://doi.org/10.1016/s0166-2236(00)01581-2
Kuhn, H. G., Dickinson-Anson, H., & Gage, F. H. (1996). Neurogenesis in the dentate gyrus of the adult rat: age-related decrease of neuronal progenitor

proliferation. *J Neurosci*, *16*(6), 2027-2033. https://doi.org/10.1523/JNEUROSCI.16-06-02027.1996
Lecuyer, E., Yoshida, H., Parthasarathy, N., Alm, C., Babak, T., Cerovina, T., Hughes, T. R., Tomancak, P., & Krause, H. M. (2007). Global analysis of mRNA localization reveals a prominent role in organizing cellular architecture and function. *Cell*, *131*(1), 174-187. https://doi.org/10.1016/j.cell.2007.08.003
Lee, M. H., Wu, X., & Zhu, Y. (2020). RNA-binding protein PUM2 regulates mesenchymal stem cell fate via repression of JAK2 and RUNX2 mRNAs. *J Cell Physiol*, *235*(4), 3874-3885. https://doi.org/10.1002/jcp.29281
Leslie, J. H., & Nedivi, E. (2011). Activity-regulated genes as mediators of neural circuit plasticity. *Prog Neurobiol*, *94*(3), 223-237. https://doi.org/10.1016/j.pneurobio.2011.05.002
Licatalosi, D. D., & Darnell, R. B. (2010). RNA processing and its regulation: global insights into biological networks. *Nat Rev Genet*, *11*(1), 75-87. https://doi.org/10.1038/nrg2673
Lim, D. A., & Alvarez-Buylla, A. (2014). Adult neural stem cells stake their ground. *Trends Neurosci*, *37*(10), 563-571. https://doi.org/10.1016/j.tins.2014.08.006
Lin, K., Qiang, W., Zhu, M., Ding, Y., Shi, Q., Chen, X., Zsiros, E., Wang, K., Yang, X., Kurita, T., & Xu, E. Y. (2019). Mammalian Pum1 and Pum2 Control Body Size via Translational Regulation of the Cell Cycle Inhibitor Cdkn1b. *Cell Rep*, *26*(9), 2434-2450 e2436. https://doi.org/10.1016/j.celrep.2019.01.111
Lois, C., & Alvarez-Buylla, A. (1994). Long-distance neuronal migration in the adult mammalian brain. *Science*, *264*(5162), 1145-1148. https://doi.org/10.1126/science.8178174
Lu, B., Nagappan, G., & Lu, Y. (2014). BDNF and synaptic plasticity, cognitive function, and dysfunction. *Handb Exp Pharmacol*, *220*, 223-250. https://doi.org/10.1007/978-3-642-45106-5_9
Lugert, S., Basak, O., Knuckles, P., Haussler, U., Fabel, K., Gotz, M., Haas, C. A., Kempermann, G., Taylor, V., & Giachino, C. (2010). Quiescent and active hippocampal neural stem cells with distinct morphologies respond selectively to physiological and pathological stimuli and aging. *Cell Stem Cell*, *6*(5), 445-456. https://doi.org/10.1016/j.stem.2010.03.017
Lukong, K. E., Chang, K. W., Khandjian, E. W., & Richard, S. (2008). RNA-binding proteins in human genetic disease. *Trends Genet*, *24*(8), 416-425. https://doi.org/10.1016/j.tig.2008.05.004
Lv, X., Ren, S. Q., Zhang, X. J., Shen, Z., Ghosh, T., Xianyu, A., Gao, P., Li, Z., Lin, S., Yu, Y., Zhang, Q., Groszer, M., & Shi, S. H. (2019). TBR2 coordinates neurogenesis expansion and precise microcircuit organization via Protocadherin 19 in the mammalian cortex. *Nat Commun*, *10*(1), 3946. https://doi.org/10.1038/s41467-019-11854-x
Macchi, P., Brownawell, A. M., Grunewald, B., DesGroseillers, L., Macara, I. G., & Kiebler, M. A. (2004). The brain-specific double-stranded RNA-binding protein Staufen2: nucleolar accumulation and isoform-specific exportin-5-dependent export. *J Biol Chem*, *279*(30), 31440-31444. https://doi.org/10.1074/jbc.C400226200
Malberg, J. E., Eisch, A. J., Nestler, E. J., & Duman, R. S. (2000). Chronic antidepressant treatment increases neurogenesis in adult rat hippocampus. *J Neurosci*, *20*(24), 9104-9110. https://doi.org/10.1523/JNEUROSCI.20-24-09104.2000

Marblestone, A. H., Wayne, G., & Kording, K. P. (2016). Toward an Integration of Deep Learning and Neuroscience. *Front Comput Neurosci*, *10*, 94. https://doi.org/10.3389/fncom.2016.00094
Marin, O., Valdeolmillos, M., & Moya, F. (2006). Neurons in motion: same principles for different shapes? *Trends Neurosci*, *29*(12), 655-661. https://doi.org/10.1016/j.tins.2006.10.001
Marina, N., Christie, I. N., Korsak, A., Doronin, M., Brazhe, A., Hosford, P. S., Wells, J. A., Sheikhbahaei, S., Humoud, I., Paton, J. F. R., Lythgoe, M. F., Semyanov, A., Kasparov, S., & Gourine, A. V. (2020). Astrocytes monitor cerebral perfusion and control systemic circulation to maintain brain blood flow. *Nat Commun*, *11*(1), 131. https://doi.org/10.1038/s41467-019-13956-y
Martin, K. C., & Ephrussi, A. (2009). mRNA localization: gene expression in the spatial dimension. *Cell*, *136*(4), 719-730. https://doi.org/10.1016/j.cell.2009.01.044
Martin, M. S., Tang, B., Papale, L. A., Yu, F. H., Catterall, W. A., & Escayg, A. (2007). The voltage-gated sodium channel Scn8a is a genetic modifier of severe myoclonic epilepsy of infancy. *Hum Mol Genet*, *16*(23), 2892-2899. https://doi.org/10.1093/hmg/ddm248
Martinez, J. C., Randolph, L. K., Iascone, D. M., Pernice, H. F., Polleux, F., & Hengst, U. (2019). Pum2 Shapes the Transcriptome in Developing Axons through Retention of Target mRNAs in the Cell Body. *Neuron*, *104*(5), 931-946 e935. https://doi.org/10.1016/j.neuron.2019.08.035
Masjosthusmann, S., Becker, D., Petzuch, B., Klose, J., Siebert, C., Deenen, R., Barenys, M., Baumann, J., Dach, K., Tigges, J., Hubenthal, U., Kohrer, K., & Fritsche, E. (2018). A transcriptome comparison of time-matched developing human, mouse and rat neural progenitor cells reveals human uniqueness. *Toxicol Appl Pharmacol*, *354*, 40-55. https://doi.org/10.1016/j.taap.2018.05.009
Masoli, S., Sanchez-Ponce, D., Vrieler, N., Abu-Haya, K., Lerner, V., Shahar, T., Nedelescu, H., Rizza, M. F., Benavides-Piccione, R., DeFelipe, J., Yarom, Y., Munoz, A., & D'Angelo, E. (2024). Human Purkinje cells outperform mouse Purkinje cells in dendritic complexity and computational capacity. *Commun Biol*, *7*(1), 5. https://doi.org/10.1038/s42003-023-05689-y
Maugeri, G., D'Agata, V., & Musumeci, G. (2023). Role of exercise in the brain: focus on oligodendrocytes and remyelination. *Neural Regen Res*, *18*(12), 2645-2646. https://doi.org/10.4103/1673-5374.373683
McAllister, A. K. (2000). Cellular and molecular mechanisms of dendrite growth. *Cereb Cortex*, *10*(10), 963-973. https://doi.org/10.1093/cercor/10.10.963
McEwen, B. S., & Gianaros, P. J. (2011). Stress- and allostasis-induced brain plasticity. *Annu Rev Med*, *62*, 431-445. https://doi.org/10.1146/annurev-med-052209-100430
Medioni, C., Mowry, K., & Besse, F. (2012). Principles and roles of mRNA localization in animal development. *Development*, *139*(18), 3263-3276. https://doi.org/10.1242/dev.078626
Mee, C. J., Pym, E. C., Moffat, K. G., & Baines, R. A. (2004). Regulation of neuronal excitability through pumilio-dependent control of a sodium channel gene. *J Neurosci*, *24*(40), 8695-8703. https://doi.org/10.1523/JNEUROSCI.2282-04.2004
Menon, K. P., Andrews, S., Murthy, M., Gavis, E. R., & Zinn, K. (2009). The translational repressors Nanos and Pumilio have divergent effects on

presynaptic terminal growth and postsynaptic glutamate receptor subunit composition. *J Neurosci*, *29*(17), 5558-5572. https://doi.org/10.1523/JNEUROSCI.0520-09.2009
Menon, K. P., Sanyal, S., Habara, Y., Sanchez, R., Wharton, R. P., Ramaswami, M., & Zinn, K. (2004). The translational repressor Pumilio regulates presynaptic morphology and controls postsynaptic accumulation of translation factor eIF-4E. *Neuron*, *44*(4), 663-676. https://doi.org/10.1016/j.neuron.2004.10.028
Miller, E. K., & Cohen, J. D. (2001). An integrative theory of prefrontal cortex function. *Annu Rev Neurosci*, *24*, 167-202. https://doi.org/10.1146/annurev.neuro.24.1.167
Miller, J. A., Horvath, S., & Geschwind, D. H. (2010). Divergence of human and mouse brain transcriptome highlights Alzheimer disease pathways. *Proc Natl Acad Sci U S A*, *107*(28), 12698-12703. https://doi.org/10.1073/pnas.0914257107
Miller, R. A. (2001). Biomarkers of aging: prediction of longevity by using age-sensitive T-cell subset determinations in a middle-aged, genetically heterogeneous mouse population. *J Gerontol A Biol Sci Med Sci*, *56*(4), B180-186. https://doi.org/10.1093/gerona/56.4.b180
Miranda-Negron, Y., & Garcia-Arraras, J. E. (2022). Radial glia and radial glia-like cells: Their role in neurogenesis and regeneration. *Front Neurosci*, *16*, 1006037. https://doi.org/10.3389/fnins.2022.1006037
Mirescu, C., & Gould, E. (2006). Stress and adult neurogenesis. *Hippocampus*, *16*(3), 233-238. https://doi.org/10.1002/hipo.20155
Mitchell, S. F., & Parker, R. (2014). Principles and properties of eukaryotic mRNPs. *Mol Cell*, *54*(4), 547-558. https://doi.org/10.1016/j.molcel.2014.04.033
Mofatteh, M., & Bullock, S. L. (2017). SnapShot: Subcellular mRNA Localization. *Cell*, *169*(1), 178-178 e171. https://doi.org/10.1016/j.cell.2017.03.004
Moore, F. L., Jaruzelska, J., Fox, M. S., Urano, J., Firpo, M. T., Turek, P. J., Dorfman, D. M., & Pera, R. A. (2003). Human Pumilio-2 is expressed in embryonic stem cells and germ cells and interacts with DAZ (Deleted in AZoospermia) and DAZ-like proteins. *Proc Natl Acad Sci U S A*, *100*(2), 538-543. https://doi.org/10.1073/pnas.0234478100
Morales, A. V., & Mira, H. (2019). Adult Neural Stem Cells: Born to Last. *Front Cell Dev Biol*, *7*, 96. https://doi.org/10.3389/fcell.2019.00096
Nakahata, S., Kotani, T., Mita, K., Kawasaki, T., Katsu, Y., Nagahama, Y., & Yamashita, M. (2003). Involvement of Xenopus Pumilio in the translational regulation that is specific to cyclin B1 mRNA during oocyte maturation. *Mech Dev*, *120*(8), 865-880. https://doi.org/10.1016/s0925-4773(03)00160-6
Nauer, R. K., Dunne, M. F., Stern, C. E., Storer, T. W., & Schon, K. (2020). Improving fitness increases dentate gyrus/CA3 volume in the hippocampal head and enhances memory in young adults. *Hippocampus*, *30*(5), 488-504. https://doi.org/10.1002/hipo.23166
Nestler, E. J., & Hyman, S. E. (2010). Animal models of neuropsychiatric disorders. *Nat Neurosci*, *13*(10), 1161-1169. https://doi.org/10.1038/nn.2647
Nishanth, M. J., & Jha, S. (2022). Global Exploration of RNA-Binding Proteins in Exercise-Induced Adult Hippocampal Neurogenesis: A Transcriptome Meta-analysis and Computational Study. *Biochem Genet*, *60*(6), 2471-2488. https://doi.org/10.1007/s10528-022-10230-7
Niu, W., Zang, T., Smith, D. K., Vue, T. Y., Zou, Y., Bachoo, R., Johnson, J. E., & Zhang, C. L. (2015). SOX2 reprograms resident astrocytes into neural

progenitors in the adult brain. *Stem Cell Reports*, *4*(5), 780-794. https://doi.org/10.1016/j.stemcr.2015.03.006
Noctor, S. C., Flint, A. C., Weissman, T. A., Dammerman, R. S., & Kriegstein, A. R. (2001). Neurons derived from radial glial cells establish radial units in neocortex. *Nature*, *409*(6821), 714-720. https://doi.org/10.1038/35055553
Nolde, M. J., Saka, N., Reinert, K. L., & Slack, F. J. (2007). The Caenorhabditis elegans pumilio homolog, puf-9, is required for the 3'UTR-mediated repression of the let-7 microRNA target gene, hbl-1. *Dev Biol*, *305*(2), 551-563. https://doi.org/10.1016/j.ydbio.2007.02.040
Nowakowski, R. S., Lewin, S. B., & Miller, M. W. (1989). Bromodeoxyuridine immunohistochemical determination of the lengths of the cell cycle and the DNA-synthetic phase for an anatomically defined population. *J Neurocytol*, *18*(3), 311-318. https://doi.org/10.1007/BF01190834
Pan, X., Wang, J., Guo, L., Na, F., Du, J., Chen, X., Zhong, A., Zhao, L., Zhang, L., Zhang, M., Wan, X., Wang, M., Liu, H., Dai, S., Tan, P., Chen, J., Liu, Y., Hu, B., & Chen, C. (2022). Identifying a confused cell identity for esophageal squamous cell carcinoma. *Signal Transduct Target Ther*, *7*(1), 122. https://doi.org/10.1038/s41392-022-00946-8
Parisi, M., & Lin, H. (2000). Translational repression: a duet of Nanos and Pumilio. *Curr Biol*, *10*(2), R81-83. https://doi.org/10.1016/s0960-9822(00)00283-9
Park, H. Y., Lim, H., Yoon, Y. J., Follenzi, A., Nwokafor, C., Lopez-Jones, M., Meng, X., & Singer, R. H. (2014). Visualization of dynamics of single endogenous mRNA labeled in live mouse. *Science*, *343*(6169), 422-424. https://doi.org/10.1126/science.1239200
Parra, A. S., & Johnston, C. A. (2022). Emerging Roles of RNA-Binding Proteins in Neurodevelopment. *J Dev Biol*, *10*(2), 23. https://doi.org/10.3390/jdb10020023
Pereira, B., Billaud, M., & Almeida, R. (2017). RNA-Binding Proteins in Cancer: Old Players and New Actors. *Trends Cancer*, *3*(7), 506-528. https://doi.org/10.1016/j.trecan.2017.05.003
Pilaz, L. J., & Silver, D. L. (2015). Post-transcriptional regulation in corticogenesis: how RNA-binding proteins help build the brain. *Wiley Interdiscip Rev RNA*, *6*(5), 501-515. https://doi.org/10.1002/wrna.1289
Pilz, G. A., Bottes, S., Betizeau, M., Jorg, D. J., Carta, S., April, S., Simons, B. D., Helmchen, F., & Jessberger, S. (2018). Live imaging of neurogenesis in the adult mouse hippocampus. *Science*, *359*(6376), 658-662. https://doi.org/10.1126/science.aao5056
Rakic, P. (1972). Mode of cell migration to the superficial layers of fetal monkey neocortex. *J Comp Neurol*, *145*(1), 61-83. https://doi.org/10.1002/cne.901450105
Saelens, W., Cannoodt, R., Todorov, H., & Saeys, Y. (2019). A comparison of single-cell trajectory inference methods. *Nat Biotechnol*, *37*(5), 547-554. https://doi.org/10.1038/s41587-019-0071-9
Sahay, A., & Hen, R. (2007). Adult hippocampal neurogenesis in depression. *Nat Neurosci*, *10*(9), 1110-1115. https://doi.org/10.1038/nn1969
Sahay, A., Scobie, K. N., Hill, A. S., O'Carroll, C. M., Kheirbek, M. A., Burghardt, N. S., Fenton, A. A., Dranovsky, A., & Hen, R. (2011). Increasing adult hippocampal neurogenesis is sufficient to improve pattern separation. *Nature*, *472*(7344), 466-470. https://doi.org/10.1038/nature09817
Sahoo, P. K., Lee, S. J., Jaiswal, P. B., Alber, S., Kar, A. N., Miller-Randolph, S., Taylor, E. E., Smith, T., Singh, B., Ho, T. S., Urisman, A., Chand, S., Pena, E.

A., Burlingame, A. L., Woolf, C. J., Fainzilber, M., English, A. W., & Twiss, J. L. (2018). Axonal G3BP1 stress granule protein limits axonal mRNA translation and nerve regeneration. *Nat Commun*, *9*(1), 3358. https://doi.org/10.1038/s41467-018-05647-x

Sanai, N., Nguyen, T., Ihrie, R. A., Mirzadeh, Z., Tsai, H. H., Wong, M., Gupta, N., Berger, M. S., Huang, E., Garcia-Verdugo, J. M., Rowitch, D. H., & Alvarez-Buylla, A. (2011). Corridors of migrating neurons in the human brain and their decline during infancy. *Nature*, *478*(7369), 382-386. https://doi.org/10.1038/nature10487

Sanai, N., Tramontin, A. D., Quinones-Hinojosa, A., Barbaro, N. M., Gupta, N., Kunwar, S., Lawton, M. T., McDermott, M. W., Parsa, A. T., Manuel-Garcia Verdugo, J., Berger, M. S., & Alvarez-Buylla, A. (2004). Unique astrocyte ribbon in adult human brain contains neural stem cells but lacks chain migration. *Nature*, *427*(6976), 740-744. https://doi.org/10.1038/nature02301

Santello, M., Toni, N., & Volterra, A. (2019). Astrocyte function from information processing to cognition and cognitive impairment. *Nat Neurosci*, *22*(2), 154-166. https://doi.org/10.1038/s41593-018-0325-8

Sartor, F., Anderson, J., McCaig, C., Miedzybrodzka, Z., & Muller, B. (2015). Mutation of genes controlling mRNA metabolism and protein synthesis predisposes to neurodevelopmental disorders. *Biochem Soc Trans*, *43*(6), 1259-1265. https://doi.org/10.1042/BST20150168

Scala, F., Kobak, D., Bernabucci, M., Bernaerts, Y., Cadwell, C. R., Castro, J. R., Hartmanis, L., Jiang, X., Laturnus, S., Miranda, E., Mulherkar, S., Tan, Z. H., Yao, Z., Zeng, H., Sandberg, R., Berens, P., & Tolias, A. S. (2021). Phenotypic variation of transcriptomic cell types in mouse motor cortex. *Nature*, *598*(7879), 144-150. https://doi.org/10.1038/s41586-020-2907-3

Schieweck, R., Ninkovic, J., & Kiebler, M. A. (2021). RNA-binding proteins balance brain function in health and disease. *Physiol Rev*, *101*(3), 1309-1370. https://doi.org/10.1152/physrev.00047.2019

Schieweck, R., Riedemann, T., Forne, I., Harner, M., Bauer, K. E., Rieger, D., Ang, F. Y., Hutten, S., Demleitner, A. F., Popper, B., Derdak, S., Sutor, B., Bilban, M., Imhof, A., & Kiebler, M. A. (2021). Pumilio2 and Staufen2 selectively balance the synaptic proteome. *Cell Rep*, *35*(12), 109279. https://doi.org/10.1016/j.celrep.2021.109279

Schieweck, R., Schoneweiss, E. C., Harner, M., Rieger, D., Illig, C., Sacca, B., Popper, B., & Kiebler, M. A. (2021). Pumilio2 Promotes Growth of Mature Neurons. *Int J Mol Sci*, *22*(16), 8998. https://doi.org/10.3390/ijms22168998

Schmidt-Hieber, C., Jonas, P., & Bischofberger, J. (2004). Enhanced synaptic plasticity in newly generated granule cells of the adult hippocampus. *Nature*, *429*(6988), 184-187. https://doi.org/10.1038/nature02553

Schoenberg, D. R., & Maquat, L. E. (2012). Regulation of cytoplasmic mRNA decay. *Nat Rev Genet*, *13*(4), 246-259. https://doi.org/10.1038/nrg3160

Schweers, B. A., Walters, K. J., & Stern, M. (2002). The Drosophila melanogaster translational repressor pumilio regulates neuronal excitability. *Genetics*, *161*(3), 1177-1185. https://doi.org/10.1093/genetics/161.3.1177

Seri, B., Garcia-Verdugo, J. M., McEwen, B. S., & Alvarez-Buylla, A. (2001). Astrocytes give rise to new neurons in the adult mammalian hippocampus. *J Neurosci*, *21*(18), 7153-7160. https://doi.org/10.1523/JNEUROSCI.21-18-07153.2001

Sidman, R. L., & Rakic, P. (1973). Neuronal migration, with special reference to developing human brain: a review. *Brain Res*, *62*(1), 1-35. https://doi.org/10.1016/0006-8993(73)90617-3
Siemen, H., Colas, D., Heller, H. C., Brustle, O., & Pera, R. A. (2011). Pumilio-2 function in the mouse nervous system. *PLoS One*, *6*(10), e25932. https://doi.org/10.1371/journal.pone.0025932
Simons, M., & Nave, K. A. (2015). Oligodendrocytes: Myelination and Axonal Support. *Cold Spring Harb Perspect Biol*, *8*(1), a020479. https://doi.org/10.1101/cshperspect.a020479
Smialek, M. J., Ilaslan, E., Sajek, M. P., & Jaruzelska, J. (2021). Role of PUM RNA-Binding Proteins in Cancer. *Cancers (Basel)*, *13*(1). https://doi.org/10.3390/cancers13010129
Snyder, J. S., Soumier, A., Brewer, M., Pickel, J., & Cameron, H. A. (2011). Adult hippocampal neurogenesis buffers stress responses and depressive behaviour. *Nature*, *476*(7361), 458-461. https://doi.org/10.1038/nature10287
Sobecki, M., Mrouj, K., Colinge, J., Gerbe, F., Jay, P., Krasinska, L., Dulic, V., & Fisher, D. (2017). Cell-Cycle Regulation Accounts for Variability in Ki-67 Expression Levels. *Cancer Res*, *77*(10), 2722-2734. https://doi.org/10.1158/0008-5472.CAN-16-0707
Sorrells, S. F., Paredes, M. F., Cebrian-Silla, A., Sandoval, K., Qi, D., Kelley, K. W., James, D., Mayer, S., Chang, J., Auguste, K. I., Chang, E. F., Gutierrez, A. J., Kriegstein, A. R., Mathern, G. W., Oldham, M. C., Huang, E. J., Garcia-Verdugo, J. M., Yang, Z., & Alvarez-Buylla, A. (2018). Human hippocampal neurogenesis drops sharply in children to undetectable levels in adults. *Nature*, *555*(7696), 377-381. https://doi.org/10.1038/nature25975
Spalding, K. L., Bergmann, O., Alkass, K., Bernard, S., Salehpour, M., Huttner, H. B., Bostrom, E., Westerlund, I., Vial, C., Buchholz, B. A., Possnert, G., Mash, D. C., Druid, H., & Frisen, J. (2013). Dynamics of hippocampal neurogenesis in adult humans. *Cell*, *153*(6), 1219-1227. https://doi.org/10.1016/j.cell.2013.05.002
Spalding, K. L., Bhardwaj, R. D., Buchholz, B. A., Druid, H., & Frisen, J. (2005). Retrospective birth dating of cells in humans. *Cell*, *122*(1), 133-143. https://doi.org/10.1016/j.cell.2005.04.028
Spassov, D. S., & Jurecic, R. (2003). Mouse Pum1 and Pum2 genes, members of the Pumilio family of RNA-binding proteins, show differential expression in fetal and adult hematopoietic stem cells and progenitors. *Blood Cells Mol Dis*, *30*(1), 55-69. https://doi.org/10.1016/s1079-9796(03)00003-2
Stiles, J., & Jernigan, T. L. (2010). The basics of brain development. *Neuropsychol Rev*, *20*(4), 327-348. https://doi.org/10.1007/s11065-010-9148-4
Sudhof, T. C. (2013). Neurotransmitter release: the last millisecond in the life of a synaptic vesicle. *Neuron*, *80*(3), 675-690. https://doi.org/10.1016/j.neuron.2013.10.022
Sun, M., Ahmad, N., Zhang, R., & Graw, J. (2018). Crybb2 associates with Tmsb4X and is crucial for dendrite morphogenesis. *Biochem Biophys Res Commun*, *503*(1), 123-130. https://doi.org/10.1016/j.bbrc.2018.05.195
Sun, W., Cornwell, A., Li, J., Peng, S., Osorio, M. J., Aalling, N., Wang, S., Benraiss, A., Lou, N., Goldman, S. A., & Nedergaard, M. (2017). SOX9 Is an Astrocyte-Specific Nuclear Marker in the Adult Brain Outside the Neurogenic Regions. *J Neurosci*, *37*(17), 4493-4507. https://doi.org/10.1523/JNEUROSCI.3199-16.2017

Sun, X., & Kaufman, P. D. (2018). Ki-67: more than a proliferation marker. *Chromosoma*, *127*(2), 175-186. https://doi.org/10.1007/s00412-018-0659-8
Svenson, K. L., Gatti, D. M., Valdar, W., Welsh, C. E., Cheng, R., Chesler, E. J., Palmer, A. A., McMillan, L., & Churchill, G. A. (2012). High-resolution genetic mapping using the Mouse Diversity outbred population. *Genetics*, *190*(2), 437-447. https://doi.org/10.1534/genetics.111.132597
Tam, P. P., & Behringer, R. R. (1997). Mouse gastrulation: the formation of a mammalian body plan. *Mech Dev*, *68*(1-2), 3-25. https://doi.org/10.1016/s0925-4773(97)00123-8
Tashiro, A., Sandler, V. M., Toni, N., Zhao, C., & Gage, F. H. (2006). NMDA-receptor-mediated, cell-specific integration of new neurons in adult dentate gyrus. *Nature*, *442*(7105), 929-933. https://doi.org/10.1038/nature05028
Tay, T. L., Carrier, M., & Tremblay, M. E. (2019). Physiology of Microglia. *Adv Exp Med Biol*, *1175*, 129-148. https://doi.org/10.1007/978-981-13-9913-8_6
Toni, N., Teng, E. M., Bushong, E. A., Aimone, J. B., Zhao, C., Consiglio, A., van Praag, H., Martone, M. E., Ellisman, M. H., & Gage, F. H. (2007). Synapse formation on neurons born in the adult hippocampus. *Nat Neurosci*, *10*(6), 727-734. https://doi.org/10.1038/nn1908
Urban, N., & Guillemot, F. (2014). Neurogenesis in the embryonic and adult brain: same regulators, different roles. *Front Cell Neurosci*, *8*, 396. https://doi.org/10.3389/fncel.2014.00396
Uyhazi, K. E., Yang, Y., Liu, N., Qi, H., Huang, X. A., Mak, W., Weatherbee, S. D., de Prisco, N., Gennarino, V. A., Song, X., & Lin, H. (2020). Pumilio proteins utilize distinct regulatory mechanisms to achieve complementary functions required for pluripotency and embryogenesis. *Proc Natl Acad Sci U S A*, *117*(14), 7851-7862. https://doi.org/10.1073/pnas.1916471117
Van Etten, J., Schagat, T. L., Hrit, J., Weidmann, C. A., Brumbaugh, J., Coon, J. J., & Goldstrohm, A. C. (2012). Human Pumilio proteins recruit multiple deadenylases to efficiently repress messenger RNAs. *J Biol Chem*, *287*(43), 36370-36383. https://doi.org/10.1074/jbc.M112.373522
van Praag, H., Kempermann, G., & Gage, F. H. (1999). Running increases cell proliferation and neurogenesis in the adult mouse dentate gyrus. *Nat Neurosci*, *2*(3), 266-270. https://doi.org/10.1038/6368
Vessey, J. P., Amadei, G., Burns, S. E., Kiebler, M. A., Kaplan, D. R., & Miller, F. D. (2012). An asymmetrically localized Staufen2-dependent RNA complex regulates maintenance of mammalian neural stem cells. *Cell Stem Cell*, *11*(4), 517-528. https://doi.org/10.1016/j.stem.2012.06.010
Vessey, J. P., Schoderboeck, L., Gingl, E., Luzi, E., Riefler, J., Di Leva, F., Karra, D., Thomas, S., Kiebler, M. A., & Macchi, P. (2010). Mammalian Pumilio 2 regulates dendrite morphogenesis and synaptic function. *Proc Natl Acad Sci U S A*, *107*(7), 3222-3227. https://doi.org/10.1073/pnas.0907128107
Vessey, J. P., Vaccani, A., Xie, Y., Dahm, R., Karra, D., Kiebler, M. A., & Macchi, P. (2006). Dendritic localization of the translational repressor Pumilio 2 and its contribution to dendritic stress granules. *J Neurosci*, *26*(24), 6496-6508. https://doi.org/10.1523/JNEUROSCI.0649-06.2006
Vivar, C., Potter, M. C., Choi, J., Lee, J. Y., Stringer, T. P., Callaway, E. M., Gage, F. H., Suh, H., & van Praag, H. (2012). Monosynaptic inputs to new neurons in the dentate gyrus. *Nat Commun*, *3*, 1107. https://doi.org/10.1038/ncomms2101

Vuong, C. K., Black, D. L., & Zheng, S. (2016). The neurogenetics of alternative splicing. *Nat Rev Neurosci*, *17*(5), 265-281. https://doi.org/10.1038/nrn.2016.27

Wan, J., Yourshaw, M., Mamsa, H., Rudnik-Schoneborn, S., Menezes, M. P., Hong, J. E., Leong, D. W., Senderek, J., Salman, M. S., Chitayat, D., Seeman, P., von Moers, A., Graul-Neumann, L., Kornberg, A. J., Castro-Gago, M., Sobrido, M. J., Sanefuji, M., Shieh, P. B., Salamon, N., . . . Jen, J. C. (2012). Mutations in the RNA exosome component gene EXOSC3 cause pontocerebellar hypoplasia and spinal motor neuron degeneration. *Nat Genet*, *44*(6), 704-708. https://doi.org/10.1038/ng.2254

Wang, M., Oge, L., Perez-Garcia, M. D., Hamama, L., & Sakr, S. (2018). The PUF Protein Family: Overview on PUF RNA Targets, Biological Functions, and Post Transcriptional Regulation. *Int J Mol Sci*, *19*(2), 410. https://doi.org/10.3390/ijms19020410

White, E. K., Moore-Jarrett, T., & Ruley, H. E. (2001). PUM2, a novel murine puf protein, and its consensus RNA-binding site. *RNA*, *7*(12), 1855-1866. https://www.ncbi.nlm.nih.gov/pubmed/11780640

Wickens, M., Bernstein, D. S., Kimble, J., & Parker, R. (2002). A PUF family portrait: 3'UTR regulation as a way of life. *Trends Genet*, *18*(3), 150-157. https://doi.org/10.1016/s0168-9525(01)02616-6

Wolf, F. A., Angerer, P., & Theis, F. J. (2018). SCANPY: large-scale single-cell gene expression data analysis. *Genome Biol*, *19*(1), 15. https://doi.org/10.1186/s13059-017-1382-0

Wolf, S. A., Boddeke, H. W., & Kettenmann, H. (2017). Microglia in Physiology and Disease. *Annu Rev Physiol*, *79*, 619-643. https://doi.org/10.1146/annurev-physiol-022516-034406

Wong, A. C., Velamoor, S., Skelton, M. R., Thorne, P. R., & Vlajkovic, S. M. (2012). Expression and distribution of creatine transporter and creatine kinase (brain isoform) in developing and mature rat cochlear tissues. *Histochem Cell Biol*, *137*(5), 599-613. https://doi.org/10.1007/s00418-012-0922-7

Wong, H. H., Chou, C. Y. C., Watt, A. J., & Sjostrom, P. J. (2023). Comparing mouse and human brains. *Elife*, *12*. https://doi.org/10.7554/eLife.90017

Yang, G., Smibert, C. A., Kaplan, D. R., & Miller, F. D. (2014). An eIF4E1/4E-T complex determines the genesis of neurons from precursors by translationally repressing a proneurogenic transcription program. *Neuron*, *84*(4), 723-739. https://doi.org/10.1016/j.neuron.2014.10.022

Ye, B., Petritsch, C., Clark, I. E., Gavis, E. R., Jan, L. Y., & Jan, Y. N. (2004). Nanos and Pumilio are essential for dendrite morphogenesis in Drosophila peripheral neurons. *Curr Biol*, *14*(4), 314-321. https://doi.org/10.1016/j.cub.2004.01.052

Yoon, Y. J., Wu, B., Buxbaum, A. R., Das, S., Tsai, A., English, B. P., Grimm, J. B., Lavis, L. D., & Singer, R. H. (2016). Glutamate-induced RNA localization and translation in neurons. *Proc Natl Acad Sci U S A*, *113*(44), E6877-E6886. https://doi.org/10.1073/pnas.1614267113

Zahr, S. K., Yang, G., Kazan, H., Borrett, M. J., Yuzwa, S. A., Voronova, A., Kaplan, D. R., & Miller, F. D. (2018). A Translational Repression Complex in Developing Mammalian Neural Stem Cells that Regulates Neuronal Specification. *Neuron*, *97*(3), 520-537 e526. https://doi.org/10.1016/j.neuron.2017.12.045

Zatorre, R. J., Fields, R. D., & Johansen-Berg, H. (2012). Plasticity in gray and white: neuroimaging changes in brain structure during learning. *Nat Neurosci*, *15*(4), 528-536. https://doi.org/10.1038/nn.3045

Zeng, H., & Sanes, J. R. (2017). Neuronal cell-type classification: challenges, opportunities and the path forward. *Nat Rev Neurosci*, *18*(9), 530-546. https://doi.org/10.1038/nrn.2017.85

Zhang, M., Chen, D., Xia, J., Han, W., Cui, X., Neuenkirchen, N., Hermes, G., Sestan, N., & Lin, H. (2017). Post-transcriptional regulation of mouse neurogenesis by Pumilio proteins. *Genes Dev*, *31*(13), 1354-1369. https://doi.org/10.1101/gad.298752.117

Zhao, C., Deng, W., & Gage, F. H. (2008). Mechanisms and functional implications of adult neurogenesis. *Cell*, *132*(4), 645-660. https://doi.org/10.1016/j.cell.2008.01.033

Zhao, C., Teng, E. M., Summers, R. G., Jr., Ming, G. L., & Gage, F. H. (2006). Distinct morphological stages of dentate granule neuron maturation in the adult mouse hippocampus. *J Neurosci*, *26*(1), 3-11. https://doi.org/10.1523/JNEUROSCI.3648-05.2006

Zheng, G. X., Terry, J. M., Belgrader, P., Ryvkin, P., Bent, Z. W., Wilson, R., Ziraldo, S. B., Wheeler, T. D., McDermott, G. P., Zhu, J., Gregory, M. T., Shuga, J., Montesclaros, L., Underwood, J. G., Masquelier, D. A., Nishimura, S. Y., Schnall-Levin, M., Wyatt, P. W., Hindson, C. M., . . . Bielas, J. H. (2017). Massively parallel digital transcriptional profiling of single cells. *Nat Commun*, *8*, 14049. https://doi.org/10.1038/ncomms14049

Zhong, L., Cherry, T., Bies, C. E., Florence, M. A., & Gerges, N. Z. (2009). Neurogranin enhances synaptic strength through its interaction with calmodulin. *EMBO J*, *28*(19), 3027-3039. https://doi.org/10.1038/emboj.2009.236

Zhou, M., Tao, X., Sui, M., Cui, M., Liu, D., Wang, B., Wang, T., Zheng, Y., Luo, J., Mu, Y., Wan, F., Zhu, L. Q., & Zhang, B. (2021). Reprogramming astrocytes to motor neurons by activation of endogenous Ngn2 and Isl1. *Stem Cell Reports*, *16*(7), 1777-1791. https://doi.org/10.1016/j.stemcr.2021.05.020

Individual contributions to the work of this thesis

This doctoral thesis presents my original research. I designed the experiments, collected, analysed the data, and interpreted the results, except where collaborations are explicitly acknowledged.

Prof. Dr. Michael A. Kiebler and Prof. Dr. Jovica Ninkovic (LMU Munich) conceived and supervised the project, were involved in data analysis and data interpretation.

Dr. Max Harner and Dr. Gregor Pilz (LMU Munich) contributed to the experimental design and the data interpretation. Furthermore, Dr. Gregor Pilz contributed to experimental execution.

Christin Illig (Kiebler laboratory) performed the BrdU mouse experiments with Pum2GT mouse line (**Figure 3**, **Figure 10**, **Figure 12**) and contributed to the data of the following graphs: **Figure 3C & D, Figure 4B, Figure 5B, Figure 6B, Figure 7B, Figure 9A , B, C & D, Figure 11B, Figure 13A** with immunostaining; **Figure 3E, Figure 4C, Figure 5C, Figure 6C, Figure 7C, Figure 11A, Figure 13C** with immunostaining and analysis of the immunostaining.

Dr. Christina Koupourtidou (Ninkovic laboratory), Sabine Thomas and Dr. Stefanie Ohlig (Kiebler laboratory) performed scRNA-seq experiment (**Figure 23**).

Dr. Christina Koupourtidou (Ninkovic laboratory) performed initial scRNA-seq sequencing data preprocessing and established the Scanpy workflow (**Figure 23**). Additionally, she provided protocols and help for the RNAscope experiments (**Figure 27**).

Prof. Dr. Magdalena Götz (LMU Munich, Helmholtz Munich) provided the HEK 293GPG cells, P19 mouse cell line, cell culture material for P19 and hNPCs cells and laboratory infrastructure for training and experimental procedures. Additionally, she provided the CAG-GFP-miRNA (Scrambled) construct and material to clone miRNAs into CAG-GFP vector.

Martina Bürkle (Götz laboratory) provided training for the retrovirus production and maintenance of the HEK 293GPG cells.

Paulina Chlebik (Götz laboratory) provided training for astrocyte culture and titre verification of the retrovirus encoding miRNAs.

Dr. Giacomo Masserdotti (LMU Munich) contributed to the experimental approach in cloning miRNAs.

Dr. Ines Muehlhahn (Götz laboratory) provided protocols and plasmid maps for cloning the for the miRNA constructs.

Renate Dombi (Kiebler laboratory) assisted cloning the miRNA constructs CAG-GFP-miRNA (Pum2) – Oligo1 and – Oligo2.

Renate Dombi and Katalin Vartas (Kiebler laboratory) performed purification and maxi preparation of all miRNA constructs.

Christian Biedinger (Pilz laboratory) provided materials and protocol for consecutive immunostaining (**Figure 28**).

Yiling Li (Götz laboratory) provided the protocol for P19 cell culture.

Jovana Spalevic (Ninkovic laboratory) provided training, maintenance and help for performing experiments with hNPC cell culture.

Dr. Rico Schieweck (Kiebler laboratory) provided training and assisted in polysome profiling experiment (**Figure 38**).

Dr. Barabra Nitz (Kiebler laboratory) provided initial cartoons illustrating the DG cell composition and hypothesis figures that were adapted for this thesis (**Figure 1**, **Figure 39**, **Figure 40**, **Figure 41**).

Ulrike Kring and Gudrun Trommler (Kiebler laboratory) provided initial genotyping for the Pum2 mice until taken over by myself.

Acknowledgements

I would like to express my sincere gratitude to those who have made this dissertation possible. First, I am deeply grateful to my supervisor, Prof. Dr. Michael Kiebler, for the opportunity to work in his laboratory and for his invaluable guidance and support. I am also indebted to Prof. Dr. Jovica Ninkovic for his expertise, insightful ideas, and teaching throughout this project. Special thanks goes to Dr. Max Harner for his participation in my thesis advisory committee (TAC) and his constant availability to provide brilliant comments, suggestions, and invaluable help that greatly impacted this project. I would also like to thank Dr. Christof Osman for his role as a TAC member and my internal supervisor with constant comments and suggestions. Additionally, I would like to acknowledge Dr. Gregor Pilz for his participation in my TAC and his insightful comments, suggestions, and support especially for the lead in the *in vivo* experiments.

I deeply appreciated the support, mentoring, and positive lab environment fostered by all members of the Kiebler lab. Special thanks goes to Sabine Thomas for lab management, assistance with animal documentation, and collaboration on the scRNA-seq with Dr. Christina Koupourtidou. I would also like to thank Dr. Barbara Nitz for her help in designing the initial figure cartoons. In addition, I would like to acknowledge Andrea Wilytsch, Ralf Bigiel, and Serpil Yildirim for their invaluable help with non-scientific tasks.

I would like to thank the Graduate School Life Science Munich (LSM) for providing the ideal opportunity to learn new skills through high-quality courses and broaden scientific horizons within a diverse network. Sincere appreciation is extended to all LSM coordinators for their constant support and assistance. Special credit is given to Prof. Dr. Magdalena Götz and all members of her laboratory, particularly Martina Bürkle and Paulina Chiblek, for their help and training.

Finally, I would like to express my deepest gratitude to my girlfriend, Leonie Koch, for her unwavering love and encouragement throughout this journey. Dr. Katja Eubler and Viviane Schulz for the friendship, support, encouragement, and beer after work.

Thank you to all members of the Cell Biology Department for being part of this awesome experience.